공학박사학위논문

Non-invasive Deactivation and Spatial Control of Intracellular Chromosome with Magnetic Nanoparticle

자성 나노입자를 이용한 세포 내 염색체의 비침습식 기능 및 위치 제어

2016 년 8월

서울대학교 대학원

기계항공 공학부

홍 주 희

자성 나노입자를 이용한 세포 내 염색체의 비침습성 기능 및 위치 제어

Non-invasive Deactivation and Spatial Control of Intracellular Chromosome with Magnetic Nanoparticle

지도교수 이 정 훈

이 논문을 공학박사 학위논문으로 제출함

2016년 4월

서울대학교 대학원

기계 항공 공학부

홍 주 희

홍주희의 공학박사 학위논문을 인준함

2016년 6월

위 원 장: 현 택 환 (인)

부위원장: 이 정 훈 (인)

위 원: 전 누 리 (인)

위 원: 강 지 윤 (인)

위 원: 신 현 정 (인)

ABSRACT

Non-invasive Deactivation and Spatial Control of Intracellular Chromosome with Magnetic Nanoparticle

Juhee Hong

School of Mechanical and Aerospace Engineering

Seoul National University

The regulation of cell signaling pathway is important for understanding biological systems. Thus, various techniques to modulate cell signaling by spatial control of cellular components have been developed. Magnetic nanoparticles are emerging as promising candidates in a broad range from cell biology to biomedical application due to their unique characteristics such as remote control and their ability to interact with various cellular and molecular level of interest through their surface decoration. With the advent of advanced nanoscience and nanotechnology in the reliable production and specific tailoring of functional magnetic particles, successful applications were dedicated to a broad range of biomedical applications such as high throughput separation of biomolecules, magnetic resonance image, hyperthermia for cancer therapy, and drug delivery. Recently, fluorescent magnetic nanoparticles inside a living cell were shown to be directly attracted by an external magnetic field. In addition, the signaling transduction pathway was remotely triggered by the

functionalized magnetic nanoparticles and the microtubule nucleation and assembly inside Xenopus oocyte was spatiotemporally controlled by magnetic nanoparticles conjugated with key regulatory proteins. Moreover, it is shown that the remote induction of cell death by targeting intracellular lysosome was triggered by functionalized magnetic nanoparticles.

In this study, we demonstrate a novel strategy to non-invasively regulate chromosome activity by targeting genetic regulation materials (i.e., oocyte-specific linker histone H1 protein) in live oocyte with the functionalized magnetic nanoparticles and to spatially control the targeted chromosomes by a remote magnetic field. To this end, bacterial magnetic nanoparticles (BMPs, ~50 nm) produced by magnetotactic bacteria (Magnetosome) were used because of their peculiar features, such as high magnetism, high dispersal ability in an aqueous media and good biocompatibility. In addition, BMPs can effectively be conjugated to the diverse biomolecules due to the abundance of amine groups on particles surrounded by lipid membrane.

First, we present a novel method to regulate the chromosome activity in mature mouse (Metaphase II) oocytes by targeting the histone H1 protein in chromosome with functionalized magnetic nanoparticles. BMPs were conjugated with histone H1 antibodies (H1-BMPs), specifically targeting the oocyte-specific histone H1 protein. The dose-dependent cytotoxicity test for H1-BMPs was initially conducted before starting experiments. Our data clearly show that the oocytes are able to be tolerated up to the delivery of 1 μg/ml H1-BMPs without any developmental retardation and this concentration is optimal for regulation of a chromosome activities.

In the first stage, to verify this approach, we examined whether H1-BMPs have the specific affinity against the chromosomal histone H1 protein in live oocyte. The capability of H1-BMPs for specific targeting was easily detected by confocal microscopy. In addition, we investigated how oocyte developmental process was affected by the magnetic labeling of chromosomes. The parthenogenesis was induced to activate the cell cycle progression. When chromosomes were targeted by H1-BMPs, oocytes were developed up to the 4-cell stage, but began to degrade afterwards and failed to reach the blastocyst stage regardless of the application of magnetic field. Interestingly, in mouse oocyte, it is well known that transcriptional repression in parthenogenesis is proceeded until four cell stage and newly synthesized ribonucleic acid (RNA) begins to be transcriptionally expressed at late four cell stage. Thus, we believed that an abrupt fall in oocyte development after four cell stage is caused by the perturbation of transcriptional activity.

Second, we demonstrate the spatial control of targeted chromosomes with H1-BMPs and remaining unbound H1-BMP inside living oocyte via a remote magnetic field. In these experiments, immature oocytes at germinal vesicle breakdown (GVBD) stage were selected for subsequent experiments. For cell cycle arrest which can prevent the spontaneous chromosome movement during experiments, the nocodazole treatment was carried out to prevent.

As a first step towards the spatial control of chromosomes, the applied magnetics force was analyzed. To generate strong magnetic fields, the several neodymium magnets in various experimental condition were used. It is calculated that a large force of 780 fN was exerted on single BMP by a strong magnetic field. Based on the

specific targeting test, we attempted to rotate cell using a remote magnetic field. The orientation of cell is dictated and arranged by the direction of a magnetic field.

Next, we attempted to move the chromosomes located around the center of an oocyte by an external magnetic field. Without the antibodies, the BMPs did not conjugate with the chromosomes and the chromosomes did not move together with the BMPs in the presence of the magnetic field. The green spots from the FITC-conjugated BMPs moved in the direction of the magnetic field, whereas the blue spots from the DAPI-stained chromosomes remained close to the center. On the other hand, with antibody, the blue spots (chromosomes) coincided with the green spots (H1-BMPs) that noticeably moved to the top. For a more detailed analysis, chromosomes movement was quantitatively assessed by using image process. The mass center of the blue spots was calculated and used as a value that represents the entire distance moved. We compare the distances with and without. A substantial difference was observed between the cases with (20.59 ± 2.47 μm) and without (9.18 ± 4.23 μm) antibodies.

To gain further evidence for chromosome movement by a remote magnetic field, we observed the time course motion of the chromosomes in live oocyte. To observe lateral movement, we prevented the rotation and drift of the living oocyte by anchoring it to the substrate. To achieve this goal, we developed a vacuum-assisted microfluidic device for trapping the oocyte on a transparent substrate and tested it. The oocytes were Hoechst-stainied before immobilized on the trapping hole. When the negative pressure was applied to the microfluidic device, oocytes were rapidly attracted to and fixed on the holes. A magnetic field was applied from the side of the

trapped oocyte. The sequence of captured images shows the lateral motion of the chromosomes toward the applied magnetic field. The velocity of chromosome movement by a remote magnetic force was calculated as ~70 nm/min. Our data shows that the movement of the chromosomes linked to the H1-BMPs can be severely hindered by the meshwork of actin filament bundles.

Recently, although human stem cell was generated by somatic cell nuclear transfer (SCNT), the enucleation process is still important factor in SCNT. It is well known that the invasive enucleation (removal of human oocyte genome) leads to the failure of embryonic development after genome exchange due to the loss of meiosis-specific factors associated with the spindle removal during physical enucleation process. Thus, we suggest the non-invasive method for SCNT without enucleation, by targeting chromosome with H1-BMPs. To achieve it, two possibilities have to be pre-verified. First, there are no interaction between chromosomes in somatic cell and unbounded H1-BMPs in oocyte after somatic cell – oocyte fusion. In previous work, we showed the possibility to control the both H1-BMPs and chromosome attached to H1-BMPs by using external magnetic field. Through previous result, the position of unbounded H1-BMPs can be controlled before somatic cell chromosomes are fused with oocyte chromosomes. Second, to deactivate chromosome activity, specific time (10 hrs) is necessary to target chromosome with H1-BMPs. Thus, it is required to investigate whether oocyte move to blastocyst stage after delay in activation for 10 hrs. Thus, it is investigated whether oocyte move to blastocyst stage after delay of activation for 10 hrs. It is shown that oocytes are well developed and reached the blastocyst stage with ~ 20 % despite of delay of activation time. Second

there are no interaction between chromosomes in somatic cell and unbounded H1-BMPs in oocyte after somatic cell – oocyte fusion. These results show the possibility to apply our method to SCNT process.

In the study described above, we demonstrate the possibility to non-invasively regulate a chromosome activity by the magnetic labeling, leading to arrest of embryonic development in parthenogenesis due to abnormal transcriptional activity. Through result, our non-invasive technique can be a candidate of alternative methods in somatic cell nuclear transfer (SCNT) that suffers from cell damage during enucleation process. To validate the potential application, the long range displacement of chromosomes is verified in oocyte by external magnetic field. We showed the traction of whole chromosomes in an oocyte across the entire cell span using functionalized magnetic nanoparticles (H1-BMPs). Procedures and techniques were well developed. In addition, our technique will provide a useful tool for investigating cellular functions associated with the spatiotemporal distribution of such components.

Keywords: Bacterial magnetic nanoparticle, Specific targeting, Parthenogenesis, Perturbation of transcription activity, Denucleation, Chromosome repositioning

Student Number: 2006-30824

CONTENTS

LIST OF FIGURES

LIST OF TABLES

CHAPTER 1. INTRODUCTION

1-1. Cell

The cell discovered by Robert Hooke in 1665 is the essential unit of structural and functional living organisms. All cells contain the hereditary information, called genetic material, which controls cellular functions and transmits information to the next generation of cells. Depending on the size, shape, and function of cell, there are many types of cells. For example, our body is composed of 10^{13}~10^{14} cells with 200 different cell types [1]. The size of most cells ranges from 1 to100 μm in order to increase their surface area to volume ratio. The various shapes of cells are determined by their functions. For examples, the nerve cell is specialized for transmission of cell signal. Thus, its shape is very thin, allowing the cell signals from head to fast transmit to toes. On the other hand, sperm cell seems to be a thin rod which helps to swim long time.

Cell can be split into two categories such as prokaryotic and eukaryotic cell, depending on the presence of nuclear membrane. Prokaryotic cells including bacteria and archaea consist of simple structure with a single chromosome without nuclear membrane as shown in Fig. 1-1. The DNA in chromosome is circular shape and the binary fission occurs in cell division [2]. In addition, some prokaryotic cells use the flagellum to facilitate the movement and communication between cells.

On the other hand, eukaryotic cells are more complex and have a various organelle such as a nuclear envelope, mitochondria, ribosomes, and so on.

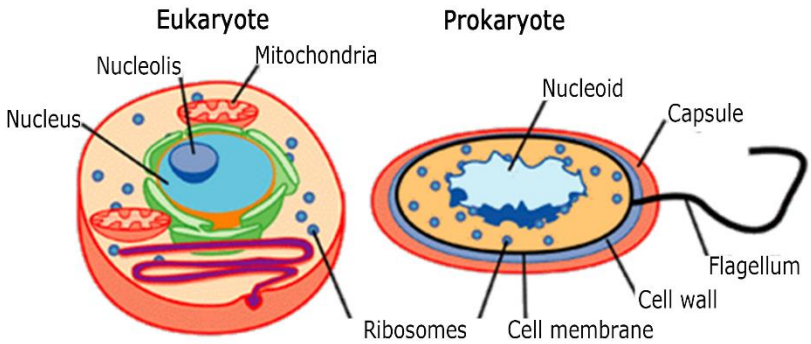

Figure 1-1 The image of eukaryotic and prokaryotic cell from Science Primer (www.scienceprimer.com).

The nuclear envelope that surrounds chromosomal DNA is a unique element in eukaryotic cells. In comparison with the binary fission of prokaryotic cell, eukaryotic cell carried out a complex and precise cell division process, called mitosis or meiosis. Figure 1-2 shows the both plant and animal cell. Although both plant and animal cell belong to a eukaryotic cell, there are some differences between a plant cell and an animal cell. One of the primary differences between plant and animal cell is that animal cell does not have a cell wall. A cell wall in plant cell prevents the cell from external high pressure without explosion and enables to take a lot of liquid through osmosis without destruction. In addition, animal cell does not have chloroplast that enables the plant cell to use the photosynthesis to convert sunlight to the nutrient. However, the centrioles that help to organize the assembly of microtubules during cell division are only found in animal cells.

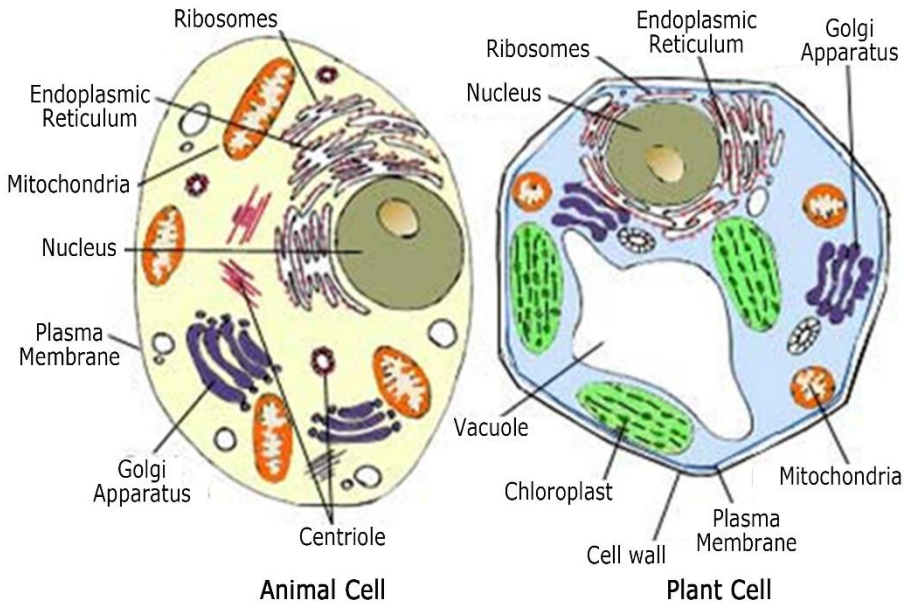

Figure 1-2 The image of animal and plant cell from Revisionworld (www. revisionworld.com).

1-2. Function of cellular organelles

All cells consist of the various components with different functions as depicted in Fig. 1-3. Some of these components, known as the cellular organelles, are the organized structures that carry out the special tasks within cell. In this section, I will describe the cellular functions.

The first organelle is the nucleus which is normally the largest component in a eukaryotic cell. The nucleus is enclosed by a nuclear envelope which separates the nuclear and cytoplasm. It serves as the control tower in cell. Thus, it enables to send the signals to cell to grow, divide, or die. It also contains the chromosome which is composed of deoxyribonucleic acid (DNA) molecules, proteins and ribonucleic acid (RNA). The coiled double-stranded DNA contains genetic information for the production of cellular components and for the reproduction of cell life. In addition, DNA which wraps around special proteins called histones protein family is tightly packed in the nucleus. The nuclear envelope consists of the double lipid bilayer membrane. It has many nuclear pores that some materials move into and out of the nucleus through them. The nucleoplasm is a highly viscous liquid similar to the cytoplasm. Next, the mitochondria is second largest organelle which is complex component that gives the energy to a cell for cellular activities such as movement, division, and protein synthesis [3]. Thus, it is called as the power centers. Mitochondria can make copies of itself since it has its own genetic material that is surrounded by the double membrane like the nucleus. The ribosome can allow cell to assemble or produce the various proteins in accordance with the genetic information from DNA [4]. Thus, the number of ribosomes is related to the level of

protein production. Ribosomes are found in the cytoplasm or the attached to the endoplasmic reticulum. The endoplasmic reticulum (ER) is a transport system, allowing molecules to transfer to one part of cell. There are two types of endoplasmic reticulum such as rough endoplasmic reticulum and smooth endoplasmic reticulum depending on its structure. Rough endoplasmic reticulum looks like sheets of bumpy membrane. It plays a key role in the synthesis and packaging of proteins [5]. On the other hand, the smooth endoplasmic reticulum synthesizes lipids and is responsible for carbohydrate metabolism and detoxification of drugs and other poisons [5]. The function of golgi apparatus is to package proteins into more complex molecules before they are transferred to next destination [6]. It also contains a large number of vesicles, which are used to send molecules to the cellular membrane. It plays a key role in molecular traffic direction inside the cell. The cytosol is the liquid inside cell. It is made up of water, salts and organic molecules like a jelly fluid [7]. The cytoplasm is composed of the cytosol and organelles inside cell. The lysosome contains the many enzymes that break down all kinds of biomolecules. Thus, it is called as the recycling system that digests the invaded foreign something into cell and removes the toxic materials from cell. Last, the cytoskeleton pervades the cytosol, helping to maintain cell shape. It plays a key role in the cellular activities including cell motility, internal movement of cell organelles, and muscle fiber contraction. The cytoskeleton consists of an organized network such as microtubules, actin filaments, and intermediate fibers. Microfilament, known as the actin filament, is the thread-like protein fibers that diameter is ~7 nm [8]. It supports the platform for cell movement, maintenance of cell shape and organelles movement inside cell.

It also provides a track for the myosin molecules movement which exerts the muscle. Microtubule is the cylindrical tubes, ~25 nm in diameter [8]. It is composed of the tubulin protein subunit that can carry out a dynamic instability, known as the coexistence process of assembly and disassembly at the end of a microtubule [9]. It provides a set of tracks for the movement of cellular organelles, vesicles and intracellular substances [10]. It also forms the spindle fibers for separating chromosomes during cell division. Intermediate filaments are about 10 nm diameter and provide basically a structural role by providing tensile strength to the cell [8].

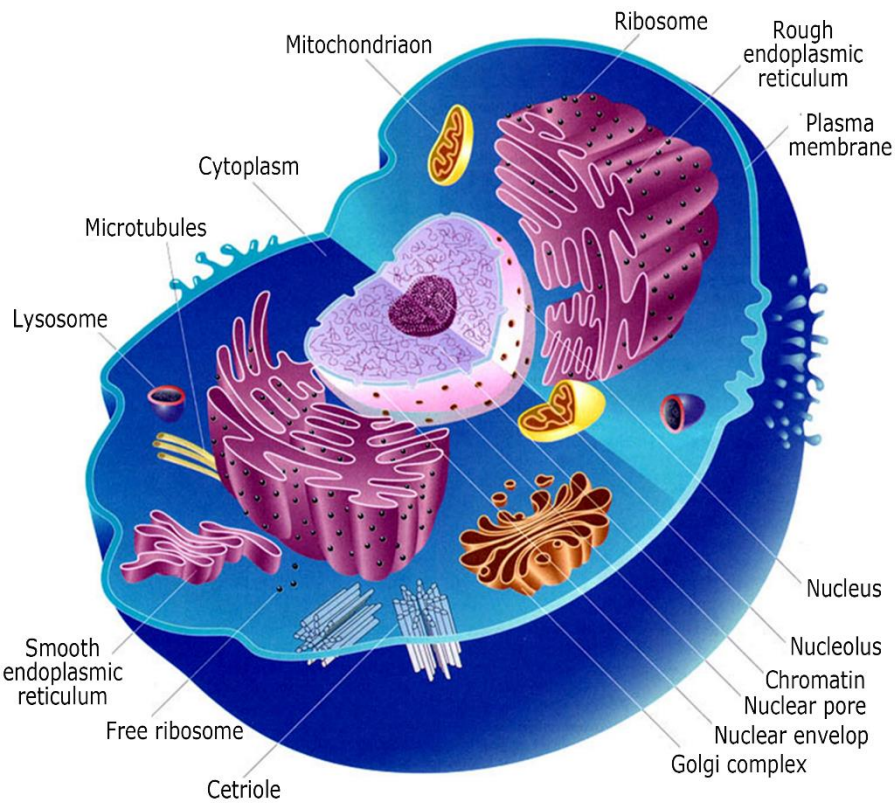

Figure 1- 3 The image of animal cell from Angelfire (www. angelfire.com).

1-3 Techniques for cell studying

Biophysical method to study cellular properties has attracted considerable attention since mechanical properties as well as chemical properties of cell play crucial roles. Thus, many approaches have tried to handle the components of cell. In here, four most techniques such as optical tweezers, atomic force microscopy, micromapulator and magnetic tweezers will be described.

1.3.1 Optical tweezers

Optical tweezers, reported in 1970 by Arthur Ashikin, are versatile instruments that used the force from high laser radiation pressure to trap and manipulate the position of the microscopic objects. The high radiation pressure from a densely focused laser beam can provide an attractive or repulsive force, depending on the refractive index mismatch. This technique has been used for long time to manipulate and measure the properties of small dielectric particles. The force is in the pN-range and can control the displacements in the nm range of objects ranging in size from 10 nm to over 100 mm. When applying a laser beam to the very small particles, the light will be reflected or refracted from the surface of small particle. The momentum of photon, refracted to the particle, will be changed and by the law of the conservation of the momentum, the force according to the variation of momentum will be exerted to the small particle. For example, the both light of **a** and **b** hit a sphere particle of high index of refraction than surrounding solution as shown in Fig. 1-4, they will be reflected and refracted at sphere surface. Thus, some momentum will be applied to the sphere due to variation of momentum conservation driven by change of light direction. The sphere will experience forces F^{i}_{R} and F^{o}_{R} due to refection at surface.

Both Forces F^{i}_{D} and F^{o}_{D} will be generated due to refraction and add to give a net force since force F^{i}_{R} and F^{o}_{R} are very small compared to force F^{i}_{D} and F^{o}_{D}.

In 1970, Ashkin group showed that one could use the forces or radiation pressure from focused laser beams to significantly affect the dynamics of small transparent micro and nanometer sized neutral particles [11]. In 1986, Ashkin group also achieved the trapping of small dielectric particles with optical tweezers, giving rise to the first steps in the field of optical nanomanipulation [12]. Recently, the optical tweezers have been applied to the study of biological system since it is able to measure the precise force and monitor the particles simultaneously. In 1987, Ashkin group showed that a single beam optical tweezers trapped bacterial cells and moved them [13]. In 1989, Walter group showed that chromosome movement on the mitotic spindle using optical tweezers [14]. Furthermore, optical tweezers are used to isolate the single chromosome [15]. Recently, many researchers have been interested in nano-scale material such as DNA, RNA, and proteins. In 1998, Allemand group investigated the biophysical properties and dynamic structures of both single stranded and double stranded DNA [16]. Wuite group revealed the mechanical force of DNA polymerase using single stranded and double stranded DNA [17].The idea of optical trapping was combined to the use of a number of tools including laser scalpel, which is capable of cutting things as small as a fragment of DNA. Despite the benefits of non-invasive and exquisite control for positioning cellular organelles, the optical trap still suffers from technical challenges, such as non-specific control, limited throughput, and photo-damage that limit the operation time [18-20]. Recent

advanced development showed that the photodamage can be reduced by using specially shaped optical tweezers [21].

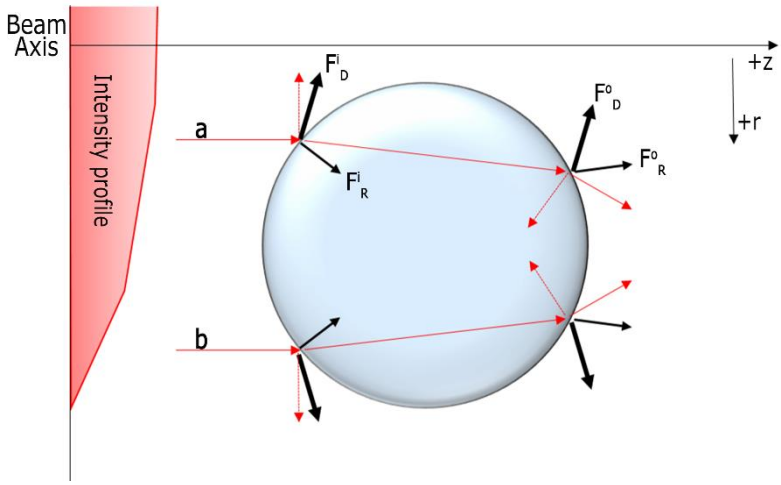

Figure 1-4 Principle of optical force

1.3.2 Micromanipulator

A micromanipulator is used to mechanically interact with a sample under an inverted microscope attached with electric motor-driven robot arms which can control precisely position as show in Fig. 1-5. It can capture cell and inject some materials into cell using control pressure. It is a powerful and versatile method for trapping single cells.

Ahring team showed that single cell captured by a micromanipulator can culture in appropriate growth medium [22]. The trapping of living cell is most important application area of micromanipulaor. Recently, other applications have been attracted much attention in basic biological research such as electrophysiological recording, in vitro fertilization, and measurement of physical cellular properties. Sigworth group in 2002 demonstrated the extracellular patch clamp technique that can detect the ionic current flow in whole cell membrane by aspirating cell into a glass pipette to form a tight electrical seal [23]. This novel technique has been contributed to the development in studying of physiological mechanism. A typical other application of micromanipulator is intracytoplasmic sperm injection [24]. Under the manual control of micromanipulation, a spermatozoon is injected into an oocyte with 100 μm diameter for in vitro fertilization. In 1979, Ellis group studied the mechanical properties of the chromosomal spindle fibers using the micromaipulator [25]. The micromanipulator was also used to study the isolated individual nuclei [26].

Figure 1-5 The image of micromanipulators from eppendorf company (www.eppendorf.de).

1.3.3 Atomic force microscopy (AFM)

Atomic force microscopy (AFM) invented by Quate and Gerber is a very high-resolution type of scanning probe microscopy[27]. A typical AFM consists of a micro-cantilever probe, a piezoelectric (PZT) actuator for mounting a sharp tip, and a photo detector for receiving a signal derived from cantilever deflection [28]. When the tip scans the surface of the sample by moving up and down with the contour of the surface, the laser beam deflected from the cantilever provides measurements of the difference in light intensities between the upper and lower photo detectors as shown in Fig. 1-6.

The AFM applications in cell biology can be divided into several categories such as imaging, micromanipulation, and measurement of physical material properties. In the beginning, AFM was almost used to characterize the material surface. Recently, the application of AFM to biological field has exponentially increased since its unique advantages over conventional other microscopes [29, 30]. AFM is suitable for obtaining image of sample. Thus, AFM has been used to investigate the changes on the cell morphology depending on change of environmental surrounding [31-33]. In addition, researchers have used AFM to investigate the interactions between DNA and RNA [34]. Gaub group measured directly the folding force of RNA at pico Newton [35]. AFM was also used to measure force to the spindle in pre-anaphase of cell division by penetrating microneedles through membrane into nucleus [36]. AFM enable to control the position of nanoneedle and measure the applied force simultaneously. Moreover, AFM was applied to measure the mechanical properties of chromosomes in cell [37] .

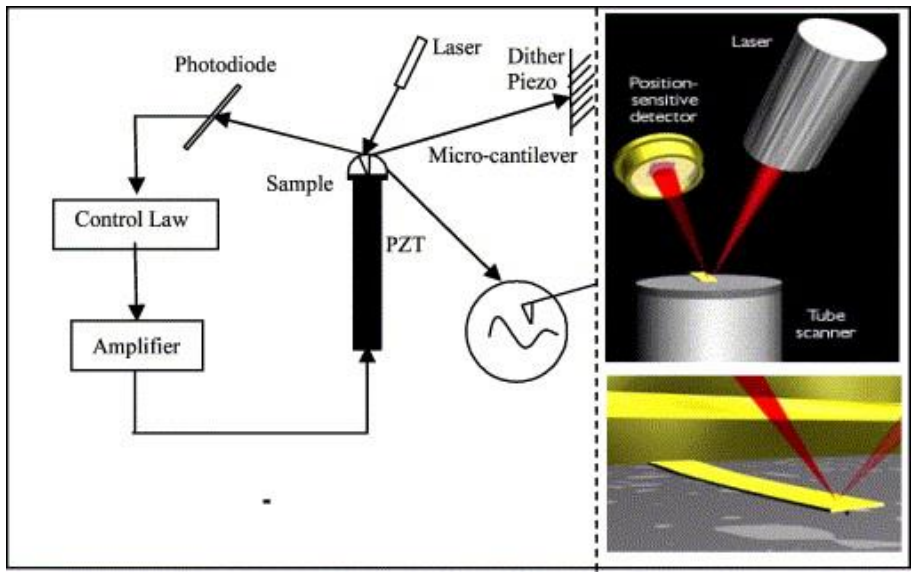

Figure 1-6 Schematic diagram of AFM operation [29].

1.3.4 Magnetic tweezers

A magnetic tweezers are a tool to exert and measure forces on magnetic particles using a gradient of magnetic field as shown in Fig. 1-7. Induced forces range from few piconewton to several nanonewton. Magnetic tweezers are popular and widespread biophysical techniques for single-molecule micromanipulation, rheology of soft matter, and measurement of force-regulated processes in living cells due to the simplicity of operation, low cost of construction, and versatility [38]. In the beginning, biophysicists applied the magnetic tweezers to study the viscoelastic properties of the cytoplasm [39]. Most applications of magnetic tweezers are used to study the physical properties of single molecules [40, 41] and filamentous macromolecular networks [42, 43]. Bustaminte group showed that single DNA molecules were stretched by magnetic bead [40]. On the other hand, Leibler group measured the local viscoelastic response in filamentous actin networks by using magnetic tweezers [43]. Most researches related to the measurement of intracellular properties have been investigated by control of the magnetic particles attached to specific components inside cell with external magnetic field. Recently, fluorescent magnetic nanoparticles in living cells were recently shown to be attracted by an external magnetic field [44]. In addition, Gueroui group showed that magnetic nanoparticles conjugated with biomolecule can artificially and spatiotemporally manipulate the Ran/RCC1 signaling pathway that regulates the cell cytoskeleton [45]. With these results, magnetic particle has been focused on a candidate for manipulating intracellular organelles. For example, chromatin elasticity has been monitored using a micro magnetic bead directly injected into the nucleus [46]. The

magnetic bead, in this case, was simply used to push the chromatin.

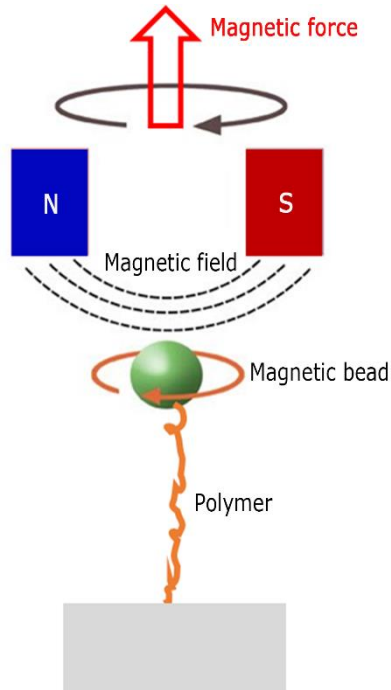

Figure 1-7 Schematic diagram of a basic magnetic tweezers setup.

CHAPTER 2. NON-INVASIVE CONTROL OF EMBRYONIC DEVELOPMENT

The regulation of cell signaling pathway is important for understanding biological systems. Thus, various techniques to modulate cell signaling by spatial control of cellular components have been developed such as optical and magnetic method [47, 48]. Despite the benefits of non-invasive and exquisite control for positioning cellular organelles, the optical trap still suffers from intrinsic technical challenges, such as non-specific control, limited throughput, and photo-damage [19, 20].

Magnetic nanoparticles are emerging as promising candidates in a broad range from cell biology to biomedical application due to their unique characteristics such as remote control and their ability to interact with various cellular and molecular level of interest through their surface decoration [49, 50]. In addition, magnetic fields show negligible effects on cell [51]. With the advent of advanced nanoscience and nanotechnology in the reliable production and specific tailoring of functional magnetic particles, successful applications were dedicated to a broad range of biomedical applications such as high throughput separation of biomolecules, magnetic resonance image, hyperthermia for cancer therapy, and drug delivery [52-55].

Recently, fluorescent magnetic nanoparticles inside a living cell were shown to be directly attracted by an external magnetic field [56]. In addition, the signaling transduction pathway was remotely triggered by the functionalized magnetic nanoparticles [57] and the microtubule nucleation and assembly inside Xenopus oocyte was spatiotemporally controlled by magnetic nanoparticles conjugated with

key regulatory proteins [45]. Moreover, it is shown that the remote induction of cell death by targeting intracellular lysosome was triggered by functionalized magnetic nanoparticles [58].

In this study, we demonstrate a novel strategy to non-invasively regulate chromosome activity by targeting genetic regulation materials (i.e., oocyte-specific linker histone H1 protein) in live oocyte with the functionalized magnetic nanoparticles. In order to evaluate biological effectiveness of magnetic nanoparticle-mediated, cellular activity modulation with the confirmation of the safety of functionalized magnetic nanoparticles, we used a mouse model employing mature oocyte -parthenogenesis-development.

2.1 Experimental concept

It has been known that the progress of the cell development after somatic cell nuclear transfer (SCNT) occurs at an extremely low efficiency presumably because of the damage or decrease of meiosis-specific factors associated with the spindle removal [59]. The first successful SCNT and derivation of human embryonic stem cells showed how this difficulty in the invasive process could be overcome by using a specific chemical treatment such as caffeine [60]. Recently it was demonstrated that one can create blastocysts with human oocytes by simply merging with somatic nucleus without enucleation [59]. The resulting blastocyst, however, keeps the haploid chromosomes (n), resulting in the mixture (3n) with paternal chromosomes (2n). In here, we attempted the non-invasive deactivation of embryonic development by targeting the genetic materials on metaphase plates by the functionalized magnetic nanoparticles. Furthermore, if the activity of the maternal chromosomes

can be silenced by the magnetic labeling as depicted in Fig. 2-1, this approach will lead to new opportunities in nuclear reprogramming. Bacterial magnetic nanoparticles (BMPs) were conjugated with histone H1 antibodies (H1-BMPs), specifically targeting the oocyte-specific histone H1 protein that clamps the linker DNA wrapped around the octameric histone core, forming nucleosome. In order to visualize and track the location of the H1-BMPs inside oocyte, the fluorescein isothiocyanate (FITC) was pre-labeled with the antibodies. Mature oocytes were obtained via superovulated C57BL/6 mice.

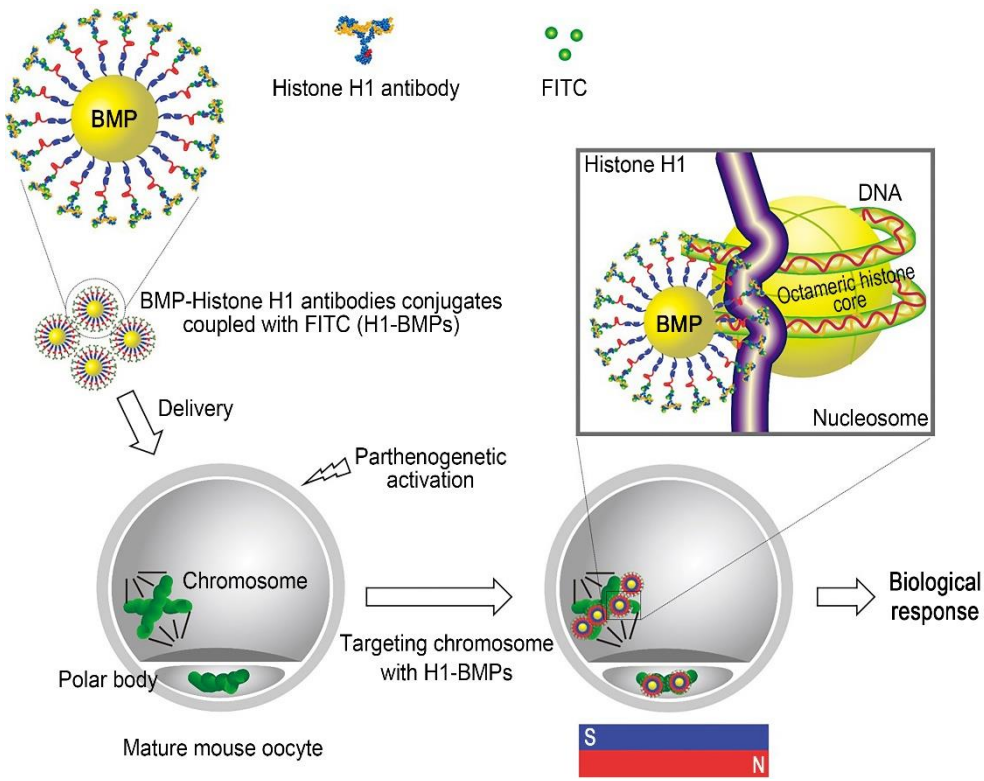

Figure 2-1 Schematic illustration of deactivation of chromosome by targeting histone H1 protein with H1-BMPs. Antibodies to histone H1 were immobilized on the BMPs for specific chromosomal targeting.

2.2 Chromosome

2.2.1 Structures and functions

Chromosome is an essential unit for cell life. It is an adequately organized chromatin which is composed of DNA tightly wrapped around histone proteins that support its structure as depicted in Fig. 2-2. Chromosome varies depending on the kind of organism. Eukaryotic cell has a large number of chromosomes. On the other hand, a number of chromosomes in prokaryotic cell are small. Chromosomes are transferred to offspring in order to ensure the genetic diversity. Thus, chromosome plays a key role that monitors whether DNA is accurately copied in the process of cell reproduction.

The DNA has the genetic information with encoding the instructions for production of proteins. The DNA double helix, found by James Watson and Francis Crick [61], is coiled many times around the histone core of eight proteins. Basically, while the DNA has the negative charge, the octametric histone core proteins have the positive charge [62, 63]. These different charges enable the DNA to easily a wrap the histone core proteins, forming the nucleosome discovered by Don and Ada Olins [64]. These nucleosomes are clamped by histone H1 that is important for maintenance of higher-order chromatin structure and the regulation of gene expression [65]. Depending on cell types, the structure of DNA can be different. For example, while chromosome in eukaryotic cell is linear shape, prokaryotic cell has chromosomes with circular shape. In eukaryotic cell, chromosomes are packaged by proteins such as Histone proteins, termed chromatin. It enables long DNA molecules to fit into the cell nucleus. In prokaryotic cell, the DNA is usually formed as circle

that is tightly coiled in on it.

In cell development, the replicated chromosomes are attached to a mitotic microtublue that aligns them and then separates the sister chromatids to produce the genetic material. This separation of the genetic material in a mitotic nuclear division is followed by a separation of the cell cytoplasm in a cellular division to produce two daughter cells.

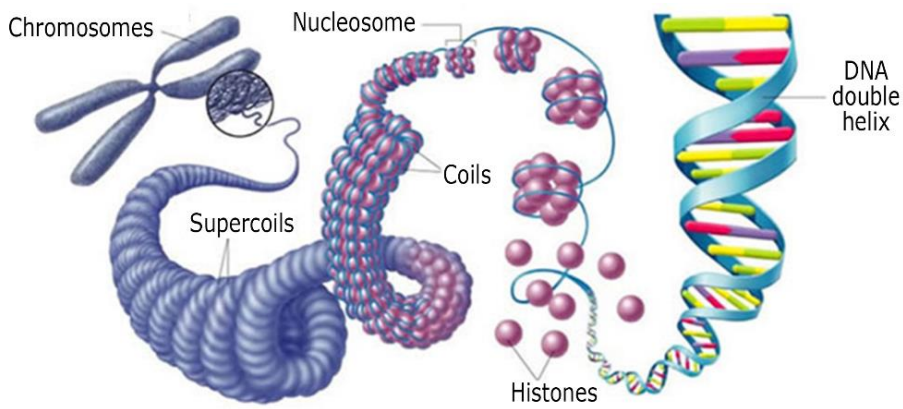

Figure 2-2 Basic chromosome structure. The image was obtained from Pearson Prentice Hall.

2.2.2 Cell cycle

The cell cycle is a serial set of processes that a cell grows, leading to the cell division that divides to form daughter cells. Thus, the cell cycle is a fundamental and essential process in all cells. It is monitored and regulated by many biomolecule events (known as checkpoint) during cell cycle process. If the cell cycle process is altered, cells get the physiological damage that can lead to cell death [66]. The sequential event of cell cycle is composed of several phase such as G1-S-G2-M phases as shown in Fig. 2-3. At G1 phase, a cell grows and prepares the chromosome replication. At a certain checkpoint, the cell is committed to division and moves into the S phase. The S phase stands for “Synthesis”. Thus, DNA start to be synthesized. Each chromosome consists of two sister chromatids. Next, the M phase means “mitotic phase”. M phase is a relatively short period during cell cycle events and can be briefly divided into 4 phases such as prophase, metaphase, anaphase, and telophase. Prometaphase can be sometime split as part of between prophase and metaphase. The detailed information of M phase will be described later.

Depending on type of cell, M phase can also divide two ways such as mitosis and meiosis as shown in Fig. 2-4. Both mitosis and meiosis are similar processes that they obtain new daughter cells through the cell cycle process. However, they are some differences. Mitosis is a process of cell duplication that produces two genetically identical daughter cells. Thus, mitosis process that is useful for the growth and repair of cells can occur in all cell types such as skin cell, bone cell, blood cell, and so on. Meiosis is a type of cellular reduction that the number of chromosomes is reduced by two fissions of the nucleus, resulting in two haploid cells

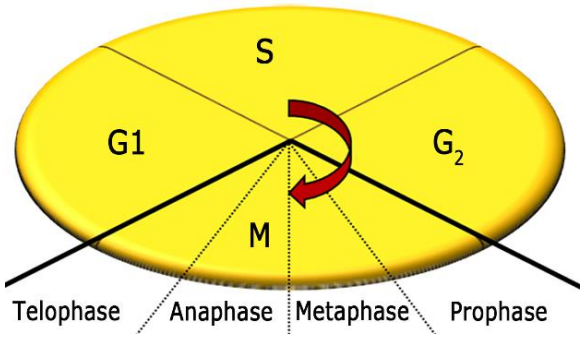

Figure 2-3 Cell cycle phases.

Thus, mitosis process that is useful for the growth and repair of cells can occur in all cell types such as skin cell, bone cell, blood cell, and so on. Meiosis, on the other hand, is a type of cellular reduction that the number of chromosomes is reduced by two fissions of the nucleus, resulting in two haploid cells. In meiosis, chromosomal crossover process occurs in prophase I. It is the exchange of genetic material between homologous chromosomes for genetic diversity in cell production. Genetic diversity makes a population more resilient and adaptable to the environment, which increases chances of survival and evolution for the long term.

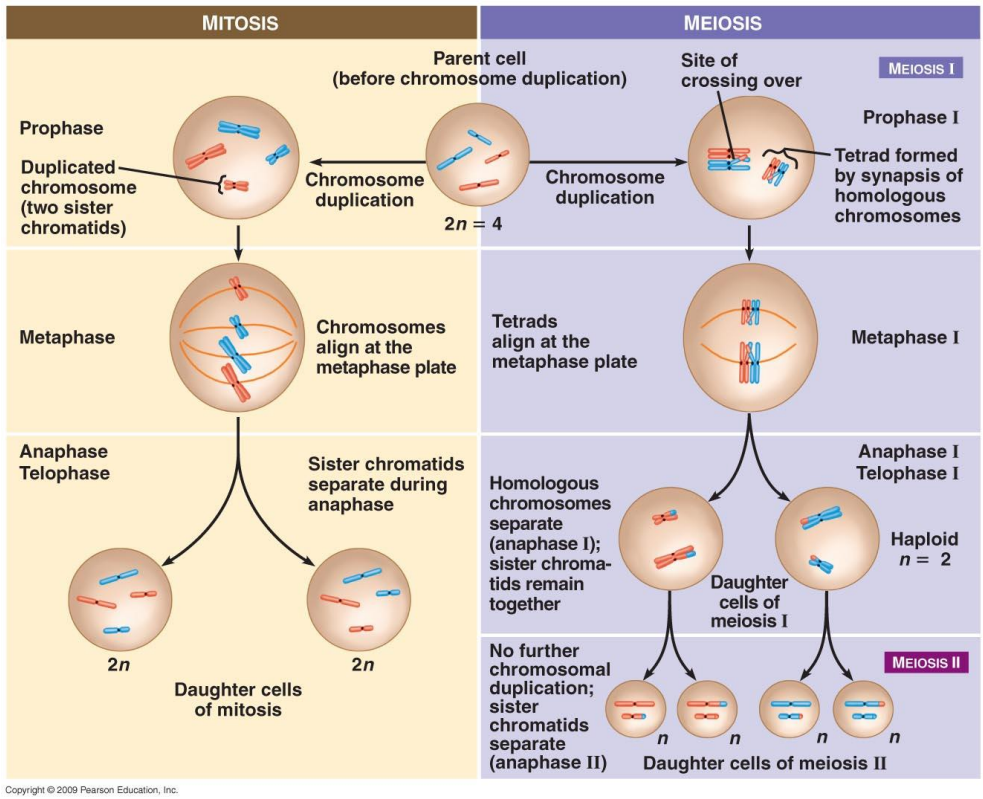

Figure 2-4 Mitosis and meiosis process from Pearson Education. Inc. (www. pearsoned.com).

2.2.2.1 Mitosis

Depending on the type of cell, mitosis process is different. In prokaryotic cell without a nucleus, the cell cycle is performed by a process of binary fission. In this process, two daughter cells are effectively produced by a single parent cell. Binary fission is classic example of asexual reproduction.

In the other hand, in eukaryotic cell, mitosis is the cell cycle process that produces two identical daughter cells through several serial events. All processes are monitored and regulated by checkpoints of cell cycle [67]. Thus, it can stop the cell cycle process when it is necessary for the verification of phase processes and repair of the damaged DNA. After completion of the checkpoint requirements, the cell cycle can move to next step. If the checkpoint requirements are incomplete, cell can be died by the apoptosis that is the process of programmed cell death. It also enables cell to mutate in cancer cell.

The M phase processes can be subdivided into several phases, known as prophase, prometaphase, metaphase, anaphase, telophase, and cytokinesis as shown in Fig. 2-5. Prophase is the first mitotic stage that chromatin begins to condense into to condense into highly ordered structure, called a chromosome. Thus, chromosomes can be visible with high magnification of the inverted microscopy. Two centrosomes which is the coordinating center for the mitotic spindle, move to opposite ends of the cell and begin to polymerize tubulin to help produce a mitotic spindle apparatus. At the prometaphase, the nuclear envelope breaks down, allowing the some mitotic spindle fiber (kinetochore microtrubules) in centrosome to invade the nuclear space and target the centromere in chromosome [62]. Prometaphase is sometimes

considered part of prophase. In metaphase, all chromosomes connected to mitotic spindle are applied by tension. Thus, the chromosomes align at the middle of cell, referred to as the metaphase plate and then two centromere start pulling the chromosome to the two ends of the cell by using mitotic spindle [63]. Metaphase leads to anaphase. When the anaphase begins, the paired chromosomes separate at the kinetochores and move to opposite sides of the cell by shortening the kinetochore microtrubules and migrate to each centrosomes. While the daughter chromosome is pulled by the kinetochore microtubules and moves toward the centrosome at the cortex of cell, the non-kinetochore microbules push against each other, allowing cell shape to change into the oval. After the cell completes the separating sister chromatins, the cell moves into the telophase. Telophase is the final stage of mitosis. Daughter chromosomes arrive at opposite poles of cell and new nuclear envelopes start to form around the daughter nuclei. As the nuclear envelopes start to rebuild, the chromosomes start to loose. Cytokinesis is the final process of the cell cycle that the cytoplasm actually divides into two daughter cells. After the cytokinesis process, cell division is completely finished. The contractile ring the consists of an overlapping array of actin filaments and myosin filaments, rebuild around the equator of the cell [8]. The strong force generated by the interaction of actin and myosin filament is capable of shrinking cell at the equator, pinching the cell membrane, and forming the cleavage furrow.

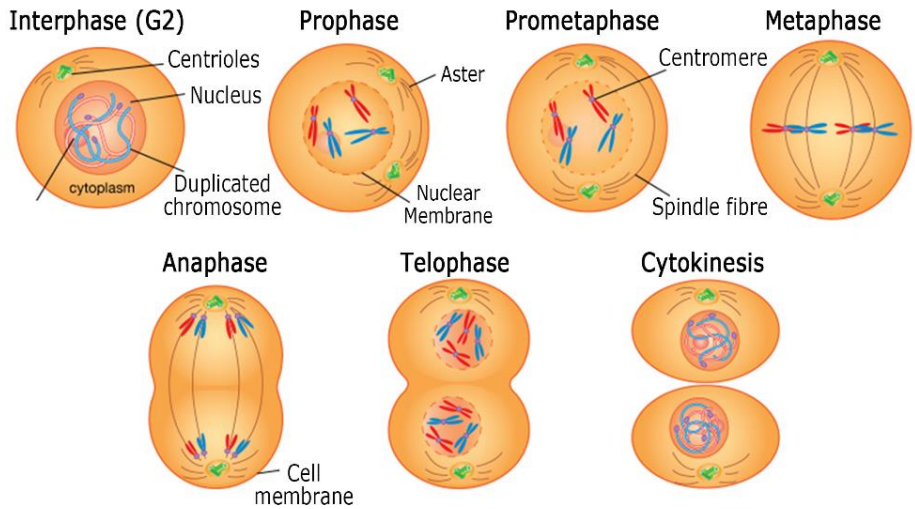

Figure 2-5 Mitosis process from Encyclopadia Britannica, Inc. (www. Britannica.com).

2.2.2.2 Meiosis

Meiosis is a specialized type of cell division that reduces the number of chromosomes and creates four gamete cells. It is necessary for sexual reproduction to produce egg and sperm cells. Comparing to the mitosis process, the meiosis is split into meiosis I and meiosis II, and both meiotic divisions have multiple phases as depicted in Fig. 2-6. While the meiosis I is a unique cell division of germ cells, meiosis II is similar to the mitosis process. The meiosis I is composed of several phases such as, prophase I, metaphase I, telophase I, anaphase I, and cytokinesis. In the meiosis I, there is a unique process that the pairs of homologous chromosome create the tetrads. Within the tetrad, any pair of chromatid arms can overlap and fuse in a process called the chromosomal crossing-over that recombines DNA to produce new combinations of genes through exchange of genetic material. Meiosis II is a mitotic division of each of the haploid cells produced in meiosis I. Through several phases such as prophase II, metaphase II, anaphase II, telophase II and cytokinesis, four haploid daughter cells that go on to develop into either sperm or egg cells are produced.

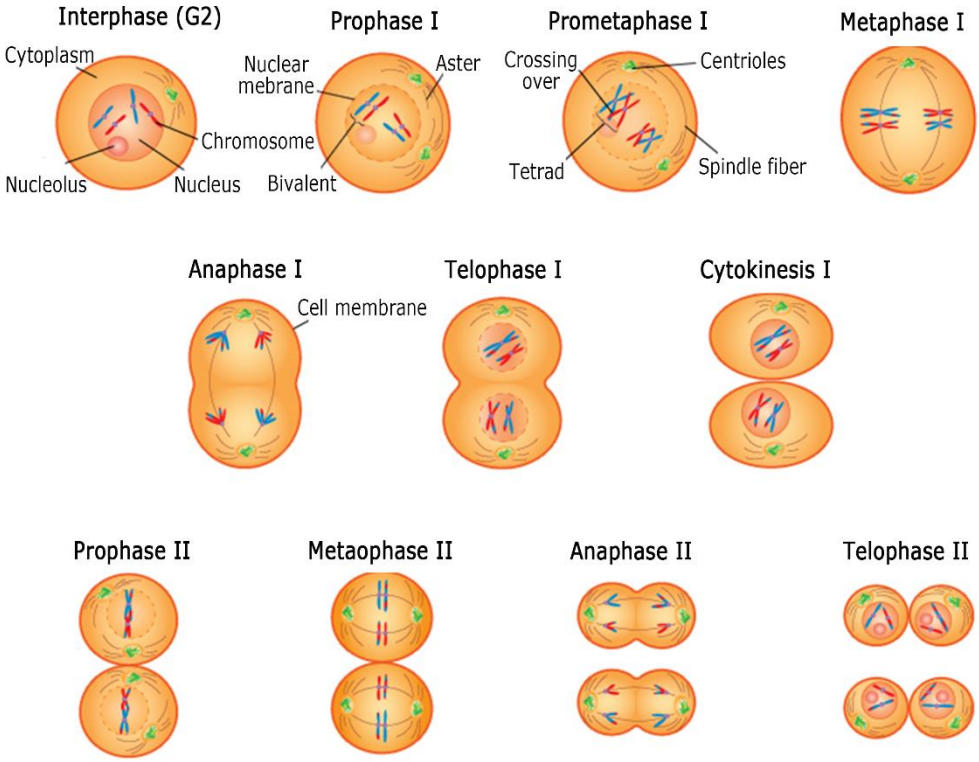

Figure 2-6 Meiosis process from Encyclopadia Britannica, Inc. (www.britannica.com).

2.2.2.3 Chromosomal crossover

The process of chromosomal crossover, or recombination is an exchange of genetic material between homologous sister chromatins at the prophase stage of Meiosis I. The chromosomal crossover occurs when two chromosomes, normally homologous chromosome, break and then reconnect but to the different end piece. This process provides the genetic variation. Chromosomal cross over is activated by a special endonuclease that simultaneously breaks both strands of the double DNA helix , forming a fragment in the DNA molecule [2]. Figure 2-7 shows the mechanism of general chromosomal crossover. First, double stand in paternal chromatin is broken by endonuclease. The 5′ ends of the broken paternal chromatin are then cut away. And an overhaning 3' end of the broken paternal chromatin invades and searches for a similar or identical DNA molecule that is not broken, leading to the formation of a joint molecule between a maternal and a paternal chromosome. The chromosomes cross over at points called chiasma. At each chiasma, the chromosomes break and rejoin, trading some of their genes.

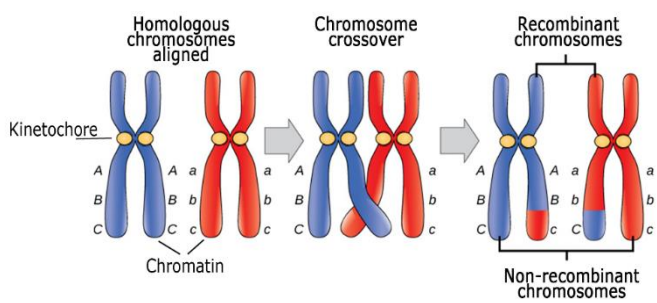

Figure 2-7 Chromosomal crossing over and recombination from Boundless (www.boundless.com).

2.3 Parthenogenesis

Parthenogenesis is a type of asexual reproduction that is development of an egg without fertilization. It is the term used to describe the process by which certain animals are able to reproduce themselves in successive female generations without intervention of a male of the species. Figure 2-8 shows the in vitro fertilization (IVF) and parthenogenetic development. It is particularly found amongst arthropods and rotifers. The activation of embryonic development generally occurs after an egg is fertilized by a sperm. In parthenogenesis, however, the diverse the stimuli for the egg is necessary to active such as electrical and chemical method [51, 52, 68]. Parthenogenesis process is widely used to produce the piglet after nuclear transfer [57, 69, 70] and intracytoplasmic sperm injection (ICSI) [71, 72]. However, the efficiency is still lower. Actually, the mechanism of parthenogenetic activation are not known but apparently include certain changes in the egg membrane.

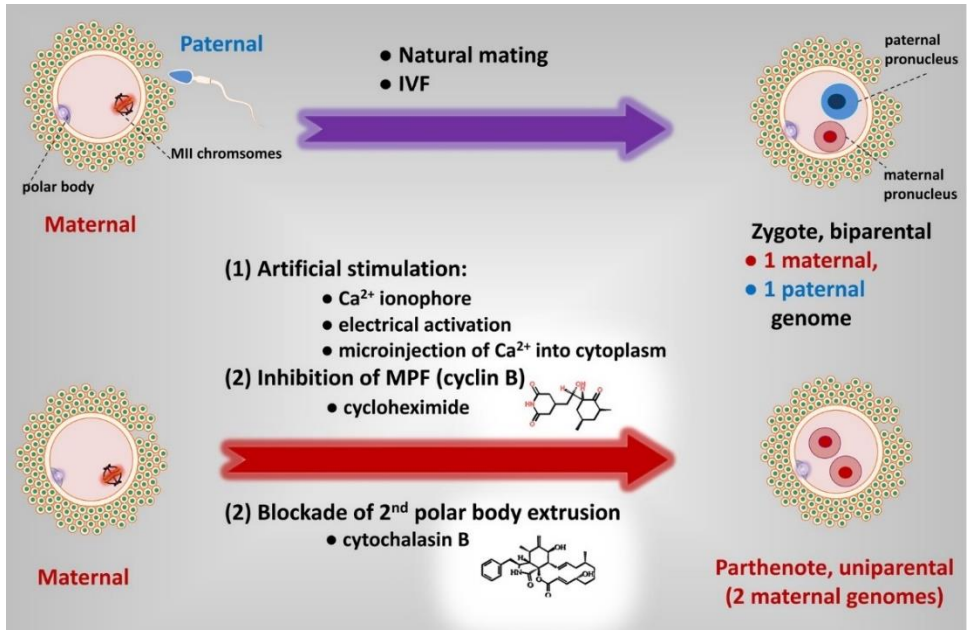

Figure 2-8 In vitro fertilization (IVF) Vs Parthenogenetic development from Creative commons (www.creativecommons.org)

2.4 Magnetic particles (MPs)

Magnetic particles have attracted great attention for researchers from a wide range of disciplines, such as magnetic fluidics, biotechnology, magnetic resonance imaging and data storage [47, 48, 50, 58, 73]. Magnetic particles, ranging from the nanometer to micrometer scale, are commonly composed of magnetic elements such as iron, nickel and cobalt. Magnetic particles have several advantages. For examples, it is possible to synthesize a various size of magnet particles with well-defined structures and magnet particles can be manipulated by a remote magnetic field. In addition, magnetic particles have a high surface to volume ratio that can provide the more loading sites for applications. Furthermore, magnetic fields show negligible attenuation in cell [51].

Magnetism, phenomenon is related to the motion of electric charges as well as elementary particles, such as the electron that have a property called spin. All matter consists of atoms that are composed of protons, neutrons and electrons. While both protons and neutrons are located in the nucleus, the electrons continue to move around the nucleus. An electromagnetic field is generated whenever an electrical charge moves. The strength of magnetic field can be defined as the magnetic moment. When an external magnetic field is applied to a material, electrons in material are influenced by one. It is well known that this effect is Faraday's Law of magnetic induction. When electron motion occurs in pairs, there is no net magnetic field since their opposite spins cause their magnetic fields to cancel each other. Most magnetic behavior of nanomaterials (magnetism) can be classified into several groups such as

diamagnetism, paramagnetism, ferromagnetism, antiferromagnetism and ferrimagnetism.

2.4.1 Diamagnetism

A diamagnetic material is a kind of characteristic of magnetism that has no permanent magnetic dipole moment. However, when an external magnetic field is applied to diamagnetic materials, they can generate a negative magnetization. In other words, when an external magnetic field is applied, a weak magnetic dipole moment is induced in the direction opposite the applied field since the magnetic susceptibility is negative as shown in Fig. 2-9. The copper, silver, and gold are representative diamagnetic materials.

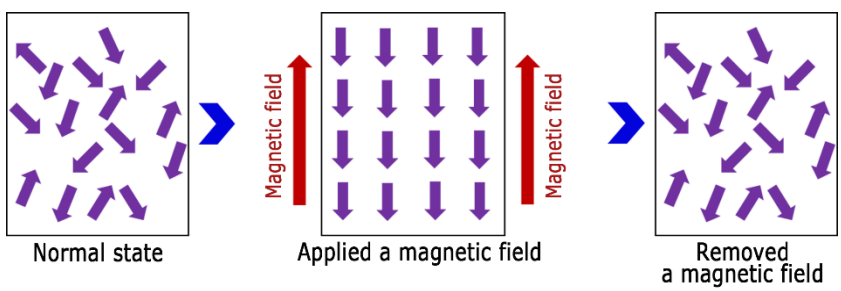

Figure 2-9 Schematic diagram of diamagnetism. The arrows indicate the direction and magnitude of the atomic magnetic moments.

2.4.2 Paramagnetism

Paramagnetism is a kind of magnetism that produces positive magnetization when applied the magnetic field. Paramagnetic materials have a relative magnetic permeability of 1 or more (a positive magnetic susceptibility). Although atoms or ions in paramagnetic materials are attracted to magnetic field when a magnetic field is applied, these materials do not retain any magnetization in the absence of an externally applied magnetic field. Magnetic moments are randomly reorient when magnetic field is removed as shown in Fig. 2-10. The arrows indicate the direction and magnitude of the atomic magnetic moments. Paramagnetic materials include magnesium, molybdenum, lithium, and tantalum.

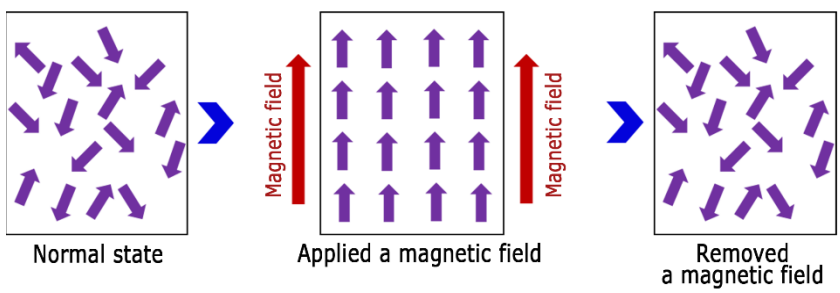

Figure 2-10 Paramagnetism. The arrows indicate the direction and magnitude of the atomic magnetic moments.

2.4.3 Ferromagnetism

Unlike paramagnetic materials, the atomic moments in ferromagnetic materials exhibit very strong interactions. It has a large and positive magnetic susceptibility to an external magnetic field. When a field is applied and then removed, the magnetization does not return to its initial state due to hysteresis as shown in Fig. 2-11. However, when a certain temperature, known as Curie point, is applied, ferromagnetic materials can lose their characteristic properties and cease to be magnetic. Two materials such as lodestone (or magnetite, an oxide of iron, Fe_3O_4) and iron, have the ability to acquire such attractive powers, and they are often called natural ferromagnets.

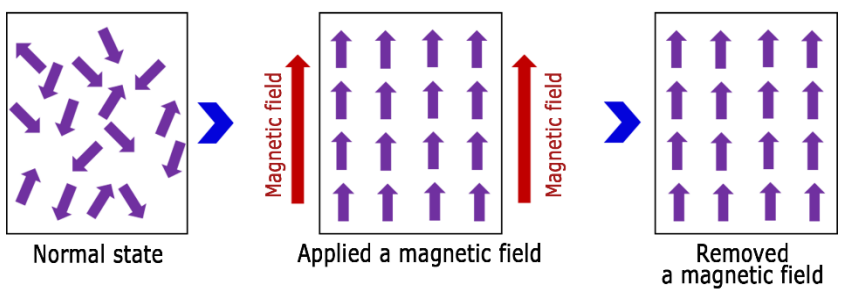

Figure 2-11 Ferromagnetism. The arrows indicate the direction and magnitude of the atomic magnetic moments.

2.4. 4 Antiferromagnetism

Antiferromagnetism is usually related to the spins of electrons that align in a regular pattern with neighboring spins pointing in opposite directions. In other words, the magnetism from magnetic atoms or ions oriented in one direction is canceled out by the set of magnetic atoms or ions that are aligned in the reverse direction as shown in Fig. 2-12. If the two sublattice moments are equal but direction is opposite, the net magnetic moment is zero when an external magnetic field is applied. The characteristic of antiferromagnetism can entirely disappears above a certain temperature, celled the Neel temperature. Above Neel temperature, antiferromagnetic materials behave like the paramagnetism.

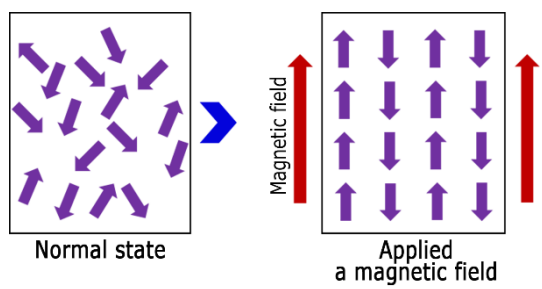

Figure 2-12 Antiferromagnetism. The arrows indicate the direction and magnitude of the atomic magnetic moments.

2.4. 5 Ferrimagnetism

Ferrimagnetisme is a type of magnetism that the magnetic fields associated with individual atoms spontaneously align themselves. In ferrimagnets, the magnetic moments of the A and B sublattices are not equal and result in a net magnetic moment as shown in Fig. 2-13. Magnetite is a well-known ferrimagnetic material. Some ferrimagnetic materials are YIG (yttrium iron garnet), cubic ferrites composed of iron oxides and other elements such as aluminum, cobalt, nickel, manganese and zinc.

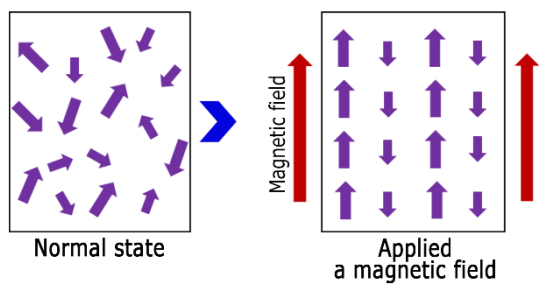

Figure 2-13 Ferrimagnetism. The arrows indicate the direction and magnitude of the atomic magnetic moments.

2.5 Methods and Materials

2.5.1 Preparation of mature oocyte

Animal care and handling were conducted in accordance with the policy and regulation for the care and use of laboratory animals at Seoul National University (SNU-070903-1and SNU-101214-1). Naturally ovulated oocytes were collected by oviduct flushing of five-week-old ICR female mice. For ovarian hyperstimulation, 7.5 IU of PMSG (Folligon, Intervet International, Boxmeer, Netherlands) was injected intraperitoneally and ovulation was induced by intraperitoneal injection of 7.5 IU of hCG (Pregnyl, Organon, Oss, the Netherlands) 48 hrs later. Oocytes were recovered 16 hrs post-hCG injection. After hormonal treatments, only mature oocytes were collected by oviduct flushing. Oocyte maturation at the metaphase II stage was verified by extrusion of the first polar body in the perivitelline space as shown in Fig. 2-14. For this analysis, oocytes were released from cumulus cells through incubation in M2 medium supplemented with 500 μl hyaluronidase (200 IU/ml, Sigma Aldrich, USA) for 5 min at 37°C. To activate oocytes parthenogenetically, oocytes released from cumulus cells were cultured in calcium-free potassium simplex optimized medium (KSOM) supplemented with 10 mM SrCl2 and 5 μg/ml cytochalasin B for 4 hrs. Oocytes that had been parthenogenetically activated in vitro were then cultured in 5 μl droplets of modified Chatot, Ziomek, and Bacister (CZB) medium consisting of 81.6 mM NaCl, 4.8 mM KCl, 1.2 mM KH_2PO_4, 1.2 mM $MgSO_4 \cdot 7H_2O$, 1.7 mM $CaCl_2 \cdot 2H_2O$, 25.1 mM $NaHCO_3$, 31.3 mM sodium lactate, 0.3 mM sodium pyruvate, 1 mM glutamine, 0.1 mM EDTA and 5 mg/ml BSA, to which 0.001 mg/ml Hb (methemoglobin) and 5.5

μM β-mercaptoethanol (Gibco Invitrogen, USA) for 120 hrs at 37 °C under an atmosphere of 5% CO_2 in air. Pronucleus formation, cleavage, and development to the 4-cell, morula, and blastocyst stages were monitored under an IX-70 inverted microscope (Olympus, Tokyo, Japan) at 6, 24, 48, 72 and 120 hrs after activation.

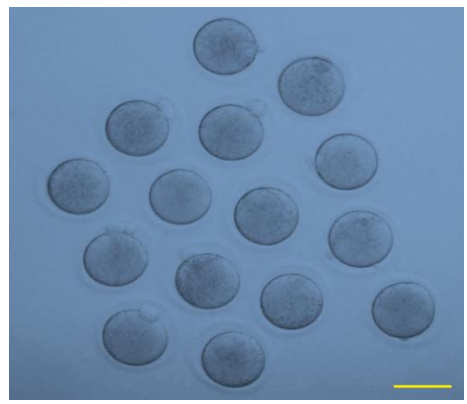

Figure 2-14 The collected mature oocytes. The scale bar is 10 μm.

2.5.2 Bacterial magnetic nanoparticles (BMPs)

2.5.2.1 Extraction of BMPs

Bacterial magnetic particles (BMPs) were obtained from Magnetospirillum sp. AMB-1 which was cultured in magnetic spirillum growth medium (MSGM) for 4–5 days at 27°C under anaerobic conditions (Biofree incubator, Korea). Cultured AMB-1 was centrifuged for 25 min at 11300×g and then lysed by sonication (VCX500, Sonics & Materials, USA) for 30 min. The BMPs were collected using a neodymium iron boron (NdFeB) magnet, washed 5 times with phosphate-buffered saline (PBS), and finally dispersed in PBS. Collected BMPs were sterilized by autoclaving (121°C, 15 min). The concentration of BMPs was measured by the inductively coupled plasma mass spectrometry (ICP, Shimadzu, Japan). The particle size of the BMPs was measured with Image J software using the obtained TEM images. The BMPs are highly uniform in shape and size ranging from 30 to 70 nm in diameter as shown in Fig. 2-15. The mean diameter of BMPs was about 49.6 ± 2.3 nm.

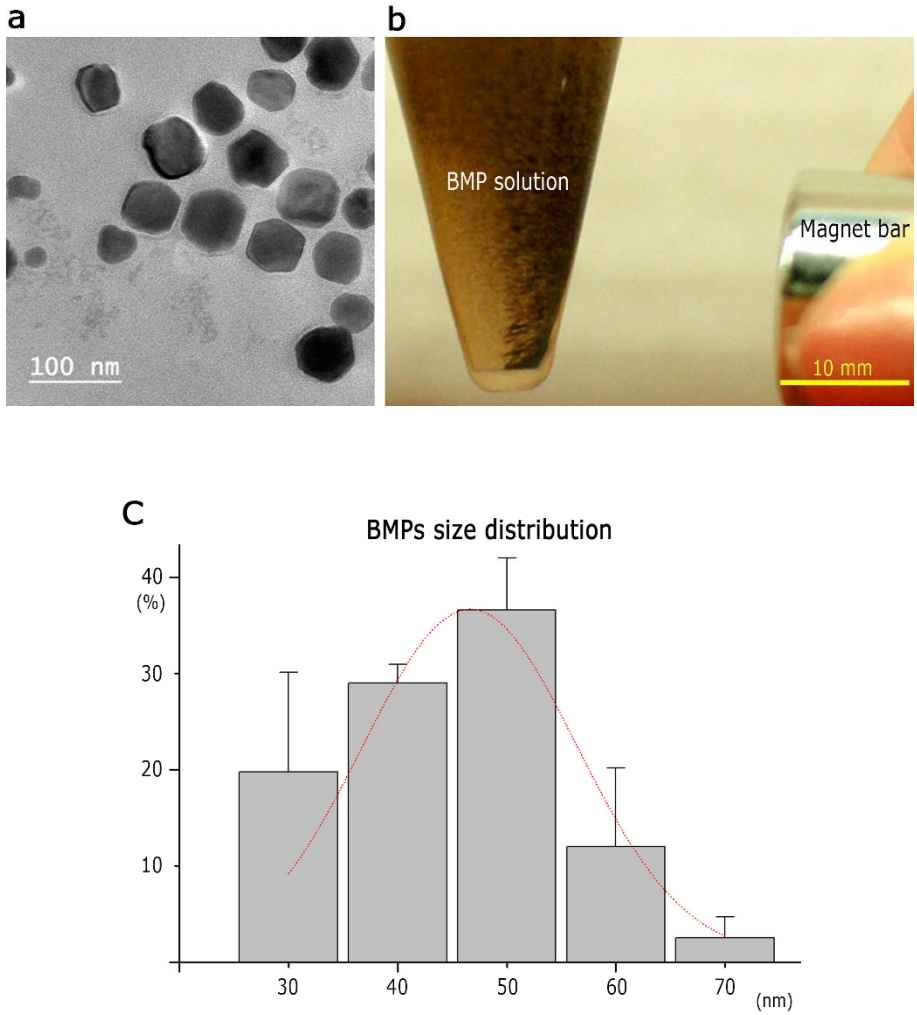

Figure 2-15 Bacterial magnetic nanoparticle (BMP). (a) TEM image of intact BMPs. (b) Photograph of concentrating process of BMPs using an external magnetic field. The BMPs quickly moved to the direction of the external magnetic field gradient. (c) The distribution of BMPs size scale is 50 nm.

2.5.2.2 Characteristics of BMPs

Magnetotactic bacteria (MTB), discovered by Richard P. Blakemore in 1975 [62, 63], can take in Fe sources and change them to magnetic nanoparticles such as magnetite (Fe_3O_4) or greigite (Fe_3S_4) [58], called bacterial magnetic nanoparticles (BMPs). In various magnetotatic bacteria, magnetic particles have different shapes such as cubo-octahedral, elongated hexagonal prismatic, and bullet-shaped morphologies [48, 73]. The BMPs are composed of magnetic core wrapped by stable lipid membranes that contain some lipids and proteins such as phosphatidylserine, phosphatidylethanol-amine, glycolipids and sulfolipids [74]. Thus, the BMPs can be easily dispersed and conjugate with other biomolecules, such as antibodies, enzymes, and polypeptides [75]. The zeta potential of BMPs ranges from -2.5 to -25.0 mV when the pH value changes from 4 to 7 [47, 76]. BMPs can generate a strong forces induced by applied magnetic field (B) due to high magnetic susceptibility [62]. BMPs is biocompatible since they are produced by bacterial cell and toxicity of iron can be negligible [70, 77]. However, it is predicted that BMPs also have potential risks due to various nonhuman proteins from bacterial cell [78]. Some works reported that the BMPs had little cytotoxic effect on various cells [57, 69, 71].

2.5.3 Bacterial magnetic nanoparticles (BMPs)-Histone H1 antibodies conjugates (H1-BMPs)

2.5.3.1 Theoretical analysis of loading efficiency of antibodies

It is hard to investigate the number of antibodies (abs) on surface of bacterial magnetic nanoparticle (BMP). Thus, we calculated the number of antibodies on surface theoretically. The number of antibodies for a monolayer was calculated from simple geometric model [79]. Figure 2-16 shows the geometric property for calculation.

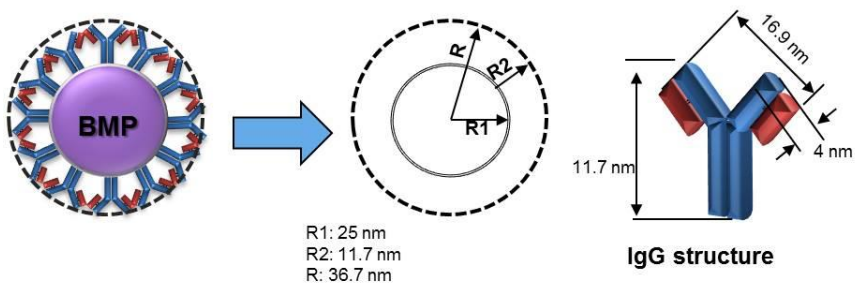

Figure 2-16 Schematic diagram of geometric H1-BMPs.

The R is defined as an effective radius from the center of the nanoparticle to the antibody. Thus, the number of antibodies is

$$N_{antibodies} = \frac{surface\ \ area\ \ of\ \ effective\ \ sphere}{Area\ \ of\ \ antibody} = \frac{4\pi R^2}{\frac{\pi r^2}{\varepsilon}}$$

Where, **R** is effective radius, **r** is length of antibody, $\boldsymbol{\varepsilon}$ is the packing density. We used the 150 KDa antibody (IgG,) because its dimension is well known [80]. In first model, the area of an antibody is assumed to be circular shape with a diameter of

16.9 nm [80]. The area of antibody is calculated as 224.2 nm^2 on the surface at **R**. Effective surface area is ~16,917 nm^2 (Radius of R: 36.7 nm). Packing density is 0.9069 [81]. Thus, 68 antibodies is calculated for a monolayer that there are no aggregated antibodies. In second model, the area of antibody is assumed to be a rectangle with length(16.9 nm) and width (4 nm) [80]. Thus, the total of antibodies is calculated as 250. Actually, we expected the number of immobilized antibodies is higher than the ideal calculation because we used 32 KDa antibody. Although the dimension of 32 KDa antibody is not known, it is certainly that the dimension of 32 KDa antibody is small compared to 150 KDa antibody

2.5.3.2 Protocol for H1-BMPs conjugates

For covalent coupling of amine-terminated BMP and oocyte-specific histone H1 antibodies (~32 KDa, abcam, USA), the surface of the BMP was pretreated with 10% glutaraldehyde solution (Sigma, USA) as the crosslinking agent. After reaction for 1-2 hrs at room temperature with continuous mixing, the BMPs were washed twice with 1 ml MES buffer (0.1x). Histone H1 antibodies (Immunoglobulin G: IgG) were labeled with fluorescein isothiocyanate (FITC) prior to the immobilization of antibodies on the BMPs. Histone H1 antibodies were coupled with the FITC by using EZ-Label FITC Protein Labeling Kit (Thermo scientific, USA). 12.48 μl FITC solution was completely mixed in 100 μl dimethylformamide (DMF) soultion, then the mixture of FITC and DMF was added into the 20 μl solution of antibodies. After incubating at room temperature for 1 hr, dialysis process was used to remove the uncoupled FITC. Based on the theoretical caculation of an average number of antibodies on nanoparticle surface [82], the resuspended ~146 μg BMPs in MES solution (0.1x) were added into reaction tube containing the histone H1 antibodies coupled with FITC. The mixture was reacted for 2-4 hrs with coninuous mixing. The BMPs conjugated with the histone H1 antibodies (H1-BMPs) were concentrated by a magnetic bar to remove the excess antibodies and washed several times with MES buffer (0.1x). After removal of the supernatant, the H1-BMPs were stored in buffer solution (0.3% Bovine serum albumin (BSA) in 1x PBS). We increased the purity of H1-BMPs using a magnetic bar (Fig. 2-17(b)). The concentration of H1-BMPs was measured by the inductively coupled plasma mass spectrometry (ICP, Shimadzu, Japan).

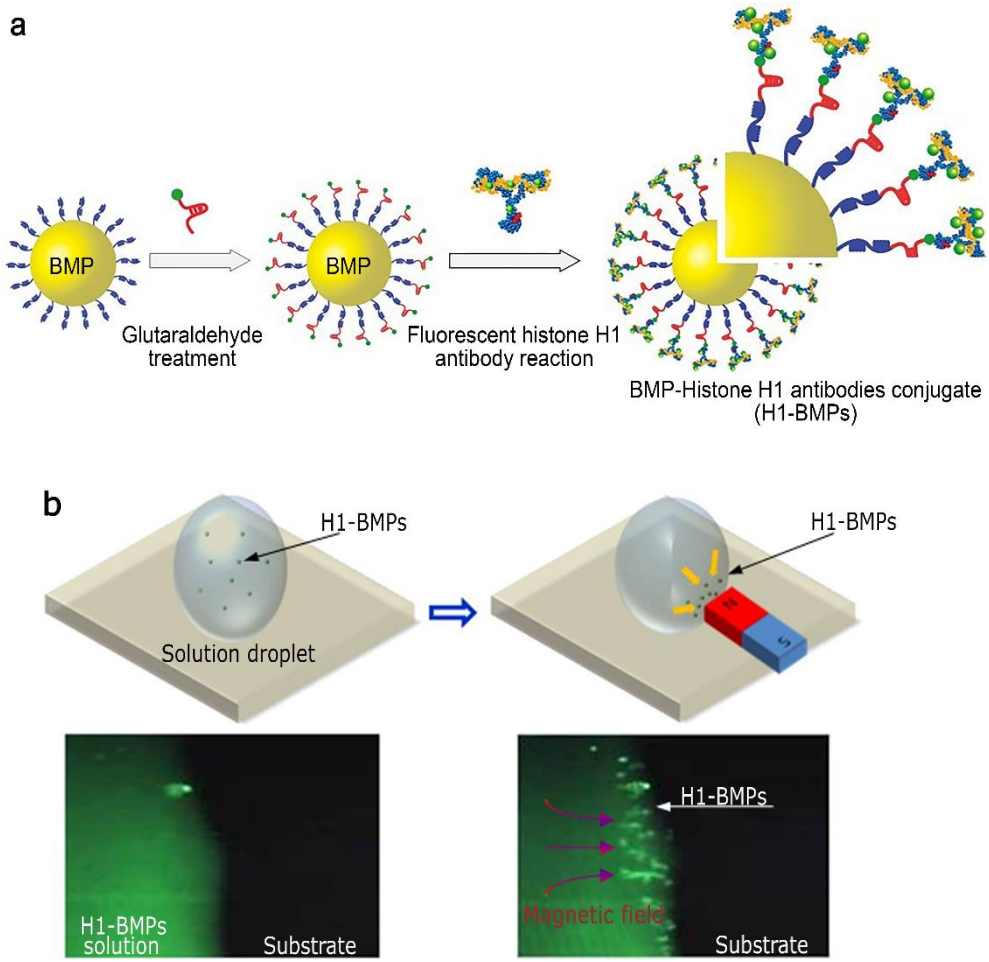

Figure 2-17 H1-BMP conjugates. (a) Sequential steps of formation of H1-BMP conjugate. (b) Focusing of H1- BMPs by external magnetic field.

2.5.3.3 Characteristics of H1-BMPs

2.5.3.3.1. TEM image

Immobilization of histone H1 antibodies on BMP surface was observed and compared with intact BMP using high resolution transmission electron microscopy (HRTEM, JEM-ARM200F, Japan) operating at 80 kV. Prior to observation by HRTEM, both samples were stained negatively using phosphotungstic acid (PTA, 2%) after the suspended samples were deposited onto carbon coated copper grid (200 mesh). The lipid layer of intact BMP has an average thickness of 4~5 nm. On the other hand, the lipid layer of H1-BMP has an average thickness of 12~13 nm. This may be due to the immobilization of the histone H1 antibodies (Immunoglobulin G: IgG) onto the lipid membrane of BMP.

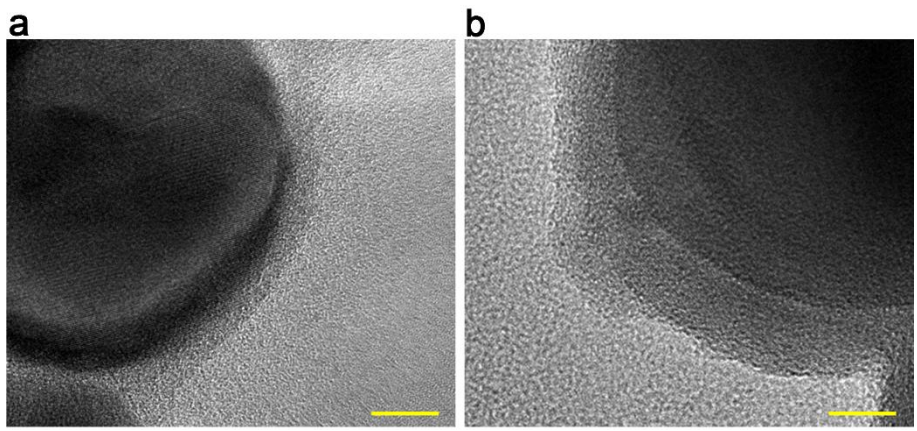

Figure 2-18 TEM image of nanoparticles. (a) Intact BMP. (b) H1-BMP conjugate. Scale bar is 10 nm.

2.5.3.3.2 BCA assay

The concentration of nanoparticles-attached protein was indirectly estimated using the bicinchoninc acid (BCA) protein assay kit (Thermo scientific, USA). A convenient standard curve can be drawn using bovine serum albumin (BSA) with concentrations of 0, 25, 125, 250, 500, 750, 1000, 1500, and 2000 µg/mL for the standard assay. The antibody content was measured in triplicates for each sample. As a first step towards the measurement of the immobilized histone H1 antibodies on BMPs surface, the measurement of the pure BMPs was performed to measure the existed proteins on BMPs as control experiment. 200 µl working reagent was mixed with 25 µl of dispersed nanoparticle (BMPs and H1-BMPs concentration: 1.75 µg/µl) by shaking for 30 sec at 37 °C. The optimal concentrations of BMPs and H1-BMPs were determined by several experiments. After 30 min, the absorbance was measured at 571 nm using a microplate reader (Thermo scientific, USA). Prior to measurement, nanoparticles in sample were removed in order to prevent the absorbance disturbance. The amount of protein was calculated from a standard curve. The protein loading efficiency (%, w/w) was expressed as the amount of measured protein relative to the amount of the initial used protein [83]. It is verified that the amount of immobilized histone H1 antibodies on BMP, which is measured as 4.06 µg. Thus, the loading efficiency is calculated as ~68% since the initially used protein was 6 µg to conjugate with 43.75 µg BMP.

2.5.3.3.3 Zeta potential

The zeta potential was determined by the electrophoretic light scattering spectrophotometer (ELS-8000, Otsuka Electronics, Japan). The zeta potentials of pure BMPs and H1-BMPs in pH 7.0 were -15.79 mV and -24.64 mV, respectively. The histone antibodies are coupled with amino groups in BMP through the cross-linking reaction (Amide bond). Thus, it is believed that this reaction decreases the positive charge in BMP membrane, leading to decrease of the zeta potential in H1-BMPs surface. These results describe that the histone antibodies were well immobilized on BMPs surface through cross-linking reaction.

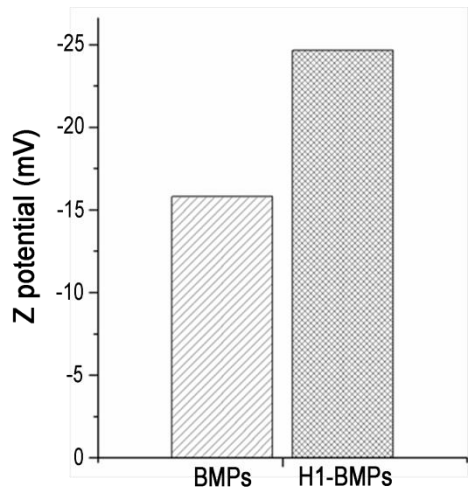

Figure 2-19 Z-potential measurement

2.5.4 Endocytosis of H1-BMPs

2.5.4.1 Preparation of TEM sample

Verification of H1-BMPs delivery into oocyte, was also carried out by transmission electron microscopy (TEM). To handle low number of cells (50~100 oocytes) without loss for TEM sample preparation, oocytes were embedded in low gelling temperature agarose (Sigma Aldrich) after delivery of H1-BMPs for 16~18 hrs. Prior to embedding, oocytes were fixed in karnovsky's solution for 2 hrs. To embed the oocytes in agarose, 2% low gelling temperature agarose was prepared in distilled water and kept at 50°C. Glass slide was kept warm on block heater at 40°C, then 20 µl drop of agarose was placed on slide and quickly oocytes were injected inside the agarose. Slide was cooled immediately to solidify the agarose before the sample reached the slide surface. Agarose-oocyte drop was cut into 1~3 mm square shape block using sharp knife. Then this agarose-oocyte block was treated with karnovsky's solution for 2 more hours for primary fixation followed by three times treatment with 0.05M sodium cacodylate buffer (Electron Microscopy Science, USA) for 10 min each. After post fixation with 2% osmium tetroxide (1ml, Sigma Aldrich) + 0.1 M cacodylate buffer (1ml) for 2 hrs, agarose-oocyte block was washed two times with distilled water. For En bloc staining process, 0.5% uranyl acetate solution (Electron Microscopy Science, USA) was used for overnight. Agarose-oocyte block was dehydrated with a graded series of ethanol (30, 50, 70, 80, 90, and 100%) for10 min each and then washed twice in propylene oxide (Electron Microscopy Science, USA) for 10 min each. For infiltration, agarose-oocyte block was treated with propylene oxide (1ml) + spurr's resin (1ml) for 2hr and transferred into spurr's resin

(2ml). After spurr's resin treatment overnight, agarose-oocyte blocks were transferred into freshly prepared spurr's resin for 2 more hr. Finally, new spurr's resin was used for polymerization of oocyte for 24 hr at 70°C. Spurr's resin was prepared after mixing Cycloaliphatic Epoxide Resin (ERL, Electron Microscopy Science, USA), DER (Electron Microscopy Science, USA), Nonenyl Succinic Anhydride (NSA, Electron Microscopy Science, USA), and 2-Dimethylaminoethanol (DMAE, Electron Microscopy Science, USA) in 23.6:14.2:61.5:0.7 ratio (weight wise). Then, an ultramicrotome was used to cut the samples into ultra-thin slices (100 nm or thinner). TEM samples are also treated with heavy metals to increase the level of contrast in the final image.

2.5.4.2 Result

It is known that a cell can engulf nanoscale extracellular matter by endocytosis and formation of endosomes. Figure 2-20 shows the mature oocyte, having polar body. Many H1-BMPs are well delivered into mature oocyte and filled with large endosomes.

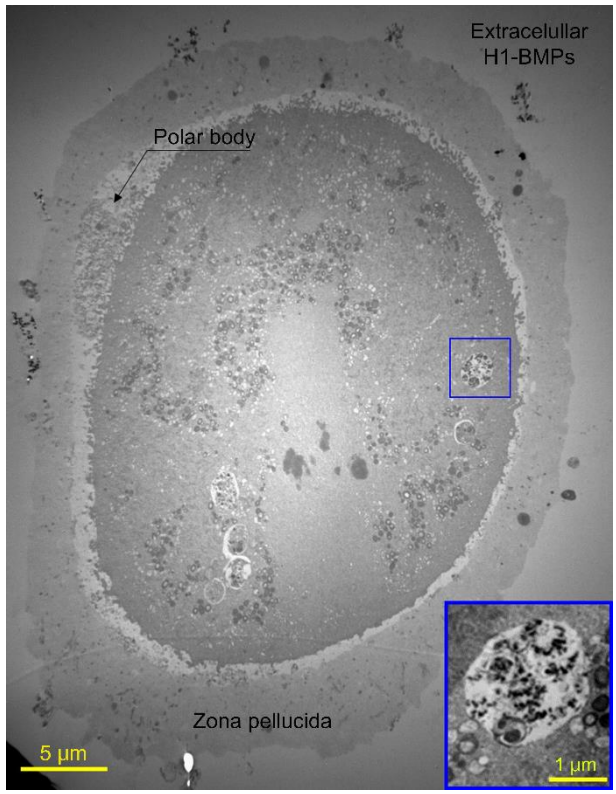

Figure 2-20 Endocytosis of H1-BMPs into oocyte

2.6 Confocal laser scanning microscopy (CLSM)

Confocal laser scanning microscopy (CLSM) developed by Marvin Minsky [84] has become an useful tool for a wide range of investigation in biology and biomedical science. Confocal microscopy has several advantages over conventional optical microscopy such as depth manipulation of field, control of background information away from the focal plane and ability to obtain the serial optical section from thick specimens. Fig. 2-21 shows the principle of confocal laser scanning microscope. The light emitted by laser source passes through a pinhole aperture and is reflected by a dichromatic mirror. From there, the laser hits two mirrors which are mounted on motors; these mirrors scan the laser across the sample in a defined focal plane. Secondary fluorescence emitted by samples is focused as a confocal point at the detector pinhole aperture and is measured by a detector (a photomultiplier detector). The detector is attached to a computer which builds up the image [85]. Basically, the confocal laser scanning microscope can collect the serial images of thin slices from a thick sample through the optical sectioning process that eliminates the contribution of out-of -focus information in each image plane depending on the changing of depth [86]. Thus, confocal microscopy has the ability to produce the three dimensional reconstruction of a sample from images captured at different focal planes.

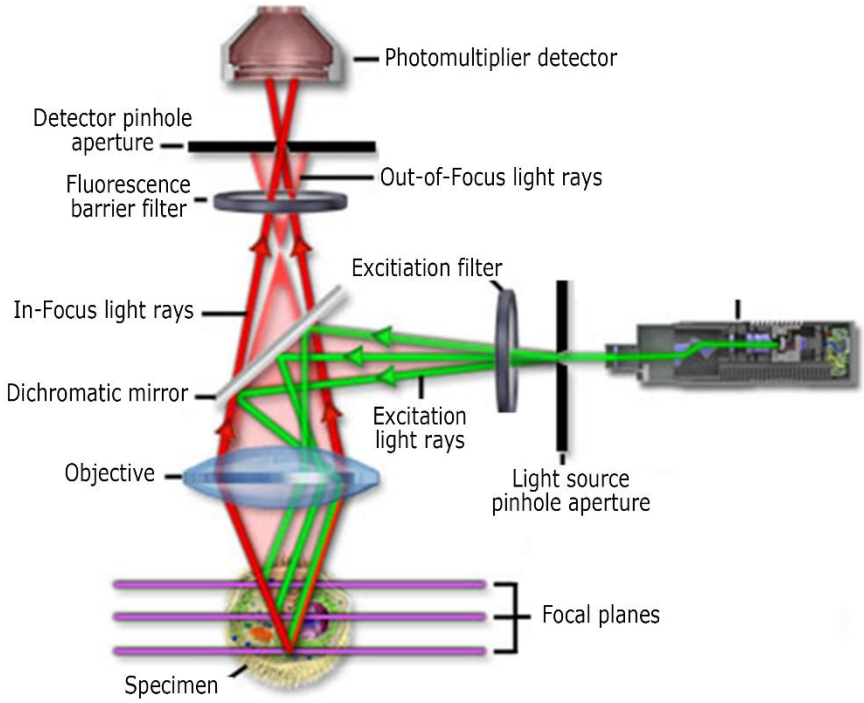

Figure 2-21 Principle of confocal laser scanning microscopy from Olympus company (www.olympus-global.com).

2.7 Portable incubator

In order to monitor the chromosome movement in real time, the portable incubator is needed. The portable incubator is composed of three components such as camera system, incubator and controller as shown in Fig. 2-22. The portable incubator is designed to fit the inverted fluorescence microscopy (Chamlide, Korea). The incubator cover is made of the glass that is patterned by the transparent heating element for prevention of a dewdrop. The controller is able to control the temperature, gas concentration and humidity.

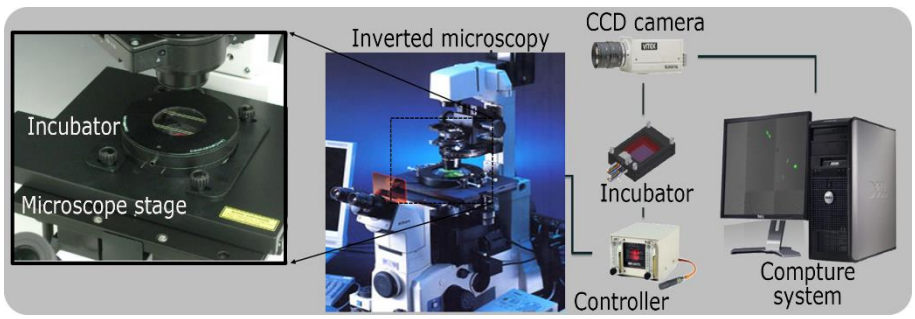

Figure 2-22 Experimental setup for observation of chromosome movement in real time

2.8 Experiment

2.8.1 Experimental procedure

Animal care and handling were conducted in accordance with the policy and regulation for the care and use of laboratory animals at Seoul National University (SNU-070903-1). Cumulus cells of cumulus-oocyte-complex retrieved from a mouse ovary after priming with PMSG and HCG were enzymatically removed. To arrest the cell cycle, 0.3 μM nocodazole (Sigma Aldrich, USA) in dimethyl-sulfoxide solution (DMSO, Sigma, USA) was used. The nocodazole was diluted in M16 medium to yield a final concentration of 0.07%. After nocodazole treatment for 16-18 hrs, the immature oocytes both with chromosome scattered in the entire cytoplasm and without nuclear membrane among retrieved oocytes were used for the following experiments. The H1-BMPs were delivered into the arrested cell. To increase the cellular uptake of the H1-BMPs, a weak magnetic field (B) was applied [87]. After internalization of the H1-BMPs, the H1-BMPs remaining outside the cells were removed by pippeting. After applying a strong magnetic field (B), the oocytes were fixed with 4% parafomaldehyde (Sigma, USA), and stained with 4', 6-diamidino-2-phenylindole (DAPI, Sigma, USA). Then, confocal laser scanning microscope (CLSM, Zeiss, USA) was used to obtain images. The confocal microscopy system is equipped with multi-photon laser that can image the FITC (excitation laser, 488 nm) and the DAPI (excitation laser, 400nm) simultaneously with the vertical resolution of 1 μm.

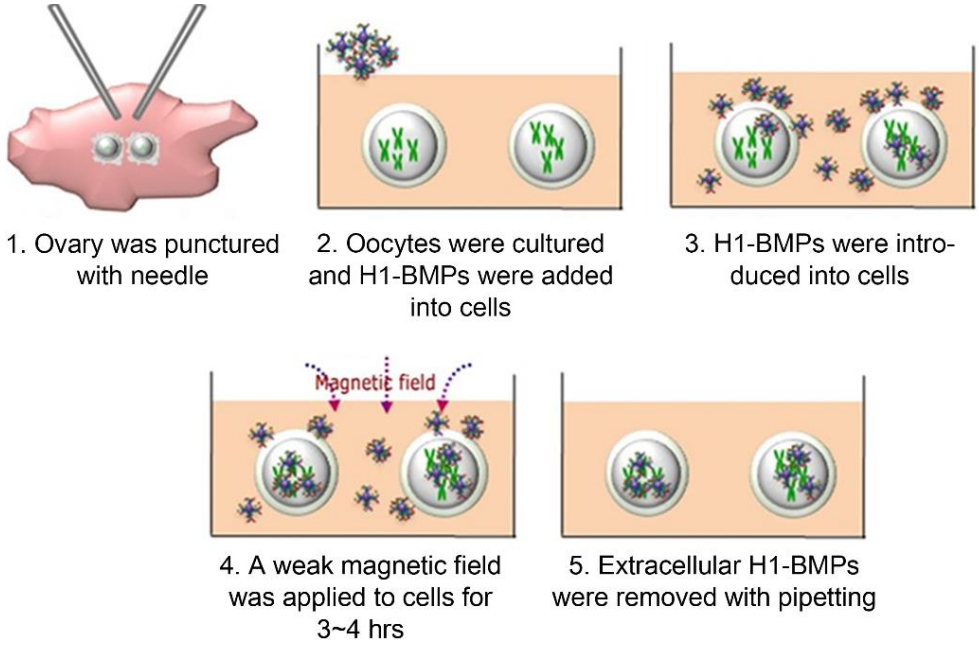

Figure 2- 23 The basic experimental procedure.

2.8.2 Cytotoxicity of H1-BMPs test

Cytotoxicity of BMPs was investigated in various doses on parthenogenetic oocyte development. Cell development was carried out in accordance with the standard protocol. In control group, the parthenogenesis activation was immediately carried out after cell collection. After oocytes were cultured in parthenogenetic activation medium for 4 hrs, cells were transferred and cultured in CZB medium. In other groups, various dose of both BMP and H1-BMPs was used to investigate the cell development in parthenogenesis, respectively. Subsequent cell development was evaluated by the morphological observations and cell developmental efficiency was calculated from four independent replicate experiments. Figure 2-24(a) shows the cytotoxicity of BMPs at 0 μg/ml (control), 1 μg/ml and 10 μg/ml doses. About 60% oocytes reached at blastocyst stage in control and sample with 1 μg/ml BMP dose. However, at 10 μg/ml BMPs, less than 40% blastocysts were obtained from activated oocyte. It is clear that BMPs at 1 μg/ml does not have significant cytotoxicity.

Figure 2-24(b) shows the result of H1-BMP at 0 μg/ml (control), 0.1 μg/ml, 1 μg/ml and 10 μg/ml doses for determination of optimal concentration. Cell viability was decreased as per increase in H1-BMPs dose. 0.1 μg/mL H1-BMPs suddenly affected the cell development at morula stage. However, 70% of cells still proceeded to the molura stage. On the other hand, the dose of 1 μg/mL and 10 μg/ml of H1-BMP effectively blocked the cell progress to morula stage by more than 90%. Although 1 μg/mL and 10 μg/ml of H1-BMP were suitable for deactivation of chromosome, the dose of 1 μg/mL was selected for experiment since oocyte development can be affected by BMP own toxicity at 10 μg/ml H1-BMP.

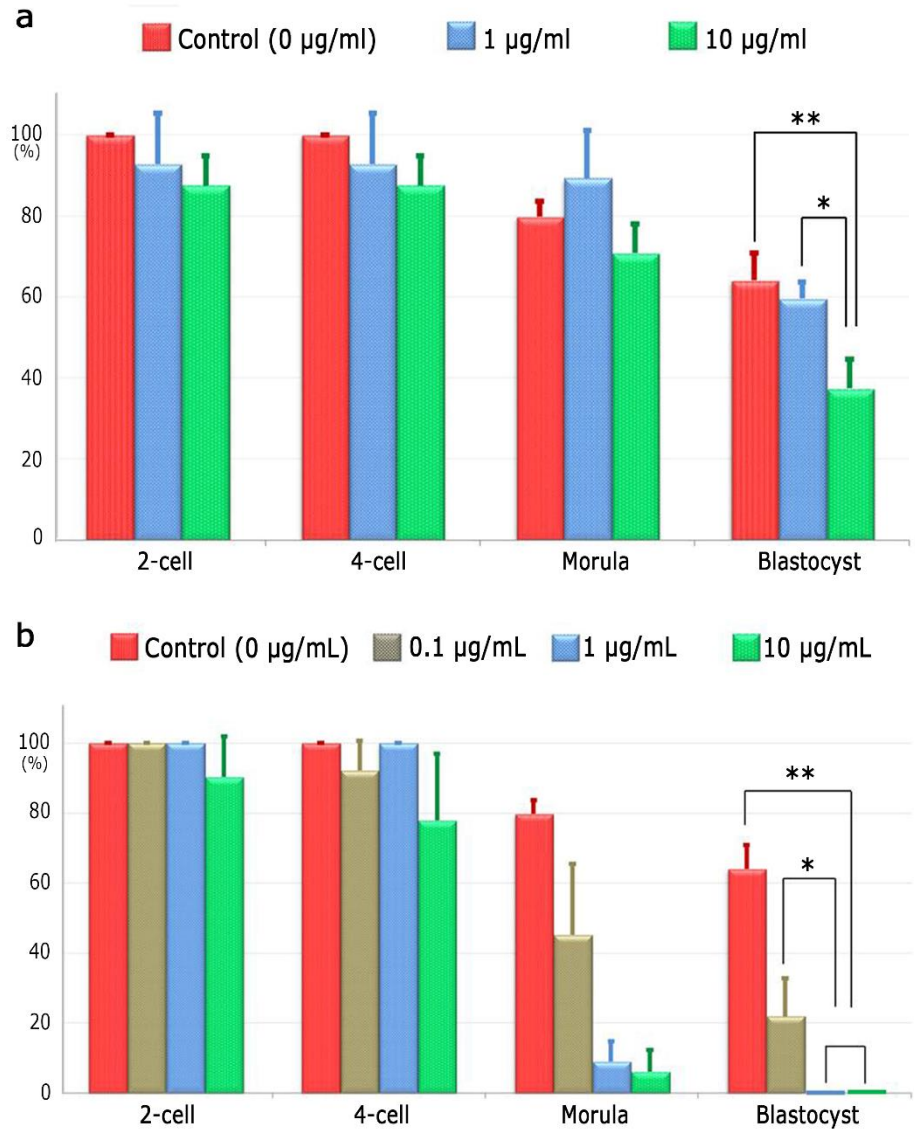

Figure 2-24 Cytotoxicity tests. (a) 0 μg/mL, 1 μg/mL, 10 μg/mL BMP. (b) 0.1 μg/mL, 1 μg/mL, 10 μg/mL H1-BMPs. Data are expressed as mean ± standard deviations. *p and **p < 0.05, ANOVA.

Table1. Data summary of cytotoxicity result

	Samples	Replicates	Activated M_2 oocytes	Number of M_2 oocyte at			
				2-cell	4-cell	Morula	Blastocyst
BMP cytotoxicity	Control	1	5	5	5	4	3
		2	14	14	14	11	9
		3	7	7	7	6	4
		4	4	4	4	3	3
	1 μg/mL	1	7	5	5	5	4
		2	7	7	7	7	4
		3	6	6	6	6	4
		4	7	7	7	6	4
	10 μg/mL	1	6	6	6	4	3
		2	6	5	5	5	2
		3	6	5	5	4	2
		4	6	5	5	4	2
H1-BMP cytotoxicity test	0.1 μg/mL	1	5	5	5	3	1
		2	6	6	6	3	1
		3	5	5	4	3	2
		4	9	9	8	1	1
	1 μg/mL	1	11	11	11	1	0
		2	6	6	6	1	0
		3	9	9	9	0	0
		4	10	10	10	1	0
	10 μg/mL	1	7	5	5	0	0
		2	10	9	9	1	0
		3	7	7	7	1	0
		4	8	6	4	0	0

2.8.3 Specific targeting

We verified whether H1-BMPs have the specific affinity against the histone H1 protein in chromosome. Confocal images of oocytes show the specific targeting of H1- BMPs to chromosomes in mature oocyte (Fig. 2-25). In both cases, without (Case 1: BMP-FITC) and with antibodies (Case 2: H1-BMPs), chromosomes in oocyte were subsequently stained with Hoechst after delivery of both BMP conjugates. In Case, “without antibodies,” FITC spots (BMP) were randomly scattered inside the mature oocyte with no correlation to chromosome distribution (Blue). In Case, “with antibodies,” most FITC spots (H1-BMPs) were found to be co-localized with blue spots (Chromosomes). This observation indicates that the internalized H1-BMPs were well guided and specifically targeted to the chromosomes, despite a highly crowded cytoplasm.

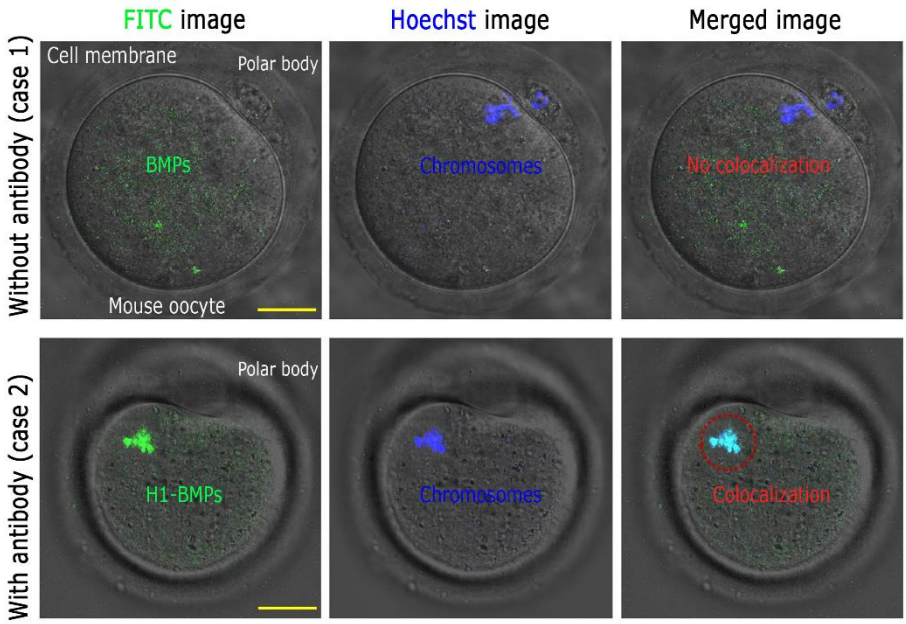

Figure 2-25 Specific targeting of H1-BMPs to chromosomes inside mature oocyte. (Upper) BMPs were randomly distributed, regardless of the condensed chromosome positions. (Lower) Green and blue spots at the same locations indicate that chromosomes were specifically attached to H1-BMPs. Confocal laser scanning microscopy was used to observe the images. The images were scanned and captured at 1-μm intervals along the Z-axis to verify the location of H1-BMPs and the chromosomes inside the cell. Scale bar is 20 μm.

2.8.4 Oocyte development in parthenogenesis

2.8.4.1 Experimental method

To investigate the artificial oocyte development in the parthenogenesis which chromosome was attached with H1-BMPs, experiments were carried out in four groups with different conditions as shown in Fig. 2-26. Subsequent cell development was only evaluated by the blastocyst morphology and the percentages of oocytes at blastocyst stage from four independent replicate experiments. In group 1, the parthenogenesis activation was immediately carried out after cell collection. After oocytes were cultured in parthenogenetic activation medium for 4 hrs, cells were transferred and cultured in CZB medium. In group 2, 1 μg/ml intact BMPs (without histone H1 antibody) were delivered into oocytes in order to investigate the BMP toxicity. In group 3, 1 μg/ml H1-BMPs were delivered into oocyte while cells were cultured in activation medium. The oocytes transferred into CZB medium with 1 μg/ml H1-BMPs 4 hrs after cell culture in activation medium. The oocytes were clearly washed to remove the extracellular H1-BMPs and cultured in fresh CZB medium 6 hrs after cell culture in CZB medium containing 1 μg/ml H1-BMPs. In group 4, the experimental condition is equal to the group 3. In this group, a magnetic field was applied to cells after cells were cultured in fresh CZB medium. Through previous work, the time to apply a magnetic field was determined.

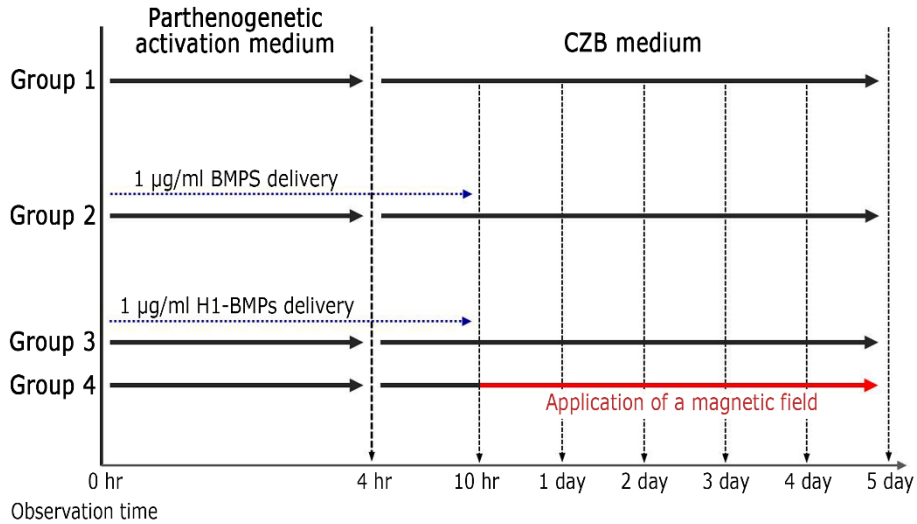

Figure 2-26 Schematic of experimental method for oocyte development in parthenogenetic activation with chromosomes captured by H1-BMPs.

2.8.4.2 Experimental result

In order to verify the feasibility of suggested approach, we investigated how oocyte developmental process after maturation was affected by the magnetic labeling of chromosomes. The parthenogenesis was induced to mimic the cell cycle after fertilization. Figure 2-27(a) shows the representative oocytes image at various stages obtaining from one experiment among five experiments. Through the images, we did analysis process. In groups 1 and 2, oocytes were well developed and reached the blastocyst stage with high efficiencies of 64.1% and 59.5 % respectively. Figure 2-27(b) shows that the intact BMPs have little toxicity up to the concentration of 1 μg/ml. In groups 3 and 4, oocytes were developed up to the 4-cell stage, but began to degrade afterwards and failed to reach the blastocyst stage regardless of the application of magnetic field. Interestingly, Figure 2-27(b) shows an abrupt fall in development process after 4-cell stage when the transcription needs to start by the maternal chromosomes. The mechanism by which this silencing occurs is elusive, but it suffices to note that the histone H1, a core protein for the stable sustaining and function of chromosome structure was disrupted by our manipulation. Unlike the traction experiments with the immature oocytes, the nocodazole treatment was not necessary for the delivery of H1-BMP to the core of the chromosomes because the oocytes used here were in the stage after maturation and nuclear envelope breakdown (NEBD).

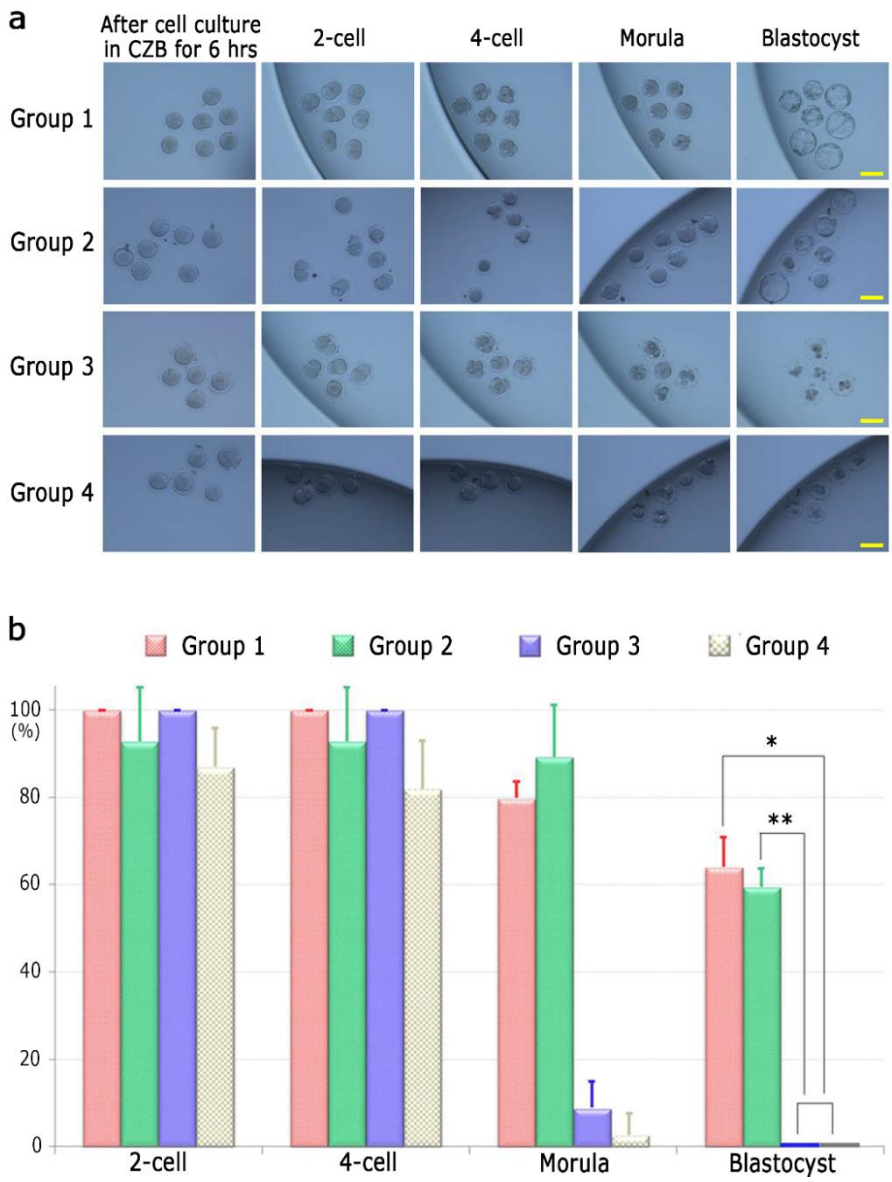

Figure 2-27 Cell development with chromosome captured by H1-BMPs derived from parthenogenetic activation. (a) Photographs (20x) showing various stages of the representative oocyte image obtaining from one experiment. (b) The graph of experimental result. Data are are expressed as mean ± standard deviations. *p and **p < 0.05 versus group 1 and group 2, ANOVA. The scale bar is 50 μm.

Table 2. Data summary of parthenogentic oocyte development with chromosomes captured by H1-BMPs

Group		Activated M_2 oocytes	Number of M_2 oocytes at			
Groups	Replicates		2-cell	4-cell	Morula	Blastocyst
Group 1	1	5	5	5	4	3
	2	14	14	14	11	9
	3	7	7	7	6	4
	4	4	4	4	3	3
	Sum	30	30	30	26	19
Group 2	1	7	5	5	5	4
	2	7	7	7	7	4
	3	6	6	6	6	4
	4	7	7	7	6	4
	Sum	27	25	25	24	16
Group 3	1	11	11	11	1	0
	2	6	6	6	1	0
	3	9	9	9	0	0
	4	10	10	10	1	0
	Sum	36	36	36	3	0
Group 4	1	10	8	7	0	0
	2	10	9	8	0	0
	3	9	9	9	0	0
	4	9	7	7	1	0
	Sum	38	33	31	1	0

2.8.5 Distribution of H1-BMPs during oocyte development

We also investigated the H1-BMPs distribution in cell development according to a presence of magnetic field. The above 4-cell stage cell was captured by confocal microscopy after cell culture for 2 day. Oocyte was stained with Hochest (Sigma, USA). 3-D images were restructured by the confocal microscopy images and the image J software was used to analyze the distribution of the chromosomes and the H1-BMPs. Figure 2-28 shows that the H1-BMPs were clearly internalized into cytosol of blastomere. Some H1-BMPs (green) trageted chromosomes (blue) and remaining H1-BMPs were still present in cytosol after four cell stage.

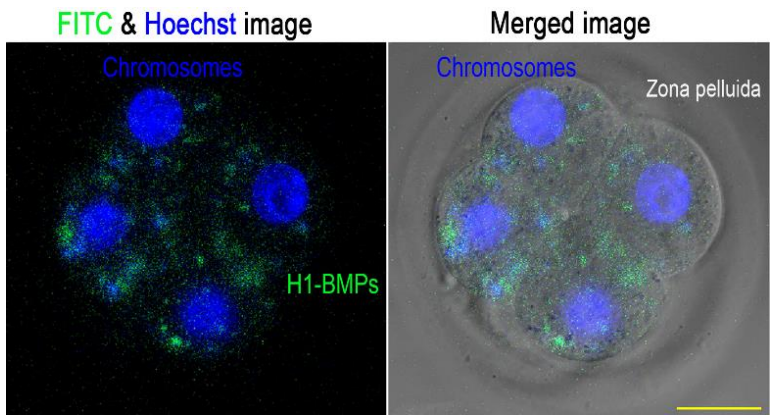

Figure 2-28 Image of H1-BMPs in blastomere cell after parthenogentic activation (green: H1-BMP, blue: chromosomes). Scale bar is 20 μm.

CHAPTER 3. INTRACELLULAR CHROMOSOME MANIPULATION

3.1 Experiments

3.1.1 Experimental concept

Recent progress in the reliable production and specific tailoring of functional magnetic particles has enabled a broad range of biomedical applications, such as contrast enhancement for magnetic resonance imaging, control of cell functions, drug delivery, and hyperthermia in cancer therapy [88-91]. Fluorescent magnetic nanoparticles in living cells were recently shown to be attracted by an external magnetic field [44]. With this possibility of remotely attracting the magnetic particles, we turn to the possibility of binding such particles to the chromosomes and relocating the whole compound.

In this work, we used bacterial magnetic particles (BMPs) functionalized with fluorescence-labeled antibodies (H1-BMPs) specifically targeting the chromosomal histone H1 in mouse oocytes as previously mentioned. Histone H1 is a key protein that staples the DNA wrapped around the octametric histone core, completing the nucleosome. Thus, the histone H1 is abundant in a chromosome and a good targeting protein for the binding of BMPs. The BMPs produced by magnetic bacteria (~50 nm) are ferromagnetic in nature and have much higher magnetic moments [62, 92]. In addition, these BMPs are inherently biocompatible, effectively conjugate with other biomolecules, and disperse well in aqueous solutions because they are enclosed by a lipid bilayer membrane [74, 75]. Figure 3-1 summarizes the experimental procedure.

First, the antibodies were labeled with the fluorescein isothiocyanate (FITC) which is used to track the location of the H1-BMPs in the mouse oocyte with a confocal laser scanning microscope. The antibodies were then covalently coupled with amine-terminated BMPs using glutaraldehyde as the homobifunctional cross-linker, resulting in the H1-BMPs. Cumulus cells of cumulus-oocyte-complex retrieved from a mouse ovary after priming with PMSG and HCG were enzymatically removed. Then immature oocytes oocytes were used for the following experiments. The H1-BMPs in 1 μl of storage buffer (at a concentration of 1.2042 μg/μl) were introduced into the oocytes, and a weak magnetic field (B) was applied at the bottom of the culture dish to increase cellular uptake [87]. For removal of the residual H1-BMPs outside the oocytes, the oocytes were washed with culture medium several times by pipetting. The external magnetic field (B) was remotely exerted on the H1-BMPs attached to chromosomes, leading to chromosome motion in the cytosol.

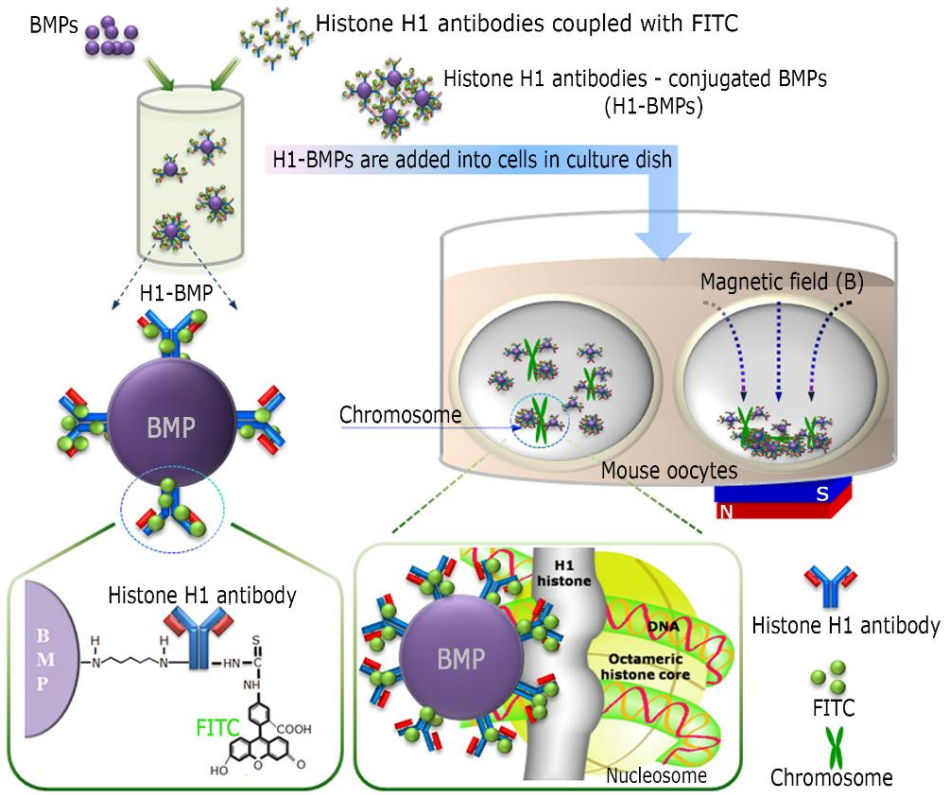

Figure 3-1 Schematic diagram of chromosomes movement by an external magnetic field.

3.1.2 Experimental procedure

Animal care and handling were conducted in accordance with the policy and regulation for the care and use of laboratory animals at Seoul National University (SNU-070903-1). Cumulus cells of cumulus-oocyte-complex retrieved from a mouse ovary after priming with PMSG and HCG were enzymatically removed. To arrest the cell cycle, 0.3 μM nocodazole (Sigma Aldrich, USA) in dimethyl-sulfoxide solution (DMSO, Sigma, USA) was used. The nocodazole was diluted in M16 medium to yield a final concentration of 0.07%. After nocodazole treatment for 16-18 hrs, the immature oocytes both with chromosome scattered in the entire cytoplasm and without nuclear membrane among retrieved oocytes were used for the following experiments. The H1-BMPs were delivered into the arrested cell. To increase the cellular uptake of the H1-BMPs, a weak magnetic field (B) was applied [87]. After internalization of the H1-BMPs, the H1-BMPs remaining outside the cells were removed by pippeting. After applying a strong magnetic field (B), the oocytes were fixed with 4% parafomaldehyde (Sigma, USA), and stained with 4', 6-diamidino-2-phenylindole (DAPI, Sigma, USA). Then, confocal laser scanning microscope (CLSM, Zeiss, USA) was used to obtain images. The confocal microscopy system is equipped with multi-photon laser that can image the FITC (excitation laser, 488 nm) and the DAPI (excitation laser, 400nm) simultaneously with the vertical resolution of 1 μm.

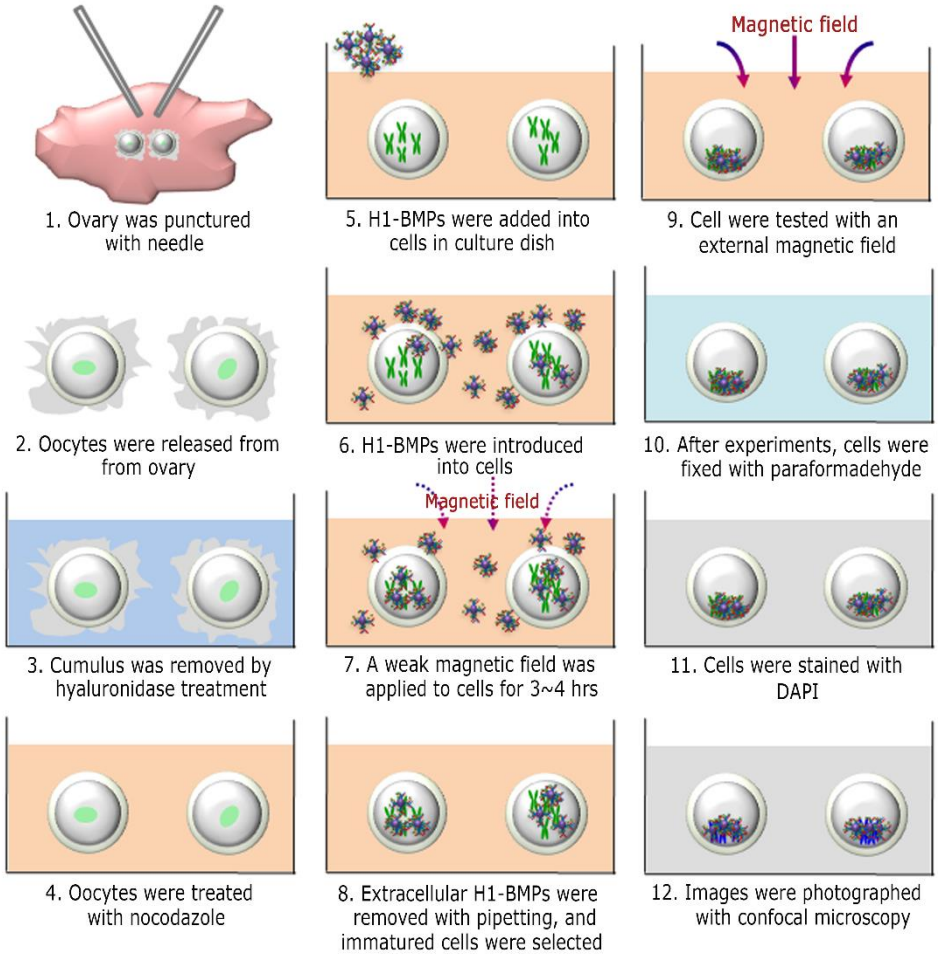

Figure 3-2 The basic experimental procedure.

3.2 Magnetic force on a BMP

3.2.1 The force on a magnetic dipole

Assuming the BMP as a point like magnetic dipole, we can calculate the magnetic force on a single BMP under external magnetic field gradient as follows. Magnetic force $\boldsymbol{F_m}$ on a point like magnetic dipole m in a magnetic field $\boldsymbol{B}$ can be calculated as [49, 93]

$$F_m = (m \cdot \nabla)B$$

the volume of a particle is V_m and effective susceptibility relative to surrounding medium is $\nabla\chi$

$$\boldsymbol{F_m} = \frac{V_m \Delta\chi}{\mu_0}(\boldsymbol{B} \bullet \nabla)\boldsymbol{B}$$

where is magnetic permeability of vacuum(μ_0) and $\nabla\chi$ ($\triangledown\chi_m$-$\triangledown\chi_w$) is the effective susceptibility of the particle relative to the water. According to Maxwell equation in time invariant magnetic field $\nabla \times B = 0$ since there is no time-varying electric fields or currents in the medium, so the above equation can be written as

$$\boldsymbol{F_m} = V_m \Delta\chi\left(\nabla|B^2| \Big/ 2\mu_0\right)$$

If the cytoplasm effective susceptibility is assumed to be equivalent to that of water (-9.035×10^{-6}), it can be neglected as compared to BMP volumetric direct current (DC) susceptibility (~1000).

3.2.2 Analysis of magnetic force

All experiments used various tools such as culture dish, and microfluidic cell trapping device. Thus, a neodymium magnetic bars in various sizes were placed at different distances from the sample. We calculated the magnetic forces based on the measurement of magnetic field in two different cases as shown in Fig. 3-3. In the culture dish experiment, a permanent neodymium magnet (50 mm × 50 mm × 25 mm) was used at 1.5 mm from oocytes. The measured magnetic field ($|\nabla B|$) at a distance of 1.5 mm was ~500 T/m which resulted in a force of ~ 780 fN on single BMP. To observe the chromosome movement in the microfluidic trapping device in real time, a combination of small magnets was used at a distance of 5 mm because of the space limitation in the device. The calculated magnetic field ($|\nabla B|$) at a distance of 5 mm was ~170 T/m which resulted in a force of ~ 230 fN on single BMP. Quantitative values for the cellular uptake and binding efficiencies are necessary to determine the total force exerted on chromosomes. Cellular uptake of particles can be affected by many factors, such as particle size, types of cell lines and cell densities, compositions of the particles and surface properties[94-96]. Currently it is hard to identify the cellular uptake efficiency because only small number of oocytes was used in our experiment. However, the magnetic force can be roughly estimated. In a separate our experiment with national institute of health (NIH) 3T3 cells, ~40% cellular uptake was measured [97]. With this uptake efficiency and 50% binding efficiency assumed, 20% of the H1-BMPs on the projected area should be delivered and bound to the chromosomes. When 1 μl H1-BMP solution (Density, ~5000 kg/m^3) was added in a culture dish (ø: 35 mm), there should be 6.4×10^{12} (H1-BMPs/m^2).

Thus, the number of the H1-BMPs on the projected area of a single oocyte (80 μm) were 3.2×10^4. If 6.4×10^3 H1-BMPs conjugated with the chromosomes, it can produce a total force of ~5 nN in the culture dish and ~1.5 nN in the microfluidic trapping device experiments. In comparison with literature, it is deemed that the force is enough to drag the chromosomes in cytoplasm.

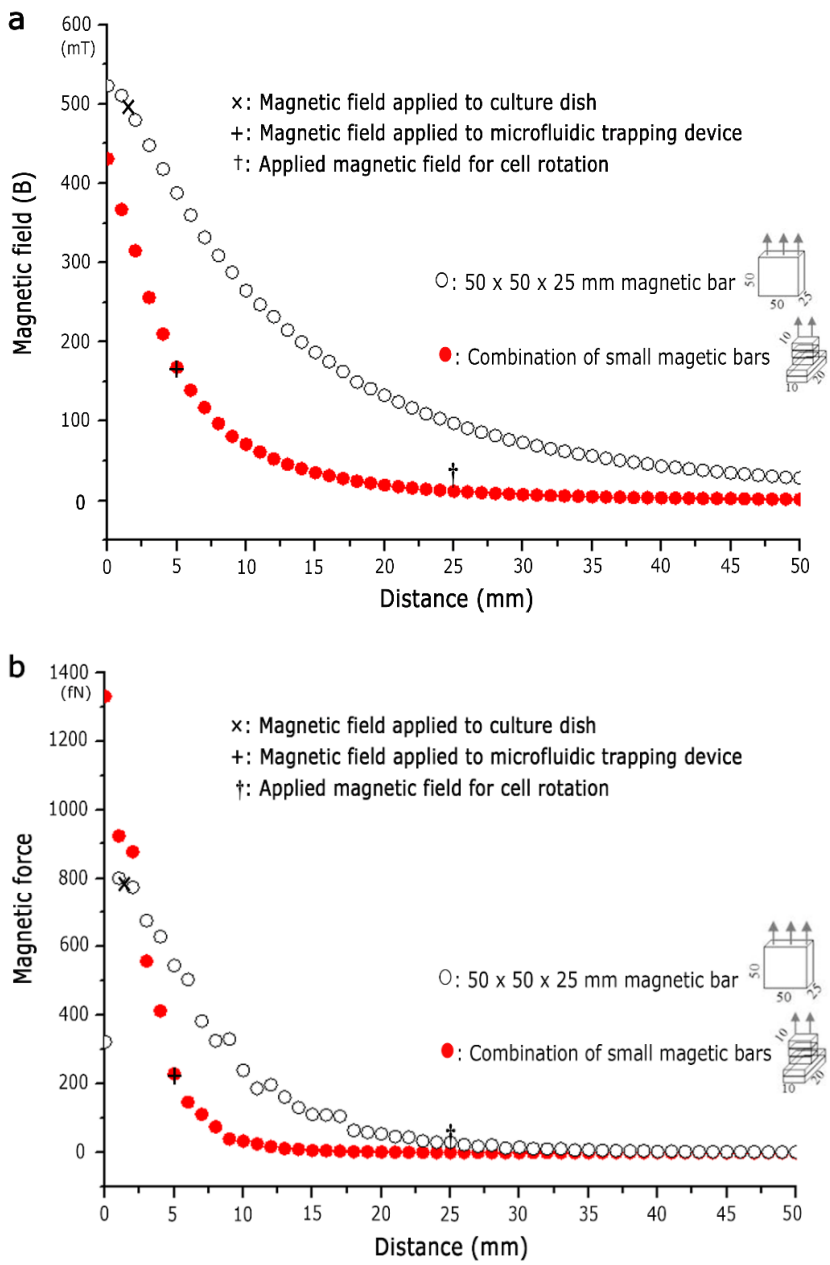

Figure 3-3 Measured magnetic field and calculated magnetic force on a single BMP. a) Magnetic field vs. distance. (b) Magnetic force vs. distance. Dimension is in mm.

3.3 Categories of experiments

3.3.1 Specific targeting test

3.3.1.1 Experimental procedure

Here, we described the specific targeting experiment in detail. Figure 3-4 shows whole procedure of the specific targeting experiment. After retrieval of mouse oocytes, nocodazole was treated to block the polymerization of microtubule for 18 hr. This process can prevent the natural chromosome movement by cell development. To determine whether the 1 μl H1-BMPs (at a concentration of 1.2042 μg) are specifically targeted to the chromosomes, we delivered two different kinds of BMP complexes: the ones with the antibodies (H1-BMPs) and the ones without them (BMP). For tracking the BMPs, the FITC was directly labeled on both two different kinds of BMP. After delivery of two BMP complexes, oocytes were cultured in incubator for 24 hrs. Generally, it is known that nanoparticle is internalized into a cell by the endocytosis, covering the various types of cellular uptake mechanisms [98]. Before investigation, extracellular BMP complexes were removed by the pipette aspiration that is to continuously aspirate oocytes by the handmade oocyte pipet. To verify the specific binding of H1-BMPs, chromosomes were stained with DAPI. The confocal laser scanning microscope (CLSM) was used to capture the images of mouse oocytes. As mentioned early, the significant feature of CLSM is the ability to obtain in-foucus images from specific depths, a process known as optical sectioning. Thus, the images were scanned and captured at interval of 1 μm along Z-axis. Image J software is used to verify the location of BMP complexes inside cell.

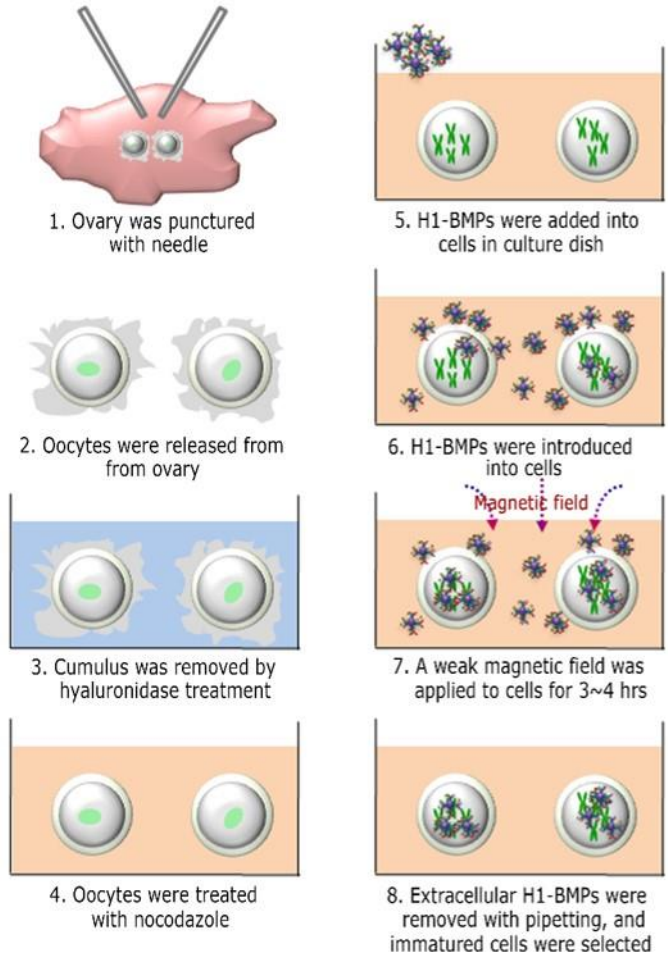

Figure 3-4 Schematic diagram of specific binding experiment

3.3.1.2 Experimental result

3.3.1.2.1 H1-BMPs distribution in immature oocytes at germinal vesicle (GV) and germinal vesicle breakdown (GVBD) stage

Prior to test of specific targeting, we investigated the effect of nuclear envelope on H1-BMPs delivery into chromosomes. Oocyte was stained with DAPI after cell fixation. The images were obtained from confocal laser scanning microscopy at intervals of 1 μm. Figure 3-5 shows that nuclear envelope disrupts the access of H1-BMPs to chromosomes. As a result, immature oocytes at GVBD stage were selected for subsequent experiments.

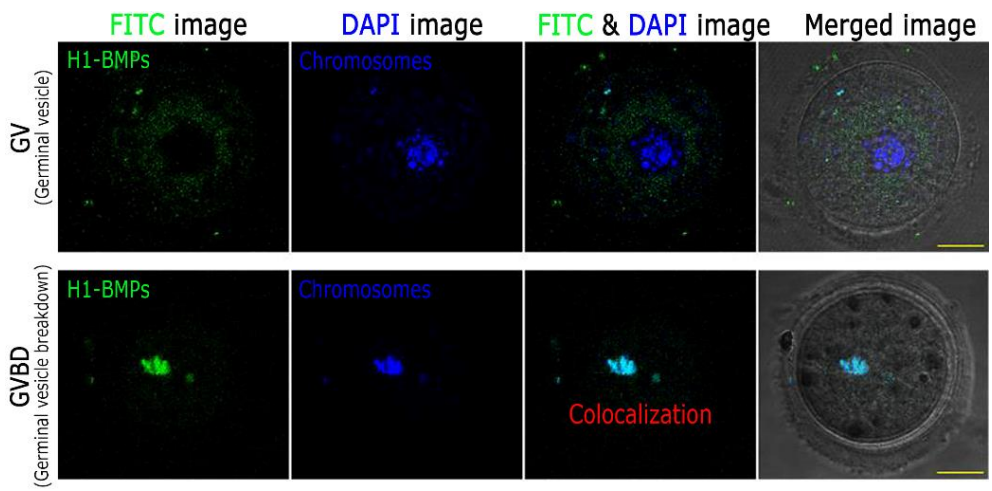

Figure 3-5 H1-BMPs distribution in immature oocytes at germinal vesicle (GV) and germinal vesicle breakdown (GVBD) stage (green: H1-BMP, blue: chromosomes). Scale is 20 μm.

3.3.1.2.2 Specific targeting in immature oocyte at GVBD stage

Figure 3-6 shows confocal images of oocytes, illustrating the specific targeting of H1- BMPs to chromosomal histones. In Case 1, “without antibodies,” FITC spots (green) were randomly scattered inside the oocyte with no correlation to chromosome distribution (blue). In Case 2, “with antibodies,” most FITC spots were found to be co-localized with DAPI-stained chromosomes. This observation indicates that the internalized H1-BMPs were well guided and specifically targeted to the chromosomes, despite a highly crowded cytosol and subcellular structures. This result shows the specific binding of BMP complexes to chromosomes inside a living cell.

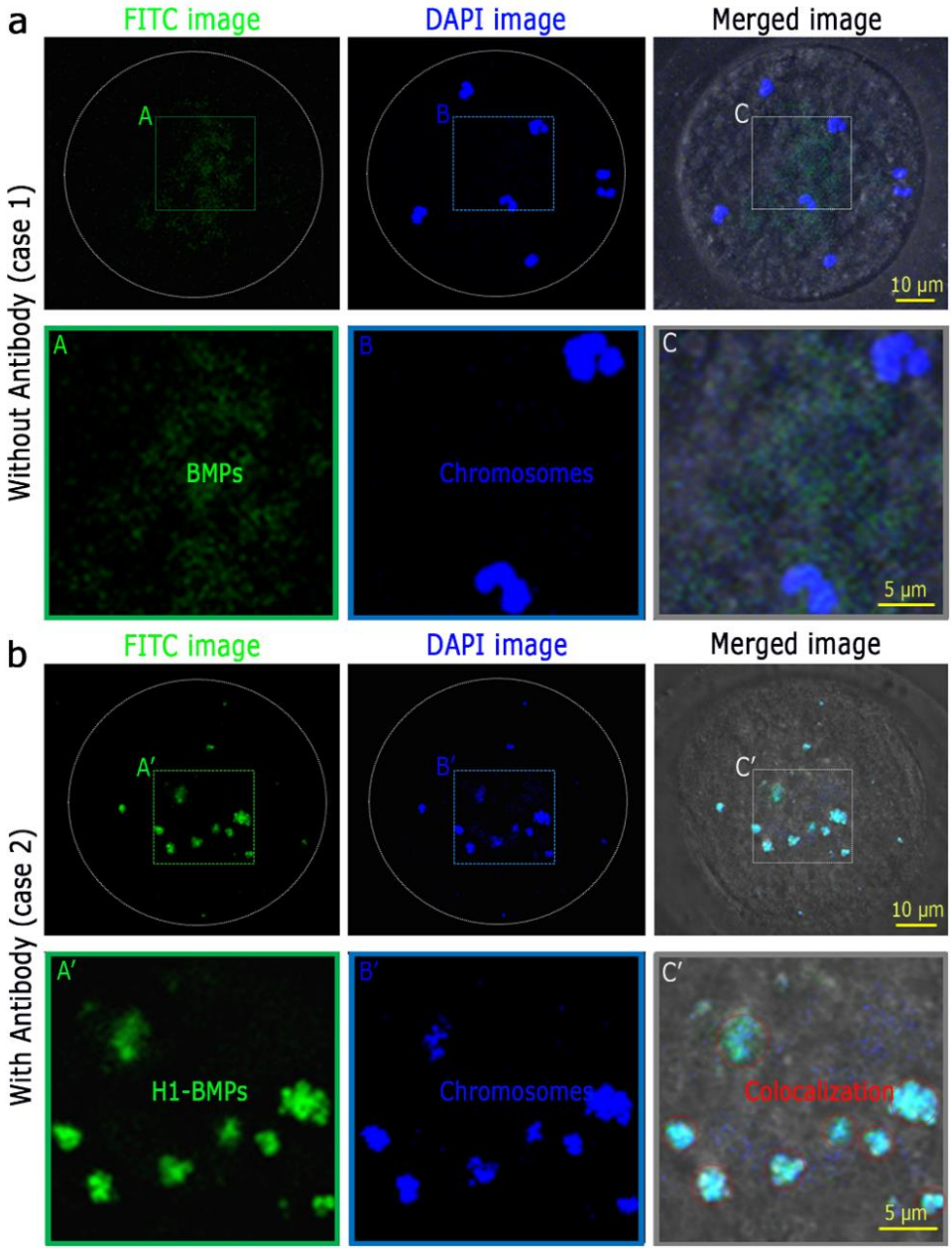

Figure 3-6 Specific targeting of H1-BMPs to chromosomes. (a) BMPs were randomly distributed without targeting of the chromosome. (b) Green and blue spots at the same locations indicate that chromosomes were specifically attached to H1-BMPs.

3.3.2 Cellular orientation control

3.3.2.1 Experimental approach

We described the cell rotation experiment in detail. Like the specific binding experiment, oocytes were prepared. All variations such as H1-BMPs concentration, nocodazole treatment, and so on are equal. After targeting chromosome with H1-BMPs, an external magnetic field was applied to the stationary cells using a neodymium magnet (45x30x10 mm) at a distance of ~ 25 mm as depicted in Fig. 3-7. For maximum torque, an oocyte, when all of the chromosomes moved toward the cortex, was selected. A magnetic bar moved from the top to bottom.

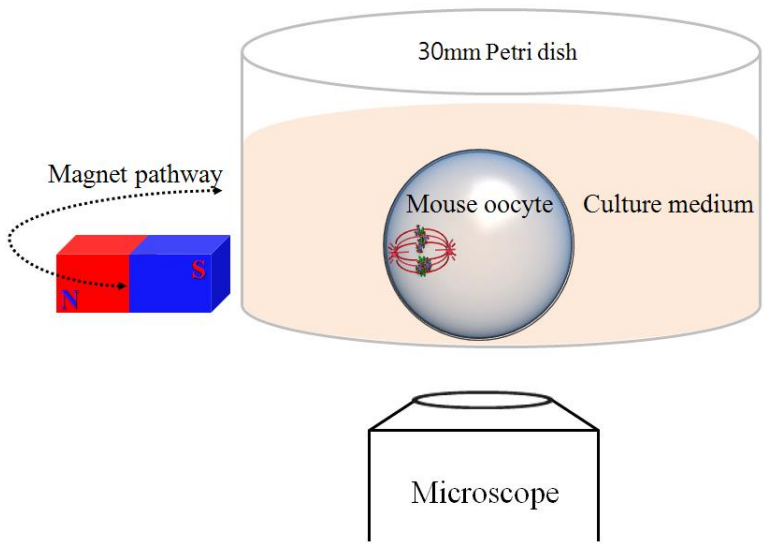

Figure 3-7 Schematic diagram of cellular orientation control.

3.3.2.2 Experimental result

A magnetic field (**B**) of 30 mT was applied to the stationary cells using a neodymium magnet at a distance of ~ 25 mm. Figure 3-8 shows the rotation of a cell along the external magnetic field. When a magnetic bar moved from the top to bottom, cell orientation was changed according to the pathway of the magnetic bar. The reverse motion of the magnetic bar created the change of the orientation in the same manner. This tracking behavior is attributed to the location of the polar body where the chromosomes are condensed with the H1-BMPs attached as a result of targeting. In the experiment, the rotation of the whole cell was preferred to the motion of the chromosomes in the cell, since the motion of the chromosomes was essentially blocked by the cytosolic resistance. Through this experiment, we observed the possibility of rearranging chromosomes inside cell by an external magnetic fields.

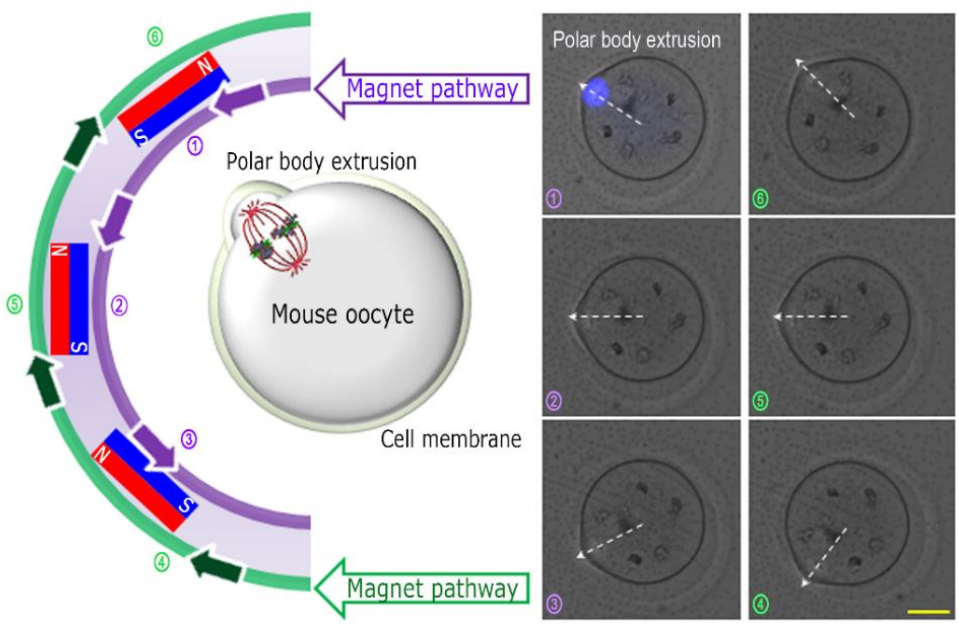

Figure 3-8 Cell rotation depending on the position of magnet bar. The bar is 20 μm.

3.3.3 Chromosome repositioning

3.3.3.1 Experimental procedure

Next, we attempted to move the chromosomes in an oocyte using the H1-BMPs attracted by the magnetic field (B). Figure 3-9 shows the detailed experimental procedure. Although mice were treated by PMSG and HCG, immature oocytes were selected for experimental purpose. Each H1-BMP and BMP of 1.2048 μ/ ml was delivered into oocyte after treatment of nocodazole for preventing the natural chromosomes movement due to cell development. All nanoparticles including H1-BMP (BMP-H1 antibodies conjugates) and BMP were coupled with FITC to monitor the position of nanoparticle inside cell. We cultured cells for 24 hrs. In order to achieve the manipulation of chromosome location in the cell, a stronger magnetic field gradient was necessary. After targeting chromosome with H1-BMPs, the magnetic field (B) was applied using a neodymium magnetic bar (45 x 30 x 10 mm) at the distance of 1.5 mm placed under the culture dish for 18~20 hrs. Extracellular H1-BMP and BMP were removed using pipette aspiration method before starting the next step. Then confocal images were taken after chromosome staining. Confocal microscopy images were processed and re-oriented to align the z-axis in the direction of the highest BMP concentration from the center. Image J was used to analyze the distribution of the chromosomes and the H1-BMPs.

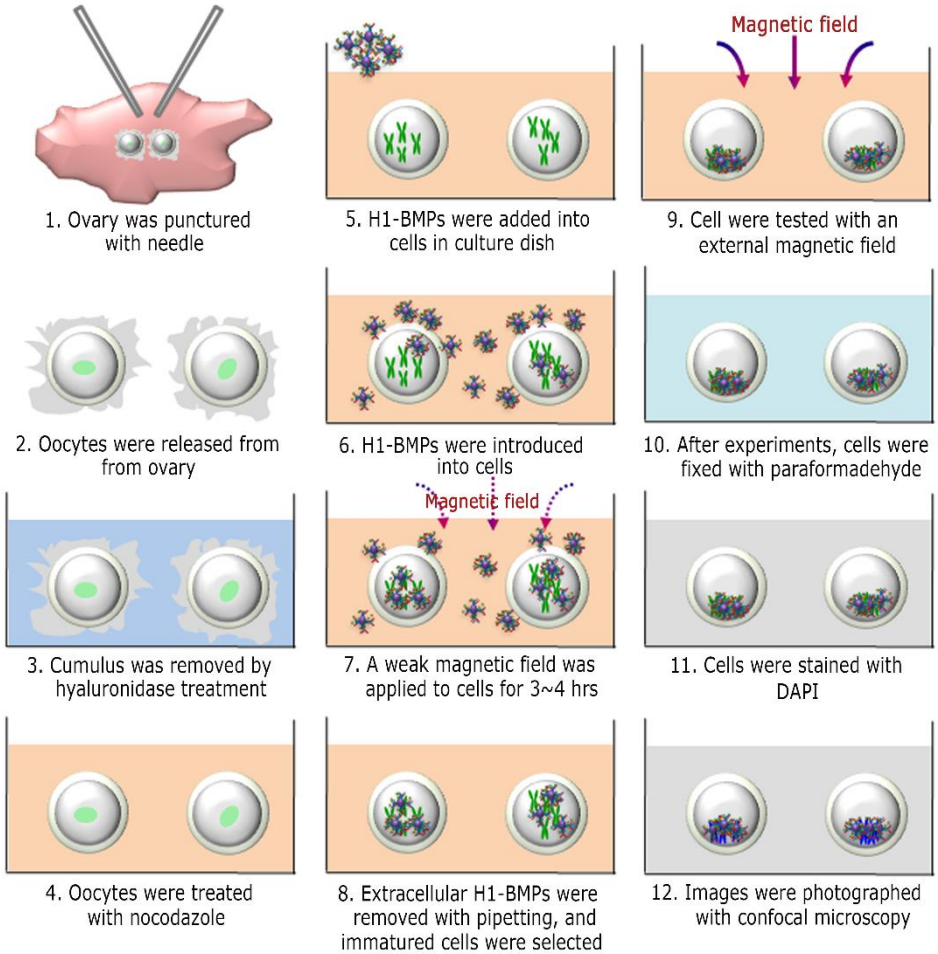

Figure 3-9 Schematic diagram of chromosome repositioning experiment.

3.3.3.2 Experimental result

In order to achieve the manipulation of chromosome location in the cell, a stronger magnetic field gradient was necessary. The magnetic field (B) was applied using a magnetic bar (495 mT at the distance of 1.5 mm) placed under the culture dish for 12 hrs. The confocal images were taken after chromosome staining. The oocyte rotated in an arbitrary direction and aligned with the direction of the magnetic field; then, the net movement of the BMPs occurred. Image J was used to analyze the distribution of the chromosomes and the H1-BMPs. The "⊙" symbol represents the direction of the magnetic field that is coming out of the page. Figure 3-10 shows the result of a control experiment in which FITC-conjugated BMPs without antibody were used. The green spots from the FITC-conjugated BMPs moved in the direction of the magnetic field (B), whereas the blue spots from the DAPI-stained chromosomes remained close to the center. Without the antibodies, the BMPs did not conjugate with the chromosome and the chromosomes did not move together with the BMPs in the presence of the magnetic field (B). In Fig. 3-10(b), the blue spots (chromosomes) coincided with the green spots (H1-BMPs) that dramatically moved to the top. These results verify that the H1-BMP bind specifically to the chromosome and manipulate the chromosomes by the magnetic field.

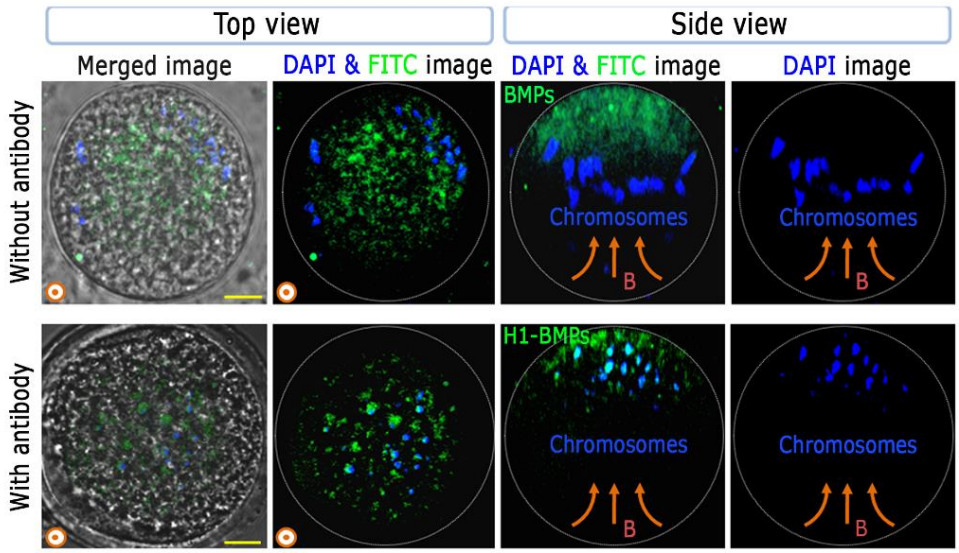

Figure 3-10 Chromosome manipulation with H1-BMPs. (a) Pure BMPs were concentrated along the magnetic field and the chromosomes not attached to the BMPs were randomly scattered. (b) the chromosomes attached to the H1-BMPs moved in the direction of the magnetic field

3.3.3.3 Quantitative calculation of chromosomes movement

The chromosome movement was quantitatively assessed based on the location data for the fluorescence spots. The mass center of the blue spots was calculated and used as a representative value for the entire distance moved. To find center of mass as a whole, all individual slides' mass center was averaged out considering the number of chromosomal pixels on each slide and then the distance of this mass center from the center of oocyte was calculated by Matlab software. Figure 3-11 compares the distances with and without antibodies (n=5 each). A substantial difference was observed between the movements with (20.6 ± 1.2 μm) and without (9.2 ± 2.1 μm) antibodies.

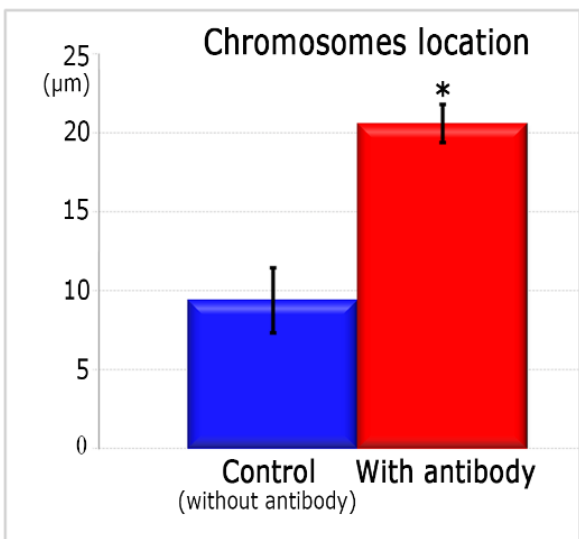

Figure 3-11 Quantitative chromosomes movement. Data are expressed as mean ± standard deviations. *$p < 0.05$ versus control.

Table 3. Data summary of chromosome distribution

Number of Samples (n)	Distance of chromosomal center from the center of cell	
	Without antibody / With magnetic field	With antibody / With magnetic field
1	3.48 μm	23.14 μm
2	14.15 μm	16.67 μm
3	12.41 μm	20.78 μm
4	7.23 μm	21.57 μm
5	8.61 μm	20.54 μm
Average distance	9.18 ± 4.23 μm	20.59 ± 2.47 μm

3.3.4 Chromosomes movement in real time

3.3.4.1 Fabrication of microfluidic cell trapping device

In order to observe the chromosome movement in real time, it was crucial to prevent the rotation of the cell by anchoring to substrate since the outer cumulus of the cell was removed as it could work like a lubrication layer that makes the rotation of the cell easy. For such anchoring purpose, we fabricated a vacuum-assisted microfluidic cell trapping device as shown in Fig. 3-12. For the observation of the chromosome movement, we used a silicon-on-glass (SOG) wafer with hole window and a transparent polydimethylsiloxane (PDMS) with microfluidic channels. Both structures were fabricated in separate steps, and assembled. First, the cell trapping holes and the observation windows were fabricated with separate etching steps on the SOG wafer with deep-reactive ion etching (DRIE) processes. Aluminum was used as a mask material for the DRIE processes and removed afterwards. Next, the microchannel was fabricated via PDMS replication process. A mold was created with SU-8 spin-coated and patterned. The PDMS mixture (curing agent: PDMS = 1: 10) was placed in a vacuum chamber for 1 hr to remove the trapped gases, and then poured onto the mold. After PDMS curing, the separate parts were assembled into the final microfluidic trapping device using biocompatible UV epoxy.

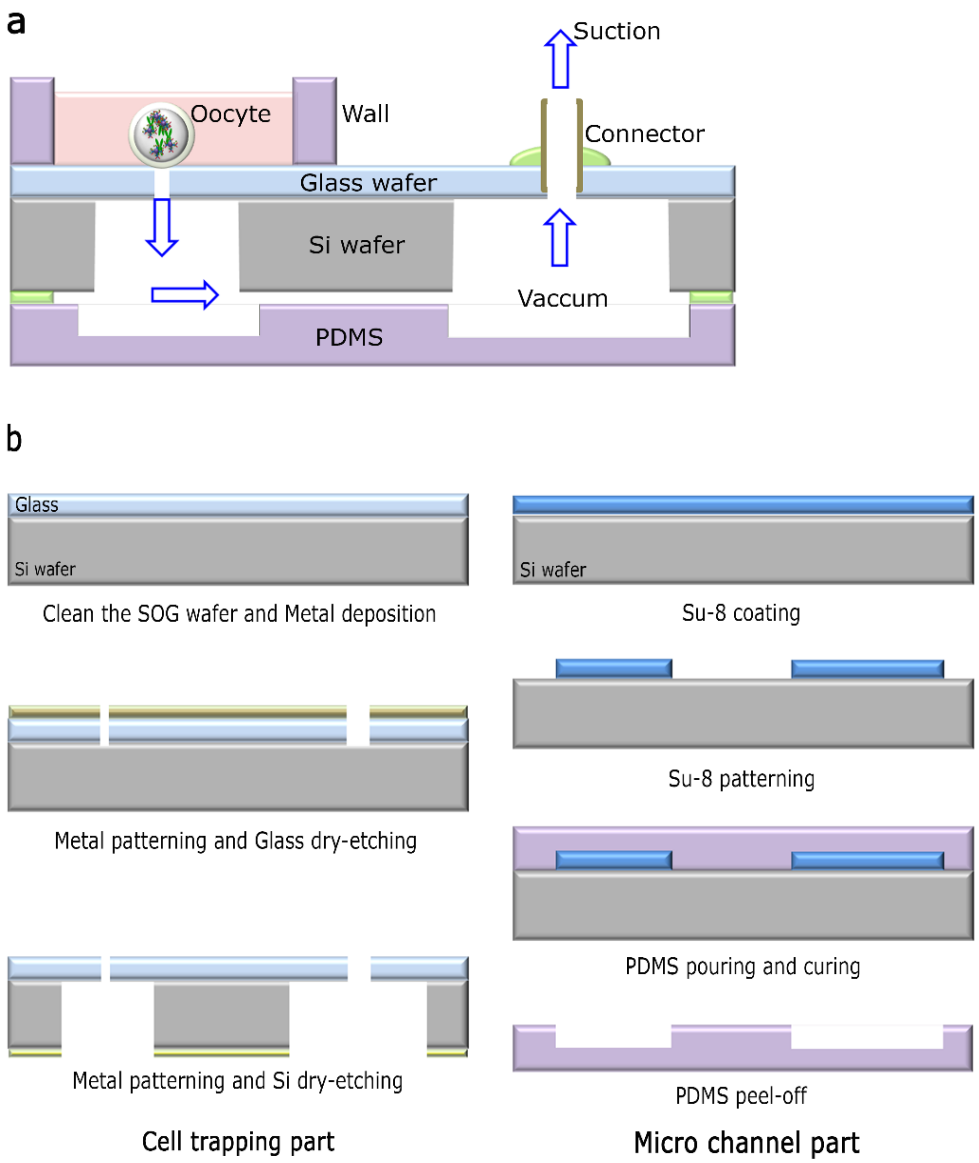

Figure 3-12 Microfluidic cell trapping device (a) concept of trapping device (b) process flow

3.3.4.2 Fabrication result

Considering the size of mouse oocytes (ø: 70-80 μm), holes of various sizes (ø = 20~40 μm) were designed to ensure the optimal capturing condition. After assembling the top and bottom substrates as shown in Fig. 3-13, we tested the micro trapping device using micro spheres (~100 μm). The micro sphere in the medium chamber was trapped at the holes connected to the vacuum chamber. Pressure of the chamber was controlled by a micromanipulator (IM- 9B and 9C, Narishige, Japan) attached to inverted microscope (TE 2000-E, Nikon, Japan). When the control pressure was applied to the device, micro sphere was rapidly attracted towards the holes as shown in Fig. 3-13 (b).

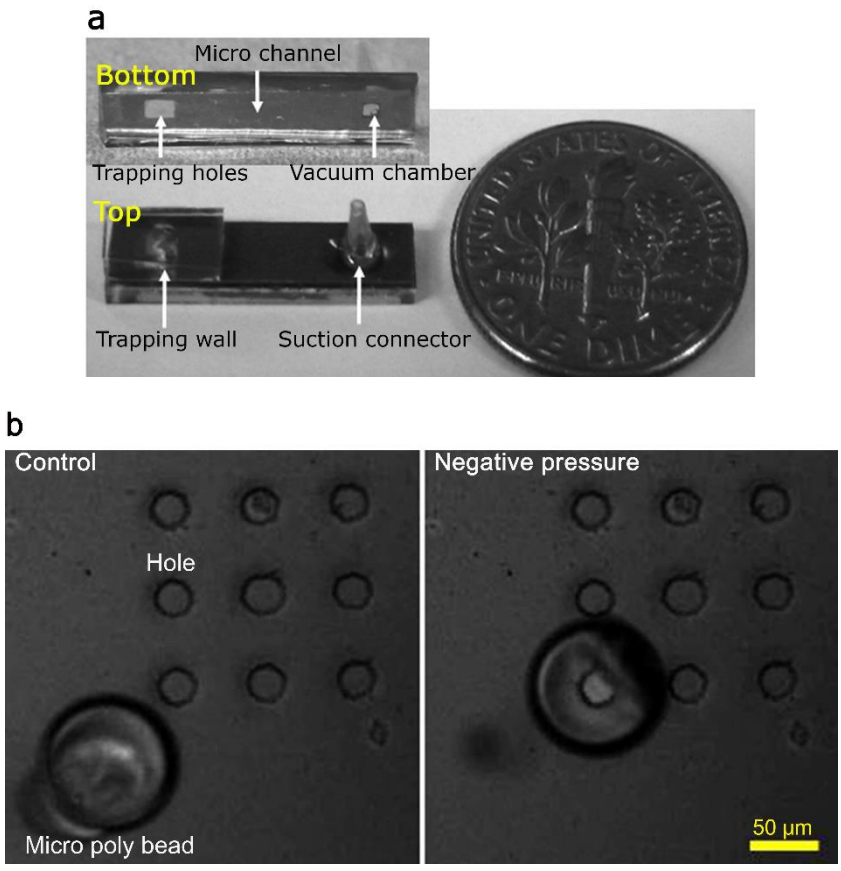

Figure 3-13 Microfluidic cell trapping device. (a) The integrated Microfluidic trapping cell device. (b) Device test by using poly bead.

3.3.4.3 Experimental setup

To observe lateral movement using the microscope, as shown in Fig. 3-14, we prevented the rotation and drift of the live oocyte by anchoring it to the substrate. The oocytes were immobilized in the trapping hole. A magnetic field (B) was applied to the oocyte at a distance of ~5 mm. The oocytes in the medium chamber were trapped at the holes connected to the vacuum chamber. Pressure of the chamber was controlled by a micromanipulator (IM- 9B and 9C, Narishige, Japan) attached to inverted microscope (TE 2000-E, Nikon, Japan). When the control pressure was applied to the device, the oocytes were rapidly attracted to and fixed on the holes in the microfluidic trapping device. After cellular internalization of H1-BMPs, the extracellular H1-BMPs were washed with fresh medium several times. The chromosomes were then stained with Hoechst for an easy observation of movement in a live cell. To monitor the chromosome position in real time, each cell was immobilized on the vacuum-assisted micro-trapping device. The images were captured by the inverted fluorescence microscope at intervals of 10 min up to 80 min. The sequence of captured images shows the lateral motion of the chromosomes toward the applied magnetic field. The maximum duration of observation was limited by photobleaching.

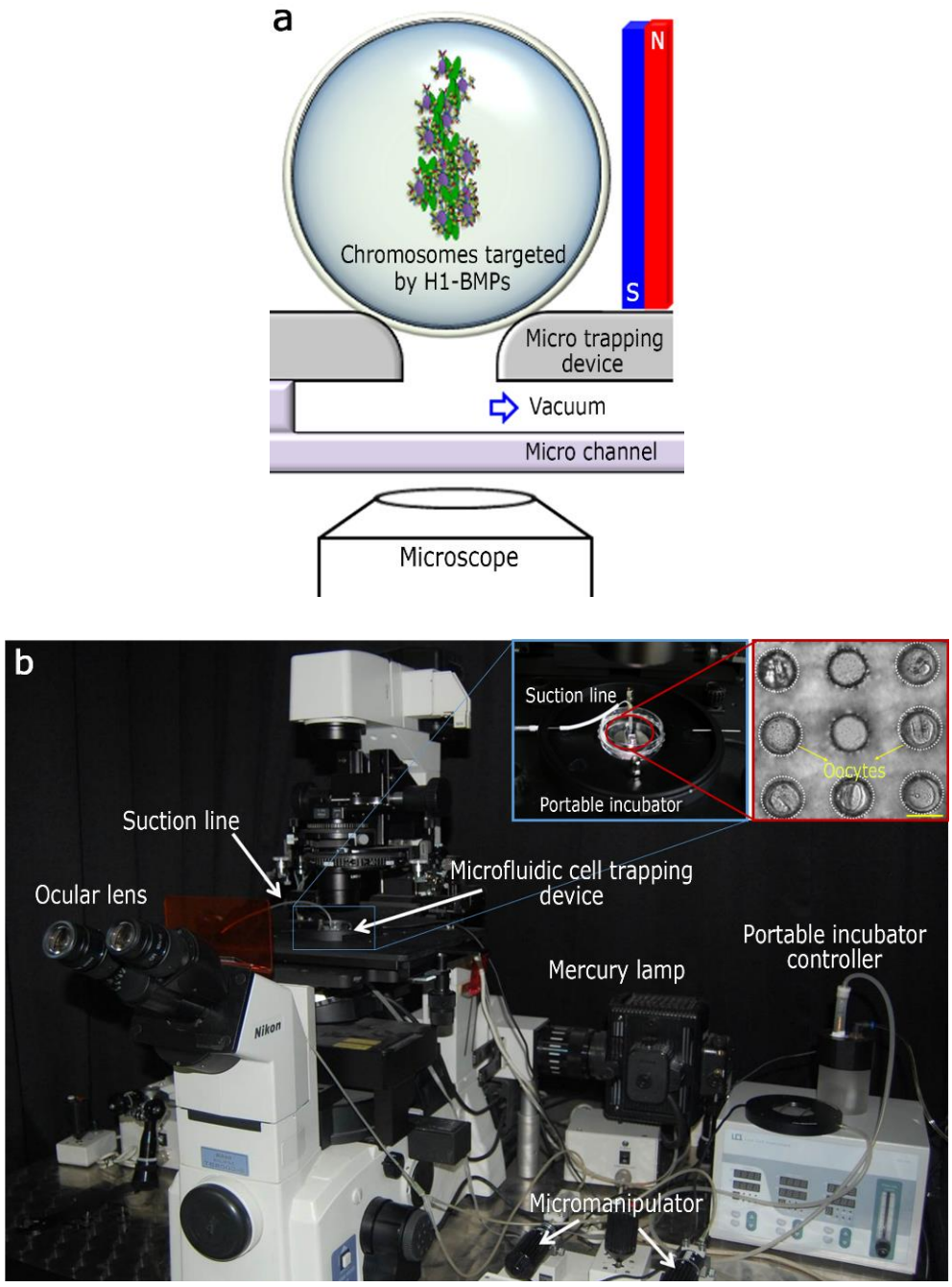

Figure 3-14 Experimental setup for observation of chromosome movement in real time. (a) Concept of setup. (b) Configuration of experimental setup.

3.3.4.4 Experimental result

We observed the motion of the chromosomes in real time. The chromosomes were then stained with Hoechst for an easy observation of movement in a live cell. To monitor the chromosome position in real time, each cell was immobilized on the vacuum-assisted micro-trapping device. The images were captured by the inverted fluorescence microscope at intervals of 10 min up to 80 min. The sequence of captured images shows the lateral motion of the chromosomes toward the applied magnetic field. The maximum duration of observation was limited by photobleaching. When the magnetic field (**B**) of 168 mT was applied to the side of microfludic trapping device at a distance of ~ 5 mm from the trapped oocyte, the chromosomes started moving to the direction of the magnetic field gradient. Since it was difficult to place the magnet at the close proximity the strength of the magnetic field was much smaller than that of the previous experiments when the magnets were directly placed under the petridish. As a result, the motion was slow, almost stopped after traveling a short distance, e.g., ~ 6 μm. We believe that the movement of the chromosomes linked to the H1-BMP can be severely hindered by cytosol viscosity and cytoskeletal network.

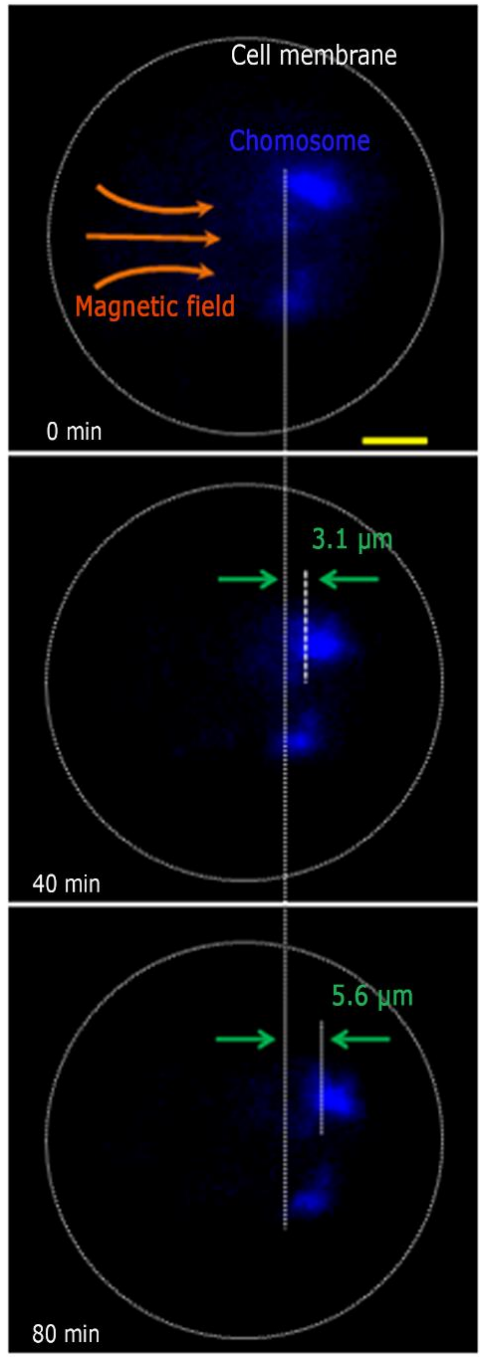

Figure 3-15 Time course monitoring of the chromosomes. Scale bar = 10 μm.

3.4 Analysis and modeling of chromosome movement in oocyte

3.4.1 Method

We stained actin filament with the actin cytoskeleton staining kit (Milliopre, USA) to investigate the chromosomes movement in cytosol since it is believed that actin filament is important barrier in the absence of microtubule. To stain the oocytes, cells were fixed with 4% faraformaldehyde in 1x PBS for 20 min at room temperature. After washing oocytes with 1x wash buffer (1x PBS containing 0.05% Tween-20), transfer them into blocking solution (1% BSA in 1x PBS) for 30 minutes at room temperature. TRITC-conjugateed phalloidin is added into blocking solution for 1 hr at room temperature. The optimal dilution for TRITC-conjugated phalloidin is 1:1000. After washing three times, cells were stained with DAPI for 5 min and then washed them three times. To prevent the photobleaching, antifade solution (Invitrogen, USA) was used.

3.4.2 Analysis and modeling

The motion of the chromosomes was significantly affected by the cytoplasmic matrix. Though the motion of the BMPs in a free solution was observed to occur instantly with application of the magnetic field (B), the chromosomes in the oocyte migrated through the cytosol very slowly. The actin filaments in a cell construct a tightly entangled meshwork with an average mesh size on the order of 100 nm to 1 μm [99]. The motion of condensed chromosomes with a size in the range of 1-2 μm would be hindered by such a network [100]. With the absence of the microtubules due to nocodazole treatment, the actin filaments are considered a major hurdle against the motion of chromosomes. Thus, we investigated the distribution of the actin filament in oocyte. After H1-BMP delivery, we cultured oocyte for 1 day. The images were captured by confocal laser scanning microscopy after staining the nuclear and actin filament. Figure 3-16(a) shows confocal images of actin filaments, chromosomes, and H1-BMPs. Chromosome was stained with DAPI. Thus blue color represented chromosomes. The green color signified the H1-BMPs. The red color indicated actin filament. It is found that H1-BMPS were well internalized and some H1-BMPs targeted chromosomes through overlapping of green and blue. We also knew that density of actin filaments increases near the surface. This result, together with the fact that the density of actin filaments increases near the surface, can elucidates why the chromosomes did not move all the way to the membrane, despite total forces ranging from tens to hundreds of pN.

Furthermore, the traction forces exerted on the multiple locations of the chromosome would create the entanglement illustrated by our model for the motion. Figure 3-16(b)

shows the model that explains the hindrance mechanism together with the confocal image of actin filaments, chromosomes, and H1-BMPs.

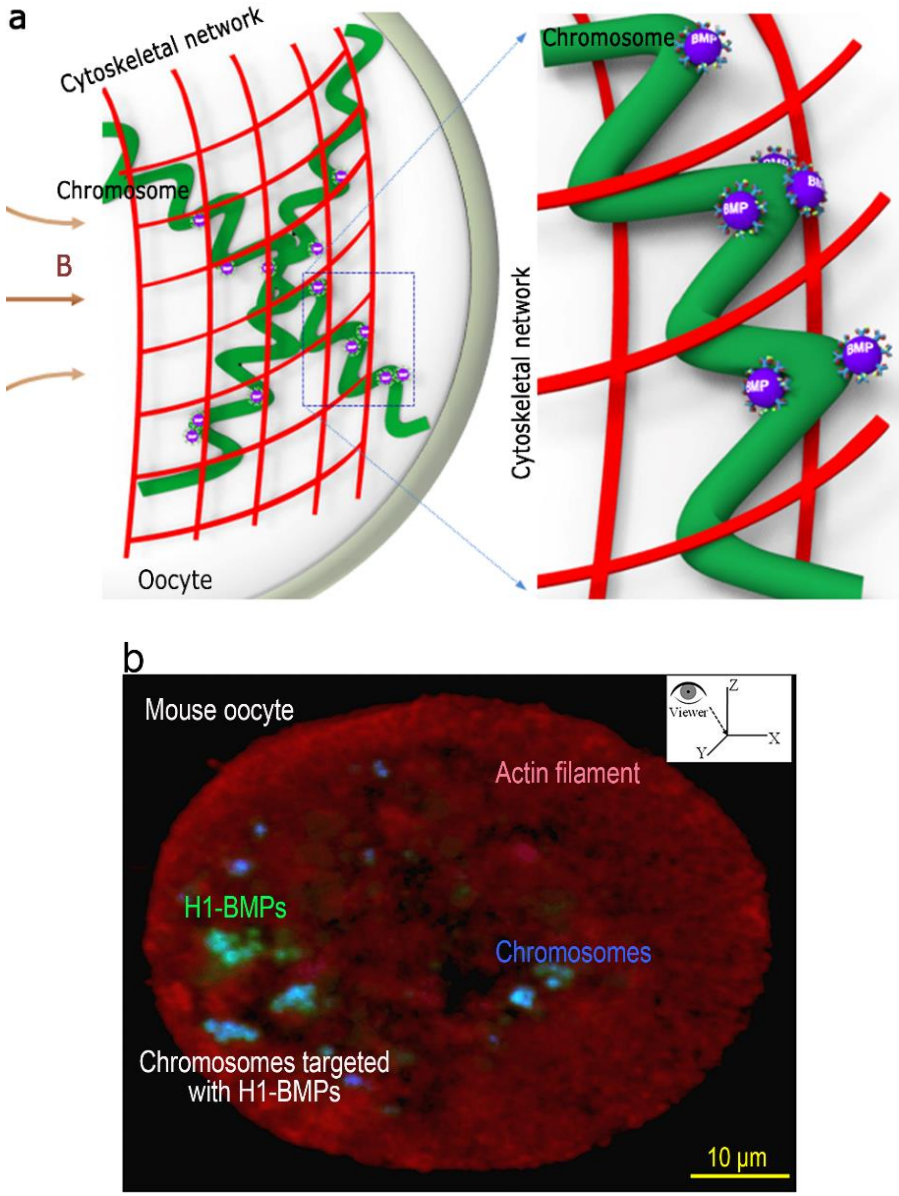

Figure 3-16 Chromosomes movement in cytosol induced by a magnetic field (B). (a) Tilted view of oocyte by restructuring confocal images (Actin filament, red; H1-BMPs, green; chromosomes, blue; light blue, overlapping of green and blue). (b) Chromosomes movement can can be strongly hindered by physical obstacle of the network of cytoskeleton filaments. The scale bar is 10 μm.

CHAPTER 4. NEW APPROACH FOR SCNT PROCESS

4-1 Stem cell

4.1.1 Stem cells

Stem cell has the remarkable potential to differentiate into various cell types in the body. When a stem cell divides, each cell has the potential either to remain a stem cell or become another type of cell with a more specialized function [101]. Stem cells can be divided as totipotent, pluripotent, and multipotent cells depending on their differential potential [54]. Totipotent cells have the ability to differentiate into embryonic and extraembryonic cell types. This indicates that the therapeutic value of totipotent stem cells is enormous. Human development begins after a sperm fertilizes an oocyte and the resulting fertilized egg generate a single totipotent cell, termed as a zygote which is examples of totipotent cells. After reaching a 16-cell stage, the totipotent cells of the morula differentiate into cells that will eventually become either the blastocyst's Inner cell mass or the outer trophoblasts. The totipotent cells can move to pluripotent cells that can differentiate into any of the three germ layers such as endoderm, mesoderm, or ectoderm. These germ layers are the embryonic source of all cells of the body such as stomach lining, lungs, muscle, bone, nervous system and so on. Unlike totipotent stem cells, pluripotent cells cannot give rise to an entire organism. As these pluripotent stem cells continue to divide, they begin to specialize further. The multipotent cells describe progenitor cells that

activate potential to differentiate into multiple. For example, a multipotent blood stem cell is a hematopoietic cell. Thus, this cell type can differentiate itself into several types of blood cell types like lymphocytes, monocytes, and neutrophils but cannot differentiate into brain cells, bone cells or other non-blood cell types.

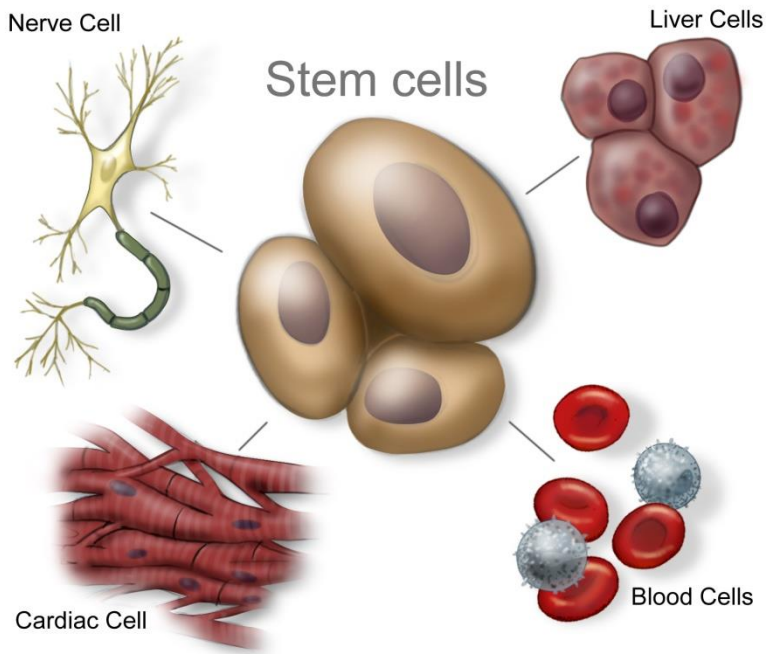

Figure 4-1 Potential of stem cell (http://www.bibalex.org)

4.1.2 Methods for generation of stem Cells

Embryonic stem cells (ESCs) are pluripotent stem cells that are derived from the inner cell mass of the blastocyst. The scientists first discovered ways to isolate and culture ESCs from early mouse embryos in 1981, nearly 35 years ago [55]. They developed a method in 1998 to derive stem cells from frozen human embryos that are no longer needed for in vitro fertilization [53]. Until recently, scientists worked with two kinds of stem cells from animals and human such as embryonic stem cells and non-embryonic stem cell. Stem cell can be generated by several methods such as fertilization, somatic cell nuclear transfer(SCNT), parthenogenesis, and transcription factor transduction.

4.1.2.1 Fertilization

A major method to generate the pluripotent stem cells for research purposes is unused embryo donated by couples undergoing in vitro fertilization (IVF). The donated embryos are placed in a media preparation in special dishes and allowed to develop for a few days. At about the fifth day the embryo reaches the blastocyst stage and forms a ball of 100-200 cells. At this stage, ES cells are derived from the blastocyst's inner cell mass (IMC). In some cases, the ES cells can be isolated even before the blastocyst stage. If an inner cell mass is obtained from a blastocyst and cultured in medium, the pluripotent cells can be generated in the laboratory.

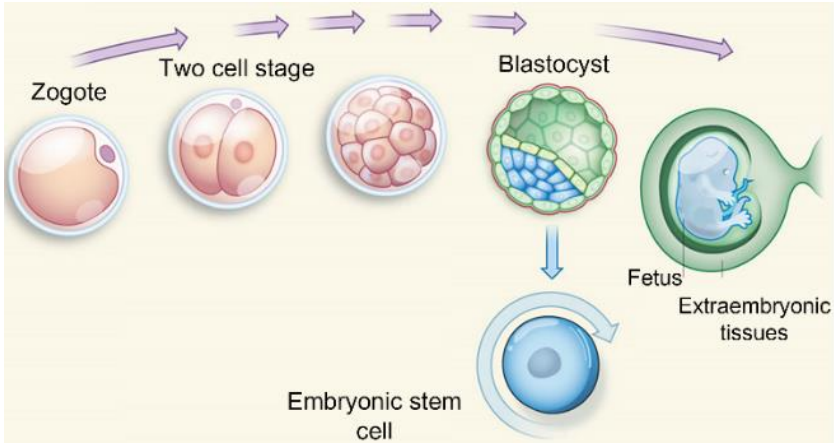

Figure 4-2 Embryonic stem cell in fertilization [15]

4.1.2.2 Somatic cell nuclear transfer (SCNT)

Of all the techniques for making pluripotent cells, nuclear transfer (NT) is the most technically demanding. Although ESCs are promising donor sources in cell transplantation therapies, they face an ethical issue regarding the destruction of human embryos. To circumvent this limitation, an existing laboratory technique was revived for creating a blastula with the transfer of a donor nucleus to a enucleated egg, laterally called somatic cell nuclear transfer [102, 103]. This technique of nuclear transfer (NT) involves a somatic cell and encleated oocyte. The nuclear DNA extracted from the somatic cells is transplanted into the enucleated oocyte that is to be removed chromosome. This hybrid oocyte is stimulated to start the development of an embryo by electric pulse or chemical agents. Various somatic cells such as mammary epithelial cells, leukocytes, and myocytes have successfully used as donor cells for SCNT.

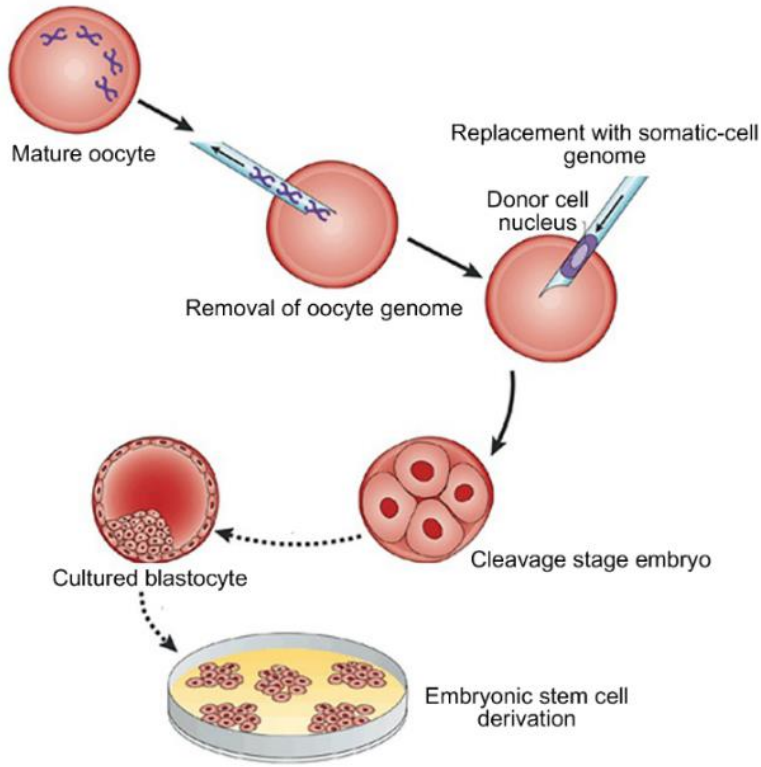

Figure 4-3 Somatic cell nuclear transfer (SCNT) procedure

4.1.2.4 Parthenogenesis

Parthenogenesis is a type of asexual reproduction that is development of an egg without fertilization. It is the term used to describe the process that certain animals are able to reproduce themselves in successive female generations without intervention of a male of the species as lizard tail. Figure 4-4 shows the in vitro fertilization (IVF) and parthenogenetic development. In fertilization process, the activation of embryonic development generally occurs after an egg is fertilized by a sperm. In parthenogenesis, however, the diverse the stimuli for the egg is necessary to active such as electrical and chemical method [51, 52, 68]. Parthenogenesis process is widely used to produce the piglet after nuclear transfer [57, 69, 70] and intracytoplasmic sperm injection (ICSI) [71, 72]. However, the efficiency is still lower. Actually, the mechanism of parthenogenetic activation is not known but apparently include certain changes in the egg membrane.

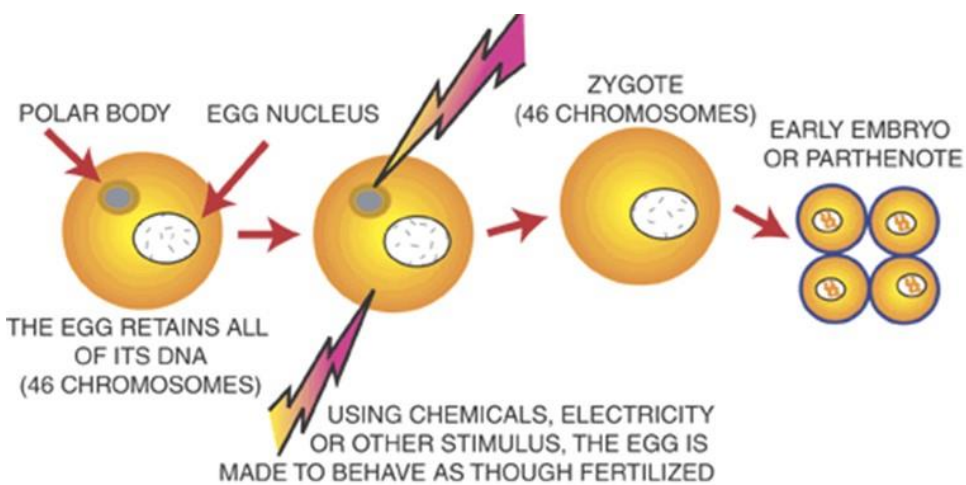

Figure 4-4 In vitro fertilization (IVF) Vs Parthenogenetic development from Creative commons (http://geneticsandsociety.org)

4.1.2.5 Transcription factor transduction

These are not adult stem cells but are created from adult skin cells after genetically programming by artificial stimulus such as chemical. In 2007, scientists published paper that described genetic reprogramming of human adult somatic cells into pluripotent human stem cells [51, 68]. Shinya Yamanaka group reported that they could use a retroviral expression vector to introduce four important stem cell factors (Oct4, Sox2, Myc, and Klf4) into adult mouse cells and reprogram them to behave like ES cells [52]. They called the reprogrammed cells "iPSCs," for induced pluripotent stem cells. Since iPSCs can be converted directly from adult tissues, they not only bypass the need for embryos, but can be made in a patient-matched manner, which means that each individual could have their own pluripotent stem cell line.

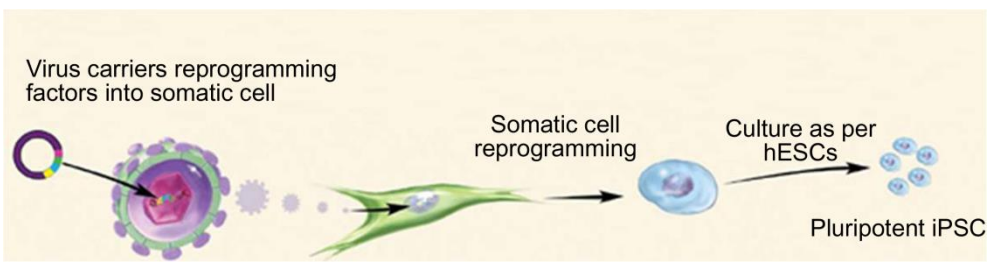

Figure 4-5. Generation of iPSC (http://stemcells.nih.gov)

4.2 Alternative approach for SCNT without enucleation

4.2.1 Experimental concept

Recently, although human stem cell were generated by somatic cell nuclear transfer (SCNT),[104, 105] the enucleation process is still important factor in SCNT. It is well known that the invasive enucleation (removal of human oocyte genome) leads to the failure of embryonic development after genome exchange due to the loss of meiosis-specific factors associated with the spindle removal during physical enucleation process.[59] Thus, we suggest the non-invasive method for SCNT without enucleation as depicted in Fig. 4-6. The control of chromosome activity is achieved by targeting chromosome with H1-BMPs. To achieve it, two possibilities have to be pre-verified. First, there are no interaction between chromosomes in somatic cell and unbounded H1-BMPs in oocyte after somatic cell – oocyte fusion. Second, to deactivate chromosome activity, specific time is necessary to target chromosome with H1-BMPs. Thus, it is required to investigate whether oocyte move to blastocyst stage after delay in activation for 10 hrs. Blastocyst formation was evaluated by the morphological observations and cell developmental efficiency was calculated from four independent replicate experiments.

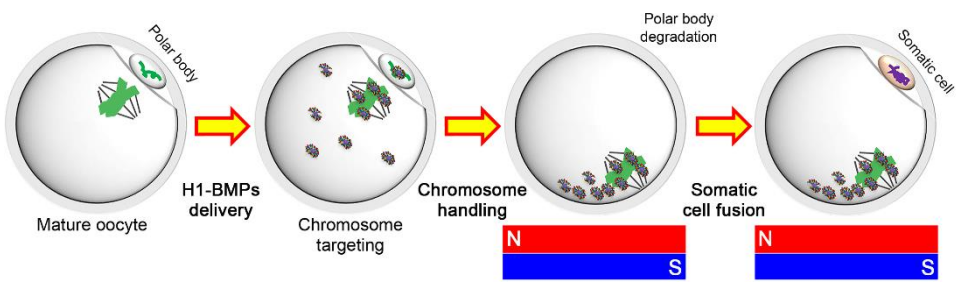

Figure 4-6. Suggested method for SCNT without enucleation.

4.2.1.1. Prevention of interaction between unbounded H1-BMPs in oocyte and chromosome in somatic cell

As we mentioned previously, H1-BMPs was designed to target the Histone H1 protein in chromosome of oocyte. Thus, oocyte-specific-histone H1 antibody was used. Through specific targeting test, it is verified that H1-BMPs have the affinity to Histone H1 proteins. Thus, it is expected that there are no interactions between H1-BMPs and chromosome in somatic cell. To verify it again, we delivered H1-BMPs into fibroblast to target chromosome. After delivery H1-BMP into fibroblast cells, we cultured cell for 24hrs. To investigate the specific binding, cells are fixed. Figure 4-7 shows that H1-BMPs do not target chromosome in somatic cell.

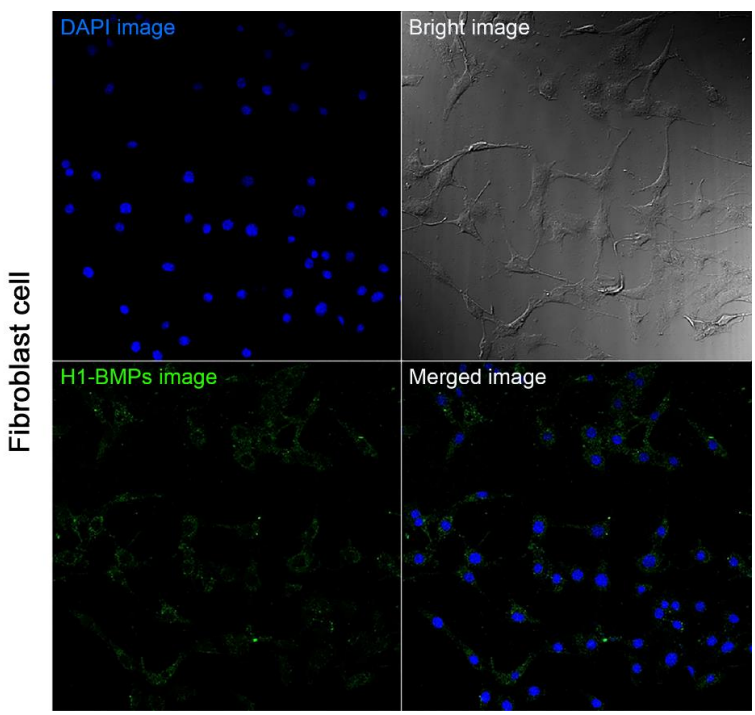

Figure 4-7 H1-BMPs targeting test to blastocyst cell

Although we know that H1-BMPs have an affinity to only chromosome in oocyte, antibody affinity is not perfect. Thus we control H1-BMPs and chromosome attached to H1-BMPs location by an external magnetic field in order to separate them from chromosome in somatic cell. Figure 4-8 shows the position of H1-BMPs and chromosome targeted by H1-BMPs can be controlled by magnetic field. Through result, if the position of unbounded H1-BMPs is controlled before somatic cell chromosomes are fused with oocyte chromosomes, the interaction can be prevented.

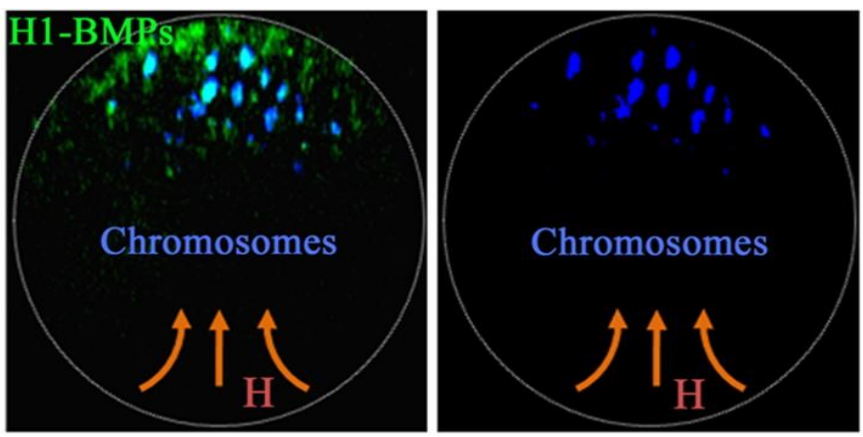

Figure 4-8. Spatial control of H1-BMPs and chromosome with a magnetic field. The image is a rotated 3D cell structure image.

4.2.1.2. Blastocyst efficiency after activation delay

To apply our technique about chromosome deactivation with H1-BMPs, specific time (10 hrs) is necessary to target chromosome with H1-BMPs as shown in Fig. 4-9. Thus, it is required to investigate whether oocyte move to blastocyst stage after delay in activation for 10 hrs. Blastocyst formation was evaluated by the morphological observations and cell developmental efficiency was calculated from four independent replicate experiments.

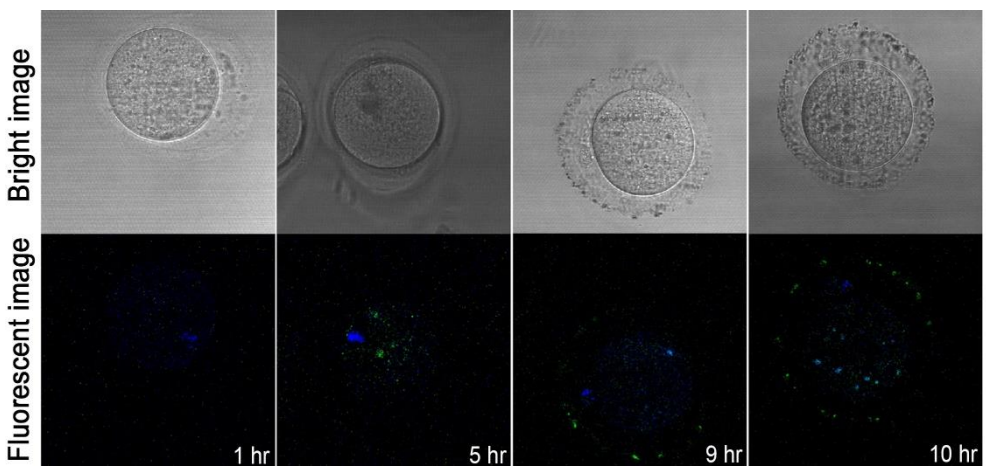

Figure 4-9 Targeting time of H1-BMPs to chromosome in oocyte

In control, there is no delay time after oocyte extraction from mouse. However, in 'sample', parthenogentic activation is delayed for 10 hrs after oocyte extraction. Figure 4-10 shows that oocytes in sample were well developed and reached the blastocyst stage with ~ 20 % efficiency against the ~60% efficiency in control sample despite the delay in activation time.

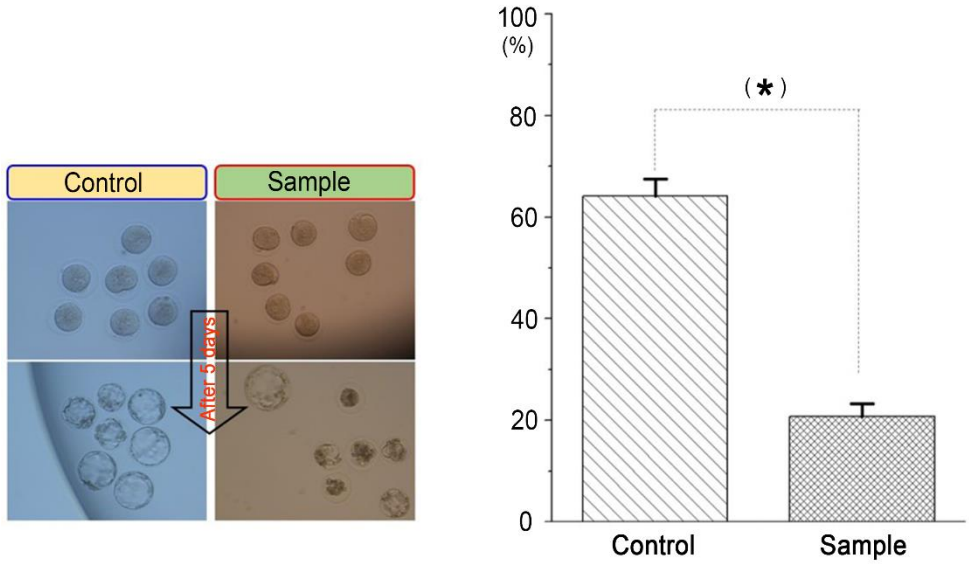

Figure 4-10 Blastocyst efficiency after activation delay

4.2.2 Future work

Through result, we can know that our technique has a potential for SCNT. Thus, we have a plan to directly do the SCNT process by using zebra fish oocyte. Oocyte in zebra fish has several advantages compared to mouse oocyte. First, it is suitable for collection of oocyte. To collect over 100 oocytes in mice, we have to kill more 3 mice. However, only a single zebra fish can generate more 100 oocytes without death. Second, the handling of oocyte in zebra fish is easy since its size is about 1 mm (mouse oocyte: ~0.1 mm).

Recently, human stem cell was generated by SCNT process. The efficiency of stem cell is about 20 % in spite of intracellular protein loss during enucleation. However, the enucleation process is still important for SCNT process. In our method, although the blastocyst efficiency is about 20% after delay of activation for 10 hrs, there are several merits instead of traditional SCNT process. First, if our method is applied, enucleation process is not necessary. The efficiency of traditional SCNT can be dependent on the skillful expert. However, there are no special skill in our method. Anybody can do this way. Second, we can do the H1-BMPs based SCNT by using microfluidic device. In previous work, we fabricated microfluidic cell trapping device. If the microfluidic cell trapping device is modified, we can handle a lot of oocyte at a time. In other words, a lot of stem cell can be generated at same time. The modified microfluidic cell trapping device have to consist of several parts such as cell trapping area, cell fusion area with electric field, cell culture long time, and so on.

CHAPTER 5. CONCLUSIONS

The physical regulation of cellular activities has attracted considerable attention in a broad range from cell biology to biomedical application. Magnetic nanoparticles have provided a powerful tool for spatiotemporal control of regulatory proteins that modulate the intracellular signaling pathway. Here, we described a novel strategy to non-invasively regulate the chromosome activity in living oocyte by using biofunctionalized magnetic nanoparticles. Bacterial magnetic nanoparticles (BMPs)-histone H1 antibodies conjugates (H1-BMPs) are used for specific targeting of chromosomes in oocyte, which hinders their transcriptional expression. Procedures and techniques were well developed. We also demonstrated the traction of whole targeted chromosomes with H1-BMPs, across the entire cell span till near cell membrane by a remote magnetic field. The capability of H1-BMPs to control chromosome activity and can further provide alternative technique to the somatic cell nuclear transfer (SCNT) which suffers from the loss of genetic materials enucleation. To verify the possibility to apply these technique, we investigated the prevention of interaction between unbounded H1-BMPs and chromosome in somatic cell. In addition, blastocyst efficiency was investigated after delay of activation for 10 hrs. These results are achieved through the non-invasive delivery of H1-BMPs into live oocyte.

In addition, our technique will provide a useful tool for investigating cellular functions associated with the spatiotemporal distribution of such components.

REFERENCE

1. Freeman, W.H., *Molecular cell biology. 4th edition.* 2000.
2. B, J.A., Lewis J, et al., *Molecular Biology of the Cell, 4th edition.* New York: Garland Science, 2002.
3. Friedman, J.R. and J. Nunnari, *Mitochondrial form and function.* Nature, 2014. **505**(7483): p. 335-343.
4. Korobeinikova, A.V., M.B. Garber, and G.M. Gongadze, *Ribosomal proteins: structure, function, and evolution.* Biochemistry (Mosc), 2012. **77**(6): p. 562-74.
5. Healy, S., et al., *Biology of the Endoplasmic Reticulum*, in *Endoplasmic Reticulum Stress in Health and Disease*, P. Agostinis and S. Afshin, Editors. 2012, Springer Netherlands. p. 3-22.
6. Andreeva, A.V., et al., *The structure and function of the Golgi apparatus: a hundred years of questions.* Journal of Experimental Botany, 1998. **49**(325): p. 1281-1291.
7. http://web.archive.org/web/20070311230518/http://sun.menloschool.org/~birchler/cells/animals/cytoplasm/.
8. Alberts B, e.a., *Essential cell biology second edition.* Garland Science, 2004.
9. van der Vaart, B., A. Akhmanova, and A. Straube, *Regulation of microtubule dynamic instability.* Biochem Soc Trans, 2009. **37**(Pt 5): p. 1007-13.
10. Vale, R.D., *The Molecular Motor Toolbox for Intracellular Transport.* Cell,

2003. **112**(4): p. 467-480.

11. Ashkin, A., *Acceleration and Trapping of Particles by Radiation Pressure.* Physical Review Letters, 1970. **24**(4): p. 156-159.

12. Ashkin, A., et al., *Observation of a single-beam gradient force optical trap for dielectric particles.* Opt. Lett., 1986. **11**(5): p. 288-290.

13. Ashkin, A., J.M. Dziedzic, and T. Yamane, *Optical trapping and manipulation of single cells using infrared laser beams.* Nature, 1987. **330**(6150): p. 769-771.

14. Berns, M.W., et al., *Use of a laser-induced optical force trap to study chromosome movement on the mitotic spindle.* Proceedings of the National Academy of Sciences, 1989. **86**(12): p. 4539-4543.

15. Haowei, W., et al., *Isolation of a single rice chromosome by optical micromanipulation.* Journal of Optics A: Pure and Applied Optics, 2004. **6**(1): p. 89.

16. Allemand, J.F., et al., *Stretched and overwound DNA forms a Pauling-like structure with exposed bases.* Proceedings of the National Academy of Sciences, 1998. **95**(24): p. 14152-14157.

17. Wuite, G.J., et al., *Single-molecule studies of the effect of template tension on T7 DNA polymerase activity.* Nature, 2000. **404**(6773): p. 103-6.

18. Neuman, K.C. and A. Nagy, *Single-molecule force spectroscopy: optical tweezers, magnetic tweezers and atomic force microscopy.* Nat Meth, 2008. **5**(6): p. 491-505.

19. Konig, K., et al., *Cell damage by near-IR microbeams.* Nature, 1995.

377(6544): p. 20-21.

20. Carlos, B., C.M. Jed, and J.L.W. Gijs, *Grabbing the cat by the tail: manipulating molecules one by one.* Nature Reviews Molecular Cell Biology, 2000. **1**(2): p. 130-136.

21. Jeffries, G.D., et al., *Using polarization-shaped optical vortex traps for single-cell nanosurgery.* Nano Lett, 2007. **7**(2): p. 415-20.

22. Ishøy, T., et al., *An improved method for single cell isolation of prokaryotes from meso-, thermo- and hyperthermophilic environments using micromanipulation.* Applied Microbiology and Biotechnology, 2006. **69**(5): p. 510-514.

23. Hamill, O.P., et al., *Improved patch-clamp techniques for high-resolution current recording from cells and cell-free membrane patches.* Pflugers Arch, 1981. **391**(2): p. 85-100.

24. Palermo, G., et al., *Pregnancies after intracytoplasmic injection of single spermatozoon into an oocyte.* Lancet, 1992. **340**(8810): p. 17-8.

25. Begg, D.A. and G.W. Ellis, *Micromanipulation studies of chromosome movement. I. Chromosome-spindle attachment and the mechanical properties of chromosomal spindle fibers.* J Cell Biol, 1979. **82**(2): p. 528-41.

26. Lammerding, J., et al., *Nuclear mechanics and methods.* Methods Cell Biol, 2007. **83**: p. 269-94.

27. Binnig, G., C.F. Quate, and C. Gerber, *Atomic Force Microscope.* Physical Review Letters, 1986. **56**(9): p. 930-933.

28. Jalili, N. and K. Laxminarayana, *A review of atomic force microscopy imaging systems: application to molecular metrology and biological sciences.* Mechatronics, 2004. **14**(8): p. 907-945.

29. Gould, S., et al., *Molecular resolution images of amino acid crystals with the atomic force microscope.* Nature, 1988. **332**(6162): p. 332-334.

30. Chang, K.-C., et al., *Atomic force microscopy in biology and biomedicine.* Tzu Chi Medical Journal, 2012. **24**(4): p. 162-169.

31. Puchner, E.M. and H.E. Gaub, *Exploring the Conformation-Regulated Function of Titin Kinase by Mechanical Pump and Probe Experiments with Single Molecules.* Angewandte Chemie International Edition, 2010. **49**(6): p. 1147-1150.

32. Gumpp, H., et al., *Ultrastable combined atomic force and total internal reflection fluorescence microscope [corrected].* Rev Sci Instrum, 2009. **80**(6): p. 063704.

33. Mandal, M. and R.R. Breaker, *Gene regulation by riboswitches.* Nat Rev Mol Cell Biol, 2004. **5**(6): p. 451-63.

34. Rippe, K., et al., *Transcriptional activation via DNA-looping: visualization of intermediates in the activation pathway of E. coli RNA polymerase·σ54 holoenzyme by scanning force microscopy.* Journal of Molecular Biology, 1997. **270**(2): p. 125-138.

35. Heus, H.A., et al., *Atomic force microscope-based single-molecule force spectroscopy of RNA unfolding.* Analytical Biochemistry, 2011. **414**(1): p. 1-6.

36. Skibbens, R.V. and E.D. Salmon, *Micromanipulation of chromosomes in mitotic vertebrate tissue cells: tension controls the state of kinetochore movement.* Exp Cell Res, 1997. **235**(2): p. 314-24.

37. Ikai, A., et al., *Mechanical measurements of a single protein molecule and human chromosomes by atomic force microscopy.* Materials Science and Engineering: C, 1997. **4**(4): p. 233-240.

38. Hosu, B.G., et al., *Magnetic tweezers for intracellular applications.* Review of Scientific Instruments, 2003. **74**(9): p. 4158-4163.

39. Crick, F.H.C., *The physical properties of cytoplasm. A study by means of the magnetic particle method. Part II. Theoretical treatment.* Experimental Cell Research, 1950. **1**(4): p. 505-533.

40. Smith, S.B., L. Finzi, and C. Bustamante, *Direct mechanical measurements of the elasticity of single DNA molecules by using magnetic beads.* Science, 1992. **258**(5085): p. 1122-6.

41. Gosse, C. and V. Croquette, *Magnetic tweezers: micromanipulation and force measurement at the molecular level.* Biophys J, 2002. **82**(6): p. 3314-29.

42. Ziemann, F., J. Rädler, and E. Sackmann, *Local measurements of viscoelastic moduli of entangled actin networks using an oscillating magnetic bead micro-rheometer.* Biophysical Journal, 1994. **66**(6): p. 2210-2216.

43. Amblard, F., et al., *Subdiffusion and Anomalous Local Viscoelasticity in Actin Networks.* Physical Review Letters, 1996. **77**(21): p. 4470-4473.

44. Gao, J., et al., *Intracellular Spatial Control of Fluorescent Magnetic Nanoparticles.* Journal of the American Chemical Society, 2008. **130**(12): p. 3710-3711.

45. Hoffmann, C., et al., *Spatiotemporal control of microtubule nucleation and assembly using magnetic nanoparticles.* Nat Nanotechnol, 2013. **8**(3): p. 199-205.

46. de Vries, A.H.B., et al., *Direct Observation of Nanomechanical Properties of Chromatin in Living Cells.* Nano Letters, 2007. **7**(5): p. 1424-1427.

47. Cho, M.H., et al., *A magnetic switch for the control of cell death signalling in in vitro and in vivo systems.* Nat Mater, 2012. **11**(12): p. 1038-1043.

48. Gorostiza, P. and E.Y. Isacoff, *Optical switches for remote and noninvasive control of cell signaling.* Science, 2008. **322**(5900): p. 395-9.

49. Pankhurst, Q.A., et al., *Applications of magnetic nanoparticles in biomedicine.* Journal of Physics D: Applied Physics, 2003. **36**(13): p. R167.

50. Lu, A.-H., E.L. Salabas, and F. Schüth, *Magnetic Nanoparticles: Synthesis, Protection, Functionalization, and Application.* Angewandte Chemie International Edition, 2007. **46**(8): p. 1222-1244.

51. Miyakoshi, J., *Effects of static magnetic fields at the cellular level.* Prog Biophys Mol Biol, 2005. **87**(2-3): p. 213-23.

52. Nam, J.M., C.S. Thaxton, and C.A. Mirkin, *Nanoparticle-based bio-bar codes for the ultrasensitive detection of proteins.* Science, 2003. **301**(5641): p. 1884-6.

53. Weissleder, R., et al., *In vivo magnetic resonance imaging of transgene*

expression. Nat Med, 2000. **6**(3): p. 351-5.

54. Lee, J.-H., et al., *Exchange-coupled magnetic nanoparticles for efficient heat induction.* Nat Nano, 2011. **6**(7): p. 418-422.

55. Dobson, J., *Gene therapy progress and prospects: magnetic nanoparticle-based gene delivery.* Gene Ther, 2006. **13**(4): p. 283-287.

56. Gao, J., et al., *Intracellular spatial control of fluorescent magnetic nanoparticles.* J Am Chem Soc, 2008. **130**(12): p. 3710-1.

57. Etoc, F., et al., *Subcellular control of Rac-GTPase signalling by magnetogenetic manipulation inside living cells.* Nat Nanotechnol, 2013. **8**(3): p. 193-8.

58. Gorostiza, P. and E.Y. Isacoff, *Optical Switches for Remote and Noninvasive Control of Cell Signaling.* Science, 2008. **322**(5900): p. 395-399.

59. Noggle, S., et al., *Human oocytes reprogram somatic cells to a pluripotent state.* Nature, 2011. **478**(7367): p. 70-5.

60. Tachibana, M., et al., *Human Embryonic Stem Cells Derived by Somatic Cell Nuclear Transfer.* Cell, 2013. **153**(6): p. 1228-1238.

61. Watson, J.D. and F.H.C. Crick, *Molecular Structure of Nucleic Acids: A Structure for Deoxyribose Nucleic Acid.* Nature, 1953. **171**(4356): p. 737-738.

62. Blakemore, R.P., *Magnetotactic bacteria.* Annu Rev Microbiol, 1982. **36**: p. 217-38.

63. Mariño-Ramírez, L., et al., *Histone structure and nucleosome stability.* Expert review of proteomics, 2005. **2**(5): p. 719-729.

64. Olins, A.L. and D.E. Olins, *Spheroid Chromatin Units (v Bodies).* Science, 1974. **183**(4122): p. 330-332.

65. Woodcock, C.L., A.I. Skoultchi, and Y. Fan, *Role of linker histone in chromatin structure and function: H1 stoichiometry and nucleosome repeat length.* Chromosome Res, 2006. **14**(1): p. 17-25.

66. Naciri, M., M. Al-Rubeai, and M.C. Flickinger, *Cell Cycle, Importance in Bioprocesses*, in *Encyclopedia of Industrial Biotechnology*. 2009, John Wiley & Sons, Inc.

67. Elledge, S.J., *Cell Cycle Checkpoints: Preventing an Identity Crisis.* Science, 1996. **274**(5293): p. 1664-1672.

68. Szobota, S., et al., *Remote Control of Neuronal Activity with a Light-Gated Glutamate Receptor.* Neuron, 2007. **54**(4): p. 535-545.

69. Funk, R.H., T. Monsees, and N. Ozkucur, *Electromagnetic effects - From cell biology to medicine.* Prog Histochem Cytochem, 2009. **43**(4): p. 177-264.

70. Chung, I., et al., *Spatial control of EGF receptor activation by reversible dimerization on living cells.* Nature, 2010. **464**(7289): p. 783-7.

71. Gupta, A.K. and M. Gupta, *Synthesis and surface engineering of iron oxide nanoparticles for biomedical applications.* Biomaterials, 2005. **26**(18): p. 3995-4021.

72. Zhang, E., et al., *Dynamic Magnetic Fields Remote-Control Apoptosis via Nanoparticle Rotation.* ACS Nano, 2014. **8**(4): p. 3192-3201.

73. Hoffman, B.D., C. Grashoff, and M.A. Schwartz, *Dynamic molecular*

processes mediate cellular mechanotransduction. Nature, 2011. **475**(7356): p. 316-323.

74. Gorby, Y.A., T.J. Beveridge, and R.P. Blakemore, *Characterization of the bacterial magnetosome membrane.* J Bacteriol, 1988. **170**(2): p. 834-41.

75. Xie, J., K. Chen, and X. Chen, *Production, Modification and Bio-Applications of Magnetic Nanoparticles Gestated by Magnetotactic Bacteria.* Nano Res, 2009. **2**(4): p. 261-278.

76. Tanaka, T. and T. Matsunaga, *Fully automated chemiluminescence immunoassay of insulin using antibody-protein A-bacterial magnetic particle complexes.* Anal Chem, 2000. **72**(15): p. 3518-22.

77. EtocF, et al., *Subcellular control of Rac-GTPase signalling by magnetogenetic manipulation inside living cells.* Nat Nano, 2013. **8**(3): p. 193-198.

78. Lee, S.E., et al., *Remote optical switch for localized and selective control of gene interference.* Nano Lett, 2009. **9**(2): p. 562-70.

79. Ma, L.L., et al., *Selective targeting of antibody conjugated multifunctional nanoclusters (nanoroses) to epidermal growth factor receptors in cancer cells.* Langmuir, 2011. **27**(12): p. 7681-90.

80. Pease, L.F., 3rd, et al., *Determination of protein aggregation with differential mobility analysis: application to IgG antibody.* Biotechnol Bioeng, 2008. **101**(6): p. 1214-22.

81. Hai-Chau Chang, L.-C.W., *A Simple Proof of Thue's Theorem on Circle Packing.* 2010.

82. http://www.sfu.ca/~fankbone/biol/index3.html.

83. Borges, O., et al., *Preparation of coated nanoparticles for a new mucosal vaccine delivery system.* Int J Pharm, 2005. **299**(1-2): p. 155-66.

84. Minsky, M., *Memoir on inventing the confocal scanning microscope.* Scanning, 1988. **10**(4): p. 128-138.

85. Claxton N S, F.T.J., Davidson M W., *Laser scanning confocal microscopy (http://www.olympusconfocal.com/theory/LSCMIntro.pdf).* December 12, 2008.

86. Conchello, J.A. and J.W. Lichtman, *Optical sectioning microscopy.* Nat Methods, 2005. **2**(12): p. 920-31.

87. Scherer, F., et al., *Magnetofection: enhancing and targeting gene delivery by magnetic force in vitro and in vivo.* Gene Ther, 2002. **9**(2): p. 102-9.

88. Kim, D.-H., et al., *Biofunctionalized magnetic-vortex microdiscs for targeted cancer-cell destruction.* Nat Mater, 2010. **9**(2): p. 165-171.

89. Arruebo, M., et al., *Magnetic nanoparticles for drug delivery.* Nano Today, 2007. **2**(3): p. 22-32.

90. Rudolf, H., et al., *Magnetic particle hyperthermia: nanoparticle magnetism and materials development for cancer therapy.* Journal of Physics: Condensed Matter, 2006. **18**(38): p. S2919.

91. Dobson, J., *Remote control of cellular behaviour with magnetic nanoparticles.* Nat Nano, 2008. **3**(3): p. 139-143.

92. Matsunaga, T. and Y. Okamura, *Genes and proteins involved in bacterial magnetic particle formation.* Trends Microbiol, 2003. **11**(11): p. 536-41.

93. Boyer, T.H., *The force on a magnetic dipole.* American Journal of Physics, 1988. **56**(8): p. 688-692.

94. Jung, T., et al., *Biodegradable nanoparticles for oral delivery of peptides: is there a role for polymers to affect mucosal uptake?* Eur J Pharm Biopharm, 2000. **50**(1): p. 147-60.

95. Zauner, W., N.A. Farrow, and A.M. Haines, *In vitro uptake of polystyrene microspheres: effect of particle size, cell line and cell density.* J Control Release, 2001. **71**(1): p. 39-51.

96. Foster, K.A., M. Yazdanian, and K.L. Audus, *Microparticulate uptake mechanisms of in-vitro cell culture models of the respiratory epithelium.* J Pharm Pharmacol, 2001. **53**(1): p. 57-66.

97. Shin, J., et al., *Cell response induced by internalized bacterial magnetic nanoparticles under an external static magnetic field.* Biomaterials, 2012. **33**(22): p. 5650-5657.

98. Berry, C.C., *Possible exploitation of magnetic nanoparticle-cell interaction for biomedical applications.* Journal of Materials Chemistry, 2005. **15**(5): p. 543-547.

99. Wong, I.Y., et al., *Anomalous diffusion probes microstructure dynamics of entangled F-actin networks.* Phys Rev Lett, 2004. **92**(17): p. 178101.

100. Wirtz, D., *Particle-tracking microrheology of living cells: principles and applications.* Annu Rev Biophys, 2009. **38**: p. 301-26.

101. Ozkumur, E., et al., *Inertial Focusing for Tumor Antigen–Dependent and –Independent Sorting of Rare Circulating Tumor Cells.* Science Translational

Medicine, 2013. **5**(179): p. 179ra47.

102. Brunet, S., et al., *Kinetochore fibers are not involved in the formation of the first meiotic spindle in mouse oocytes, but control the exit from the first meiotic M phase.* J Cell Biol, 1999. **146**(1): p. 1-12.

103. Brunet, S. and B. Maro, *Cytoskeleton and cell cycle control during meiotic maturation of the mouse oocyte: integrating time and space.* Reproduction, 2005. **130**(6): p. 801-11.

104. Tachibana, M., et al., *Human Embryonic Stem Cells Derived by Somatic Cell Nuclear Transfer.* Cell. **153**(6): p. 1228-1238.

105. Chung, Young G., et al., *Human Somatic Cell Nuclear Transfer Using Adult Cells.* Cell Stem Cell, 2014. **14**(6): p. 777-780.

KOREAN ABSTRACT

세포 내 신호 전달 경로의 조절은 생물학적 시스템을 이해하는 것에 매우 중요한 요소이다. 따라서, 다양한 방법으로 세포 내 신호를 조절하여 그 기능을 연구하고, 더불어 공간적 제어를 통하여 물리적 특성을 연구하여 왔다. 대표적으로, 광학집게(optical tweezers)가 비침습적으로 정교하게 제어 할 수 있더라도, 여전히 비특정 포획, 제한된 처리량 및 광학 에너지에 의한 세포 손상 등 고유한 문제점이 존재하고 있다. 반면에, 자기 나노 입자(magnetic particle)는 원격 제어와 표면에 다양한 물질을 고정하여 세포 내 기관들과 반응하여 결합을 할 수 있는 장점이 있어 생물의학 응용부터 세포 생물학까지 넓은 범위에 다양하게 이용 할 수 있는 장점을 가지고 있다.

최근에는 자성 나노 입자의 제조 방법의 발달 및 특정 물질의 고정방법 발달로 인하여 자기 공명 이미징(MIR), 세포 행동 제어 연구(control of cell behavior), 세포에 약물 전달(drug delivery) 및 이상 고열을 이용한 암 치료(hyperthermia in cancer therapy) 등 다양한 생물, 의학분야에 기능성 자성 나노 입자(biofunctionalized magnetic nanoparticle)가 활용되고 있다. 더욱

이, 살아 있는 세포 내에 형광을 가진 자성 나노 입자 (fluorescent magnetic nanoparticles)를 세포 내로 전달하고, 외부 자기장을 이용해서 세포 내 전달 된 나노 입자를 이동하여, 세포막 근처에 응집(accumulation) 하여 나노 입자를 이용한 세포 연구의 가능성을 제기하기도 하였다.

본 학위 논문에서는 자성 나노 입자-H1 히스톤 항체 복합체 (H1-BMPs)를 제작하여, 비침습적(non-invasive) 방법으로 쥐 난자 세포 내 염색체를 선별적으로 포획하였다. 포획한 염색체를 인하여 세포 주기를 조절 할 수 있는 가능성을 보였으며, 외부의 자기장을 인가하여, 세포 내 공간적 위치를 제어 할 수 있는 가능성을 보여 주었다. 이러한 결과를 바탕으로 새로운 체세포 핵 이식 방법을 제안하였다.

자기적 특성이 우수한 나노 입자-항체 복합체의 히스톤 H1 항체는 염색체의 전사 활동(transcriptional activity)에 관련 있는 히스톤 H1 단백질을 선별적인 포획 할 수 있도록 설계되어 있다. 복합체는 비침습적(non-invasive) 방법으로 쥐 난자세포 안으로 전달되어, 염색체를 포획하였다. 복합체의 안전성 확인하기 위한 실험으로 성숙(mature) 및 미성숙(immature) 쥐 난자의 처녀생식(parthenogenesis) 방법을 이용하여, 복합체

의 독성 시험을 진행하여 검증하였다. 쥐 난자의 염색체가 복합체에 의해 포획되었을 때, 난자 세포는 4 cell stage까지 진행되었지만, 그 후 세포 퇴화(cell degradation) 시작하여, 배반포(blastocyst)에 도달하지 못하였다. 이 결과의 원인은 쥐 난자 세포에서, 전사 활동(transcription activity)이 4 cell stage 이후에 시작되는데, 염색체를 포획한 복합체가 전사 활동을 방해한 결과로 보인다. 다음으로, 우리는 외부 자기장을 이용하여 복합체에 의해 포획된 염색체를 세포 내에서 이동 시켰다. 항체가 없는 자성을 가진 나노 입자를 세포 내로 전달하여, 자기장을 인가한 한 경우, 자성을 가진 나노 입자는 자기장에 의해 세포 막 근처로 이동하였지만, 염색체의 위치는 세포 중앙에서부터 9.18 ± 4.23 ㎛로 떨어져 분포하였다. 그러나 항체가 있는 복합체인 경우는 염색체가 세포 중앙에서부터 20.59 ± 2.47 μm로 떨어져 분포하였다.

이러한 결과를 바탕으로, 세포 핵 이식 기술(somatic cell nuclear transfer)의 새로운 대안을 제시함과 동시에 실험적 검증을 통해 가능성을 보였다. 제안된 체세포 핵 이식 방법은 난자세포의 염색체를 복합체로 포획하여, 염색체의 활동을 조절하고, 탈핵(enucleation)과정 없이 체세포를 난자세

포 내로 융합한다. 제안된 방법의 가능성을 확인하기 위해, 복합체가 염색체를 포획하는데 소요되는 시간(10시간)이 세포 발달에 미치는 영향을 확인하고, 난자세포 내 잔류해 있는 복합체와 융합 후 난자 세포 내로 들어 온 체세포의 염색체 사이에 반응을 방지하는 방안을 제시하였다.

학회논문에서 복합체를 이용한 염색체 포획·세포 주기 조절·이동 등에 관한 연구방법은, 세포 내 다양한 기관들의 기능 및 물리적 특성을 연구하기 위한 기술로 활용 될 것으로 기대된다. 또한, 탈핵 과정 없이 다량의 난자세포를 동시에 다룰 수 있는 새로운 체세포 핵 이식법을 제안함으로써, 세포 리프로그래밍(reprogramming) 연구에 중요한 역할을 할 것으로 기대된다.